STOCHASTIC MULTI DRUG ADAPTIVE CHEMOTHERAPY CONTROL OF COMPETITIVE RELEASE IN TUMORS

by

Jiyeon Park

A Dissertation Presented to the
FACULTY OF THE USC GRADUATE SCHOOL
UNIVERSITY OF SOUTHERN CALIFORNIA
In Partial Fulfillment of the
Requirements for the Degree
DOCTOR OF PHILOSOPHY
(Applied Mathematics)

May 2022

Table of Contents

List of Tables

List of Figures

Abstract

This thesis is concerned with modeling tumor growth and chemotherapy response using stochastic evolutionary game theory models. In particular we develop stochastic N-cell models of a heterogeneous (multiple cell types) tumor using a Moran process model with frequency dependent fitness, which in the limit $N \to \infty$ converges to the deterministic adjusted replicator dynamical system as its mean-field limit. This limit and some of the details of our model and background literature are described in Chapter 1. Chapter 2 develops new results associated with the fixation probability of cell types that do not necessarily depend on the assumption of weak selection, but are valid across the full range of selection strengths. Chapters 3 and 4 develop our main results on adaptive chemotherapy scheduling using our stochastic N-cell evolutionary game theory model, both single drug and multi-drug scheduling, with the goal of avoiding chemo-resistance via the mechanism of competitive release, a concept borrowed from the ecology literature. The methods we develop are superior in measurable ways to more standard chemotherapy schedules currently in use at cancer centers all over the world, such as maximum tolerated dose (MTD) schedules and low-dose metronomic schedules (LDM). The final chapter describes potential future research directions.

Chapter 1

Introduction

Cancer can be seen as a consequence of interactions of cells with their surrounding environment as well as each other all of which contribute to its development. One approach to modeling the co-evolution of cancer cell populations that make up a tumor is to apply evolutionary game theory, an approach ideally suited to model the interactions dictated by the various fitness levels of the cells [37]. In the context of evolutionary game theory, fitness means the success rate at reproduction of a cell whose genotype is passed from generation to generation. This information is quantified through a payoff matrix that defines the game being played. Each group of cells is assumed to have a different success rate which depends not only on its own frequency in the population but also other types' in a population. As the populations co-evolve, success breeds success, and failure spirals downward, which is the essence of the replicator dynamical system and reinforcement learning equations. From Darwinian evolutionary theory, we know that natural selection is the key mechanism of evolution of a co-evolving population. With no selection, the system proceeds under random drift. However, even under weak selection, some sub-populations can develop higher fitness [12]. Eventually these frequency-dependent fitness functions determine and guide the fate of groups of cells when it is compared to the averaged fitness of the entire population. These ideas form the basis for the replicator dynamical system we use as our basic model, both in its mean-field deterministic form and its stochastic finite population form.

Many people have attempted to mathematically model tumor evolution with the aim of controlling its growth at a theoretical/computational level in order to guide and motivate clinicians to try new strategies and test them in clinical trials. These efforts in turn gives rise to important insights that can aid clinicians in finding and exploring to methods and avenues of possible treatments for their patients. Chemotherapy is the most important clinical treatment that is executed for the purpose of alleviating/controlling cancer at a systemic level. When it is administered to a patient in standard treatment schedules, it often decreases the size of the tumor initially (tumor regression), but then can be followed by re-growth (tumor recurrence) due to chemo-resistance. A working hypothesis in this thesis is that designing adaptive chemotherapy schedules that change as the tumor evolves can sometimes be an effective tool in delaying tumor recurrence. We develop computational models in this thesis (based on evolutionary game theory) and test various hypothetical adaptive chemotherapy schedules for the purpose of designing schedules that combat chemo-resistance. Much like adaptive control theory, the chemo-dosing adapts to the current state of the tumor, which of course requires efficient monitoring of the sub-populations of cells making up the tumor.The idea in this approach is to focus more on controlling the tumor growth with an allowable increase in its size than on eradicating all present cancerous cells [18, 19].

To better understand the role of chemotherapy in the evolution of the tumor, we divide (coarse-grain) the tumor cells into three groups: healthy cells, chemo-sensitive cells, and chemo-resistant cells. Assuming that cancer is the outcome of interactions of only these three different types, modeling the interplay between cancer and a drug is then equivalent to designing a fitness landscape for each type by which selection dynamics result, having the concentration of a drug as a controller of the system. We interpret the tumor recurrence as a result of a continued drug use in the context of *the competitive release*, which demonstrates that when two different types of groups are competing against each other for limited resources, currently subordinate subpopulations start proliferating and nearly take over the entire population when a catalyst that decreases the fitness of presently dominant subpopulations is introduced into a population [11]. In

other words, the sensitive cell subpopulations are dominant when no drug is administered since they have higher fitness, but when chemotherapy is introduced, it lowers the fitness of the sensitive cell population allowing the resistant population to proliferate. That is, a high enough concentration of a drug acts as a catalyst that exchanges the fitness of two different cancerous subpopulations competing each other and eventually the fate of the system. With this understanding that the drug concentration is a controller of the system, we let it enter the population equations through the selection of sensitive and/or resistant cells such that a high dose reduces the fitness level of the sensitive cells.

We adopt *a Prisoner's dilemma (PD) game* to assign the payoff that each cell receives from interaction with another. In its original form, the PD game is a two-player game between a cooperator and a defector from classical game theory, which is determined by what is called *the Prisoner's dilemma inequality* [3]. It describes that the rationality of players who are selfishly interested in maximizing their own rewards in playing a game eventually results in the sub-optimal scenario, both becoming defectors and receiving a lower payoff than they would have gained if they cooperated. The PD game has received a great attention in evolutionary game theory since the emergence of cooperation, which is often seen in nature but cannot be understood if assuming rationality of participants as in classical game theory, can be explained when this game is played repeatedly by a number of individuals in a population along with the natural selection acting on [3, 21, 39, 42, 44, 55]. We model a payoff matrix for healthy, sensitive and resistant cells such that healthy cells are cooperators whereas cancerous cells (resistant cells and sensitive cells) are defectors. For the payoff from the interaction between resistant cells and sensitive cells, we take *a cost of resistance* into account [8, 13, 20]. In many studies of drug resistance, it has been shown that resistant cells are present in a population as a result of mutation long before any drug is administered, and there is a fitness cost for cells becoming resistant. We adopt a PD game for the interaction between resistant and sensitive cells such that resistant cells are cooperators (lower fitness) whereas sensitive cells are defectors (higher fitness). The payoff matrix we use assures growth of the sensitive cell population under low drug concentrations,

while allowing for the competitive release of resistant cells under drug concentrations at a high enough threshold level.

In order to understand the co-evolutionary dynamics of these sub-groups in a finite population, we develop *a Moran process* model with three strategies, which is a discrete-time stochastic process [40, 51]. Knowing that *the (adjusted) replicator dynamics*, which assumes an infinite size of population, is the asymptotic dynamic ($N \to \infty$) of the Moran process [53, 54] and that an adaptive chemotherapy schedule is able to control the growth of a tumor by allowing a slight increase in size at an acceptable level as much as desired by repeating several cycles when it is modeled with the replicator equations [36], we will apply the adaptive chemotherapy schedule associated with the adjusted replicator dynamics to the Moran process and investigate how long the application is successful in controlling tumor growth in a finite population or how badly this adaptation fails to be used as a proper treatment. Moreover, for comparative purposes, the same investigation is carried out for two typical clinical chemo-schedules that ensure the same amount of drug use as the adaptive schedule: the maximum tolerated dose (MTD) and the low-dose metronomic schedules (LDM).

The natural extension of this study is obtained by generalizing the number of drugs. When more than one drug is used simultaneously, then some combinations act synergistically while others act antagonistically, compared to the case where each drug is independently delivered. The study of drug interaction has a long history and drug interactions can be mainly divided into three cases: additive, synergistic or antagonistic drug interactions [5, 9]. Following a drug interaction parameter introduced in [30] allows those three cases to be distinguishable from each other. We the model the effect of two drugs on cancerous populations by the Moran process with three sub-populations where there are two kinds of resistant cells to each of two drugs as well as sensitive cells to both drugs. A similar but more complicated investigation compared to a single drug model is achieved with this stochastic two drug chemotherapy model. This thesis is concerned with finding the optimal single drug and two-drug chemotherapy schedule that delays

the time of the saturation of cancerous cells in a population, and discuss its advantage compared to the standard clinical approaches.

1.1 Evolutionary game theory

Classical game theory, established by J. Von Neumann and O. Morgenstern in [35] in 1928, had been studied sporadically in the 19th century. It has received great attention and been applied to various areas from social science to ecology in the 20th century in an effort to understand how this decision-making model from interactions of rational players results in human behavior [33]. A classical game theory is originally evoked in a form of two-player games, where players participate in a game receiving a certain amount of payoff according to the strategies of their choices, and are assumed to be rational and struggle for earning a maximal possible reward being selfish. In 1950, *a strict Nash equilibrium*, a solution to a game, was invented by J. Nash, which is a strategy with which a players cannot be benefited in payoff by switching a strategy [34]. Game theory had not been significantly considered valuable in biology until J. M. Smith founded the field of evolutionary game theory by taking frequency dependence into account and applying it to evolution in order to model *Darwinism* [12] in the early 1970's in [46, 47, 48, 49] while similar attempts had been preceded in the 1930s by population geneticist such as R. A. Fisher, J. B. S. Haldane and S. Wright on the purpose of modeling *random drift* with the neglect of frequency in a finite population. Evolutionary game theory is distinct from classical game theory although they share some of the same ingredients of a game such as the payoff matrix that players or populations of players receive from interactions. However, being invented to describe the dynamics of subpopulations in a well-mixed reproductive population where each individual has the ability to reproduce its copy and a genotype is passed on to its offspring by heredity. In a population of cells where each cell has unique genotypic characteristics, cells are players of a game, genotypes are strategies, and fitness or success rate of a cell at reproductions is payoff. A group of cells with a higher expected fitness produces more offspring whereas a group with a lower expected fitness

replicates less. Unlike classical game theory, the focus of evolutionary game theory is not necessarily finding an optimal strategy with which a group of cells obtains a maximal payoff, but at achieving a state in which a sub-population is stable against invasion by an infinitesimally small increase of the frequency of a mutant population when a game is repeatedly played by a number of cells in a population. Thus, evolutionary game theory is described by a dynamical system, whereas classical game theory is described by a payoff matrix.

1.1.1 (Adjusted) Replicator dynamics in an infinite population

After the term "*replicator*" was first invented by R. Dawkins in [14], *the replicator equation* has become the most popular model that describes the dynamics of coevolving populations in a well-mixed population assuming an infinite size since its first introduction by P. G. Taylor and L. B. Jonker in [52] in 1978 [23, 41, 45]. For a game with two strategies, it is defined by

$$\begin{aligned} \dot{x}_A &= (f^A - < f >)x_A, \\ \dot{x}_B &= (f^B - < f >)x_B, \end{aligned} \tag{1.1}$$

where $\vec{x} := (x_A, x_B)^\intercal$ is a frequency vector of $A-$ and $B-$subpopulations such that $x_A + x_B = 1$, $f^A := (M\vec{x})_1 = ax_A + bx_B$ and $f^B := (M\vec{x})_2 = cx_A + dx_B$ are repectively the expected fitness of $A-$ and $B-$subpopulations, and $< f >:= \vec{x}^\intercal M\vec{x} = x_A f^A + x_B f^B$ is the averaged fitness in the entire populations. Here, M is the payoff matrix defining the interactions of the two (or more) sub-populations. It is a nonlinear deterministic ordinary differential equation that describes the relative growth of competing subpopulations. It is clear from the frequency dependent equations in (1.1) not only that a certain type of subpopulations grows faster in density when it is abundant in a population but also that it grows at the rate of the relative difference of its expected fitness to the averaged fitness, $< f >$, of the whole population. We only present the replicator equations for a game with two strategies but it is similarly defined for a

game with any finite number of strategies. Having $x_A + x_B = 1$, the equations in (1.1) are equivalent to a single equation

$$\dot{x}_A = (f^A - f^B)(1 - x_A)x_A \tag{1.2}$$

which demonstrates that a certain type of subpopulations increases in frequency whenever it has a higher expected fitness than other types of subpopulations.

Deterministic evolutionary dynamic is often explained by *the adjusted replicator equation* instead of the regular replicator equation, which is defined by:

$$\begin{aligned} \dot{x}_A &= \frac{f^A - < f >}{< f >} x_A, \\ \dot{x}_B &= \frac{f^B - < f >}{< f >} x_B, \end{aligned} \tag{1.3}$$

and with $x_A + x_B = 1$, is identical to

$$\dot{x}_A = \frac{f^A - f^B}{< f >}(1 - x_A)x_A. \tag{1.4}$$

As long as the fitness function, $< f >$, of the entire populations is positive, the equations (1.3) are not qualitatively different from equations (1.1), except for a difference in time scale. The replicator equation is not the only one model that illustrates deterministic dynamical systems, and many studies in evolutionary game theory have been conducted with other models including ODEs, differential inclusions, difference equations and reaction-diffusion system as summarized in [22]. However, it is worth deserving its fame when taking its equivalence to *the Lotka-Volterra equation* into account, which is a well-known model in ecology to describe the interactions of two populations over time, having a long history [6, 43].

1.1.2 Stochastic models in a finite population

Although a deterministic model is often a convenient description of population dynamics, sometimes there is a need for a model describing finite population interactions which have inherent stochastic fluctuations. D. Foster and P. Young suggested a continuous-time stochastic model that is designed by simply adding the Wiener process to the deterministic replicator equation, presuming that the white noise is configured by the Gaussian distribution in [17]. However, a discrete-time finite-space stochastic model is enough to characterize cell division and its inheritance from generation to generation as long as the model is equipped with fitness. One of frequently used such models is a frequency-dependent *Wright-Fisher process* although it was introduced a long ago by S. Wright and R. A. Fisher in 1930's [16, 60] with the absence of frequency [57, 25]. Suppose that a population of size N consists of cells who has unique genotype between A and B. The number of cells in the subpopulation A then defines a state of the system, and it is assumed in this model to be determined by N independent Bernoulli trials where the success and failure probabilities are weighted by the expected fitness of A and B. In precise, the current state, i, changes to a state, j, in the next step with a probability, $T_{i\to j}$,

$$T_{i\to j} = \binom{N}{j} \left(\frac{if^A}{if^A + (N-i)f^B}\right)^j \left(\frac{(N-i)f^B}{if^A + (N-i)f^B}\right)^{N-j} \tag{1.5}$$

for $j = 0, \cdots, N$. This sampling method, which is binomial for two strategies and multinomial for higher strategies, produces nonoverlapping generations and defines a discrete-time finite-space Markov chain with nontridiagonal transition matrix, meaning that every states is reachable from any states except for absorbing states, $i = 0$ or $i = N$. The power of this model is not only that it is built with a well-studied distribution, but also the population size is adjustable at all times without being fixed so that the total population size, N, at the current step can jump to, say, $2N$ in the following step, which is beneficial in

describing cell divisions. However, this process being a Markov chain with a nontridiagonal transition probability even in a constant population case challenges computational complexity for analytical study.

Unlike the Wright-Fisher process not being a birth-and-death process, a birth-death process, so-called *a pairwise comparison process*, has been studied in depth [2, 50, 54, 56, 58]. In this model, a randomly chosen individual updates its strategy to another randomly chosen individual's with a bigger probability than $1/2$ if the partner has a higher payoff at each time step. Precisely, the probability, p^{Fermi}, that an $A-$individual replaces a $B-$individual is given by

$$p^{\text{Fermi}} = \frac{1}{1+e^{-\beta(f^A - f^B)}}, \tag{1.6}$$

where it is represented as a function of fitness difference, $\Delta f := f^A - f^B$, and $\beta \geq 0$ is the strength of natural selection corresponding to the random drift when $\beta = 0$. Thus, an update is more likely to occur as the fitness difference, Δf, gets bigger. The fact that the number of individuals of a certain type can change at most by ± 1 in one time step and the total population size remains fixed in evolution defines a Markov chain with a tridiagonal transition probability. For this pairwise comparison model, the transition probability, T_i^+, that the system increases the number of $A-$individuals from i to $i+1$ and the transition probability, T_i^-, that it decreases the size of $A-$individuals from i to $i-1$ are given by

$$T_i^{\pm} = \frac{i}{N} \cdot \frac{N-i}{N} \cdot \frac{1}{1+e^{\mp\beta(f^A - f^B)}}. \tag{1.7}$$

The advantages of this model is that the selection intensity parameter, β, is unbounded and hence it can be set as arbitrary strong as needed while either weak or strong selections are of major interests to be analyzed. Also, the exponential form of probabilities in (1.6) and its expression only through the fitness difference, Δf, helps to obtain fruitful analytical observations such as fixation probability and fixation time, which are of key interests for stochastic models and we will be discussed in Chapter 2. This pairwise

comparison process is much more known as *Fermi process* with the recognition of use of the Fermi function, stemming from physics, for probability of switching strategies in (1.6).

Having a specific function for switching probability (1.6), the Fermi process is one special case of *a local update model* although it generalizes selection intensity to an unbounded interval. A local update model instead has a switching probability, $p^{\text{local update}}$, given by

$$p^{\text{local update}} = \frac{1}{2} + \frac{w}{2} \cdot \frac{f^A - f^B}{\Delta f_{\max}}, \tag{1.8}$$

where $\Delta f_{\max}$ is the maximum possible fitness difference and $0 \leq w \leq$ indicates the selection intensity. With this local update model, the transition probabilities similar to (1.7) are given by

$$T_i^{\pm} = \frac{i}{N} \cdot \frac{N-i}{N} \cdot \left(\frac{1}{2} \pm \frac{w}{2} \cdot \frac{f^A - f^B}{\Delta f_{\max}} \right). \tag{1.9}$$

The local update model has been mainly studied in 2×2 game especially in the comparison to other stochastic processes [54, 57] and it experienced a generalization in the number of strategies of a game in [53]. At the expense of complexity of functions of interest such as transition or fixation probability, it can also be generalized by modifying the switching or imitating probability, shown in (1.8), such that it possesses the same quality that the fitter grows more rapidly with a higher probability of switching and that a bigger fitness difference leads to a higher updating probability. Defining the updating probability by a function, $g(\beta \Delta f)$, of both selection and fitness difference such that $g'(\beta \Delta f)$ is nondecreasing in Δf, a generalized local update model was discussed in [61]. These local update models were discussed at a group level as well as an individual level in the context of spatial dynamics in [44] with the consideration that cells are more interacting with their neighbors than ones in a far distance.

1.2 Moran process in a finite population

Among many stochastic processes describing co-evolving finite populations, the one that has attracted many researchers in evolutionary game theory is the frequency-dependent *Moran process* since it was developed by M. A. Nowak *et al.* in [40] in 2004 [1, 2, 10, 29, 31, 32, 40, 51, 53, 54]. A local update model that only requires local information, which is the fitness difference of two randomly chosen individuals, for an update in each evolution time step is advocated by some researchers in the sense that cell interactions also depend on the physical distance and it can be then easily extended to the study of spatial dynamics. However, the computational simplicity, leading to a wide range of analytical observations besides numerical results while capturing the same amount of essence of description for selection dynamics acting on asexual cell divisions as other processes do, is enough to have fascinated and convinced scientists the use of the frequency-dependent Moran process. The Moran process was originally introduced by an Australian statistician, P. A. P. Moran, in [31, 32] in 1958 to express population dynamics, especially random drift, in a finite population in the absence of frequency in describing fitness. That is, the model in his introduction assumed that the each individual has a constant fitness that is never affected by the number of its own groups' or other groups' fitness during evolution. However, M. A. Nowak *et al.* insisted that how fast a mutant reproduces its offspring takes the frequencies of all different types into account and they modified it to be a frequency-dependent model.

1.2.1 Moran process: A birth-and-death process

The Moran process is a birth-and-death model that describes population dynamics in a well-mixed population, in which all individuals compete and interact with each other for limited resources, without imposing a population structure. For a basic Moran process, one individual is chosen and reproduces its offspring of the same type with a probability that is proportional to its expected fitness, and one individual, possibly the same one, is randomly chosen and eliminated in one evolution time step. This reproduction and

elimination in one time step thus results in a constant total population size during the whole evolution though the number of subpopulations are ever changing until it get absorbed to a homogeneous state. With this model, the number of at most two different types of subpopulations are affected and each group either increases or decreases at most by 1 in one time step, without both increasing or both decreasing, while the number of other types keeps unchanged. For example, consider a population of size N with two genotypes, A and B, in which every pair of two cells in one generation interact each other equally likely and their fitness is evaluated according to the payoff matrix, M, in (1.1). A state of the Moran process is determined by the number of subpopulations of one type, say type A, since a constant total population size is maintained during the whole evolution process, and then the number of cells in the subpopulation, B, is automatically given by the difference of the number of cells in the subpopulation, A, from the total population size, N.

Knowing that the state of the Moran process can change at most by 1 in one time step, this defines a discrete-time $1-$dimensional Markov chain on a finite space, $\{0, 1, \cdots, N\}$, with a $(N+1) \times (N+1)$ tridiagonal transition probability matrix. To be precise, let i be the number of individuals in the subpopulation, A, at the current step. Let T_i^+ be the transition probability that the state, i, increases by 1 to $i+1$, and T_i^- the transition probability that the state decreases to $i-1$ from i. These are the only possible nonzero transition probabilities with the probability, $T_i^0 = 1 - T_i^+ - T_i^-$, that the system stays at the current state under the assumption of no mutation. Both $i = 0$ and $i = N$ are two absorbing states that correspond to a homogeneous $B-$population and a homogeneous $A-$population, respectively, and these obviously lead to $T_0^+ = 0$ and $T_N^- = 0$, or in other words, $T_0^0 = 1$ and $T_N^0 = 1$. At all other internal states, the transition probability, $T_i^{\pm}$, at the state, i, is computed by considering the birth rate and the random

death. The birth rate is assumed to be proportional to the expected fitness, f_i^A and f_i^B, of A and B which interpret the expected payoffs, π_i^A and π_i^B, that are given by excluding the self-interaction:

$$\begin{aligned} \pi_i^A &= \frac{a(i-1)+b(N-i)}{N-1}, \\ \pi_i^B &= \frac{ci+d(N-i-1)}{N-1}. \end{aligned} \tag{1.10}$$

As introduced as a key mechanism by Darwin, it is common for the Moran process that natural selection whose intensity parameter, w, ranges between 0 and 1 goes through fitness function in a way that when $w = 0$, it reduces to the background fitness which is usually normalized to 1 for all types while when $w = 1$, it is exactly the same as the expected payoffs in (1.10). Thus, $w = 0$ corresponds to neutral drift where all subpopulations of different types are equally likely at reproduction whereas $w = 1$ is where the payoff, on which the researchers' preliminary knowledge and background about the components of a game is reflected, has the greatest influence on the selection dynamic. Fitness functions are then defined by:

$$\begin{aligned} f_i^A &:= 1 - w^A + w^A \pi_i^A = 1 - w^A + w^A \frac{a(i-1)+b(N-i)}{N-1}, \\ f_i^B &:= 1 - w^A + w^A \pi_i^B = 1 - w^B + w^B \frac{ci+d(N-i-1)}{N-1}, \end{aligned} \tag{1.11}$$

where w^A and w^B are selection intensities of A and B, respectively. Finally, the birth rates of $A-$ and $B-$subpopulations at the state, i, are given by $\frac{if_i^A}{if_i^A+(N-i)f_i^B}$ and $\frac{(N-i)f_i^B}{if_i^A+(N-i)f_i^B}$, and these help to compute the transition probabilities for the Moran process:

$$\begin{aligned} T_i^+ &= \frac{if_i^A}{if_i^A+(N-i)f_i^B} \cdot \frac{N-i}{N}, \\ T_i^- &= \frac{(N-i)f_i^B}{if_i^A+(N-i)f_i^B} \cdot \frac{i}{N} \end{aligned} \tag{1.12}$$

for $i \in \{1, \cdots, N-1\}$. It allows the Moran process to have an explicit $(N+1) \times (N+1)$ tridiagonal transition probability, T, such as:

$$T = \begin{pmatrix} 1 & 0 & 0 & \cdots & 0 & 0 & 0 \\ T_1^- & T_1^0 & T_1^+ & \cdots & 0 & 0 & 0 \\ \vdots & \vdots & \vdots & \ddots & \vdots & \vdots & \vdots \\ 0 & 0 & 0 & \cdots & T_{N-1}^- & T_{N-1}^0 & T_{N-1}^+ \\ 0 & 0 & 0 & \cdots & 0 & 0 & 1 \end{pmatrix}. \tag{1.13}$$

Due to the facts that the fitness functions in (1.11) become the expected payoffs in (1.10) when $w = 1$ and that these fitness functions are factors of transition probabilities in (1.12), it is necessary to assume that both f_i^A and f_i^B are nonnegative for all i's. These are satisfied if either selection intensities are small or all entries of a payoff matrix P in (1.1) are nonnegative. It is common to implicitly assume that $a, b, c, d \geq 0$ for the Moran process when the process with the whole range of selection is aimed to be analyzed. Whenever no one is fitter than another at all states, that is, $f_i^A = f_i^B$ for all i's , we have $T_i^+ = T_i^-$ and neither genotype is favored for reproduction at all states. This is the case to which the neutral drift case belongs. Also, it is a random walk in $\mathbb{Z}_0^+$ though not simple since it still does not have a stationary property, in fact, $T_i^\pm \neq T_j^\pm$ for $i \neq j$. Thus, many known theories in a random walk in $\mathbb{Z}_0^+$ are ready-to-use, allowing fruitful analytical results available.

Along the studies of evolutionary game theory by modeling a population with the Moran process since its reinterpretation as a frequency-dependent model, it has experienced generalizations in many aspects. For example, imposing a structure into a population by placing all individuals at vertices, and giving a weight to a directed edge, which represents a probability that an adjacent vertex is replaced by the offspring of the vertex from which the edge flies on a graph, a stochastic model can be designed to a various extents by varying either structures and weights as discussed in [29] in 2005. From their design, a

homogeneous population illustrated by the Moran process is considered as a particular case of a complete graph on which all edges have the same weight. They deduced that evolution is greatly dependent on the underlying structure and characterized graphs for which the quality of fixation coincides with that of a homogeneous population when it is modeled by the Moran process. On the other hand, P. M. Altrock and A. Traulsen proposed another generalization of the Moran process by introducing fitness-dependency in death rate as well as in birth rate for 2×2 game in [1] in 2009. According to their design, a cell is chosen for elimination not at random but at a probability proportional to inverse fitness, and the transition probabilities, $T_i^{\pm}$, in (1.12) are then modified as:

$$\begin{aligned} T_i^+ &= \frac{ie^{+w^b\pi_i^A}}{ie^{+w^b\pi_i^A} + (N-i)e^{+w^b\pi_i^B}} \cdot \frac{(N-i)e^{-w^d\pi_i^B}}{ie^{-w^d\pi_i^A} + (N-i)e^{-w^d\pi_i^B}}, \\ T_i^- &= \frac{(N-i)e^{+w^b\pi_i^B}}{ie^{+w^b\pi_i^A} + (N-i)e^{+w^b\pi_i^B}} \cdot \frac{ie^{-w^d\pi_i^A}}{ie^{-w^d\pi_i^A} + (N-i)e^{-w^d\pi_i^B}}, \end{aligned} \tag{1.14}$$

where $w^b \geq 0$ and $w^d \geq 0$ are the selection intensities at birth and death, respectively, and the fitness is defined in the form of an exponential function. Leaving these for further studies, we model a finite well-mixed population using the fitness-dependent Moran process in this thesis.

1.2.2 Connection of Moran process to the adjusted replicator dynamics

Evolutionary game theory, which classically began with the replicator dynamics equations for an infinite population, was later developed for a finite (stochastic) population. How the stochastic process for a finite population is related to the replicator system for an infinite population as the population size increases was a natural question in this field. A. Traulsen *et al.* first proved in [54] in 2005 for 2×2 game that the replicator dynamic is the expected system of a local update stochastic model defined with a switching probability in (1.8) in the population size limit whereas the adjusted replicator dynamic is the mean system for the Moran process. They generalized this result for a general stochastic process with an arbitrary finite number of strategies, where mutation is also allowed in [53] in 2006. We briefly discuss the derivation of

the adjusted replicator system from the Moran process in the population size limit for a 2×2 game and the maximal selection intensity in this section since it captures the essence of the argument in its simplest form, and the generalization to higher dimension is straightforward.

The Moran process with two strategies is described at a microscopic level in terms of the probability, $P_i(\tau)$, that the system is in the state, i, at time τ, with the transition probabilities:

$$\begin{aligned} P_i(\tau+1) - P_i(\tau) = P_{i-1}(\tau)T^+_{i-1} + P_{i+1}(\tau)T^-_{i+1} \\ - P_i(\tau)T^-_i - P_i(\tau)T^+_i, \end{aligned} \tag{1.15}$$

where i is the number of agents in subpopulation A in a population of size N as before. This equation (1.15) is called *the master equation* and it describes the net change in probability from state, i, in one time step from time, τ. Letting

$$x = i/N, \tag{1.16}$$

$$t = \tau/N, \tag{1.17}$$

$$T^{\pm}(x) = T^{\pm}_i, \tag{1.18}$$

the equation in (1.15) is rewritten in terms of the probability density function, $\rho(x,t) := NP_i(\tau)$, as follows:

$$\begin{aligned} \rho(x, t+N^{-1}) - \rho(x,t) =& \rho(x-N^{-1},t)T^+(x-N^{-1}) + \rho(x+N^{-1},t)T^-(x+N^{-1}) \\ & - \rho(x,t)T^-(x) - \rho(x,t)T^+(x). \end{aligned} \tag{1.19}$$

For a large N, the Taylor expansion at x and t for both the probability density function, ρ, and the transition probabilities, $T^{\pm}$, up to the first order term in N^{-1} gives rise to *the Kolmogorov forward equation*:

$$\frac{\partial}{\partial t}\rho(x,t) = -\frac{\partial}{\partial x}[a(x)\rho(x,t)] + \frac{1}{2}\frac{\partial^2}{\partial x^2}[b^2(x)\rho(x,t)] \tag{1.20}$$

with the drift term, $a(x) = T^+(x) - T^-(x)$, and the diffusion term, $b(x) = \sqrt{(T^+ + T^-)/N}$. Applying the Itô calculus on $\rho(x,t)$, the equation (1.20) is equivalent to a stochastic differential equation, called *the Langevin equation*:

$$dX_t = a(X_t)dt + b(X_t)dB_t, \tag{1.21}$$

where B_t is the one dimensional standard *Wiener process* and X_t is the state of the system at time t. Noting that the diffusion term, $b(X_t)$, vanishes with the rate of $1/\sqrt{N}$ as $N \to \infty$, the limiting system is solely determined by the drift term, $a(X_t)$, as follow:

$$\dot{x} = \lim_{N\to\infty}(T_i^+ - T_i^-). \tag{1.22}$$

By equations in (1.12), it becomes

$$\begin{aligned}\dot{x} &= \lim_{N\to\infty}\frac{f_i^A - f_i^B}{(if_i^A + (N-i)f_i^B)/N}\cdot\frac{N-i}{N}\cdot\frac{i}{N} \\ &= \frac{f^A - f^B}{< f >}(1-x)x\end{aligned} \tag{1.23}$$

and finally the adjusted replicator equation in (1.4) is recovered in the limit of N from the master equation for the Moran process with $x = x_A$.

This derivation is available in [53] even when the Moran process is applied to a population having more than two strategies, say d strategies. However, this stochastic process with $d > 2$ strategies is no longer a random walk on $(\mathbb{Z}_0^+)^{d-1}$. In the same manner, the Fermi process defined by (1.6) and the local

update process defined by (1.8) are also shown to converge to the regular replicator system with a constant factor that only re-scales the time.

1.3 Moran process and a chemotherapy concentration applied to the selection

Chemotherapy is a standard systemic clinical approach and is ubiquitous in various cancers as a treatment to alleviate disease by generally focusing on killing as many malignant cells as possible in order to reduce the size of tumor. The goal of this thesis is to develop adaptive chemotherapy protocols that prevent the deterministic adjusted replicator system from saturating the population with cancer cells, in the spirit of [36] and [59], then to test these strategies with the stochastic Moran process model, both using the single drug and multi-drug protocols. We will then highlight the advantages of using the adaptive chemotherapy schedules with respect to avoiding chemo-resistance of the tumor.

Our approach is to view tumor growth as the outcome of the interactions of three subpopulations of cells: healthy cells (H), sensitive cancer cells (S) and resistant cancer cells (R) to a drug. The model we employ is the $2-$dimensional Moran process for a population of size N with three cell types, H, S and R. Since the Moran process keeps a constant population size during the whole evolution, the frequency of the different cell types determines the state of the system. We specify the number of healthy cells and the number of resistant cells as independent variables, so $2-$dimensional process, and let i be the size of healthy subpopulations and j the size of resistant subpopulations. Then for each N, the set

$$\Lambda_N := \{(i,j) \in \mathbb{Z}_0^+ \times \mathbb{Z}_0^+ | 0 \leq i \leq N, 0 \leq j \leq N, i+j \leq N\} \tag{1.24}$$

defines the space of states for the Moran process with three strategies, and the number of elements, $|\Lambda_N| = \frac{(N+1)(N+2)}{2}$, of Λ_N increases in the order of $O(N^2)$. When we refer to a state in Λ_N in (1.24), we interchangeably use $(H, R) = (i, j)$ or $(H, S, R) = (i, N-i-j, j)$.

We assume that a finite population is well-mixed and every pair of cells in this population interacts and each cell receives a payoff from that interaction according to a 3×3 payoff matrix, A:

$$A = \begin{array}{c} \\ H \\ S \\ R \end{array} \begin{array}{c} \begin{array}{ccc} H & S & R \end{array} \\ \begin{pmatrix} a_{11} & a_{12} & a_{13} \\ a_{21} & a_{22} & a_{23} \\ a_{31} & a_{32} & a_{33} \end{pmatrix} \end{array}. \tag{1.25}$$

From those equally likely interactions, a cell of type X, $X \in \{H, S, R\}$, receives the expected payoff, $\pi^X_{i,j}$, at the state, (i, j), excluding self-interaction as it does for the $1-$dimensional Moran process in (1.10):

$$\begin{aligned} \pi^H_{i,j} &= \frac{a_{11}(i-1) + a_{12}(N-i-j) + a_{13}j}{N-1}, \\ \pi^S_{i,j} &= \frac{a_{21}i + a_{22}(N-i-j-1) + a_{23}j}{N-1}, \\ \pi^R_{i,j} &= \frac{a_{31}i + a_{32}(N-i-j) + a_{33}(j-1)}{N-1}. \end{aligned} \tag{1.26}$$

The expected fitness function, $f^X_{i,j}$, is defined, similarly to (1.11), by

$$f^X_{i,j} = 1 - w^X + w^X \pi^X_{i,j}, \tag{1.27}$$

where $w^X \in [0, 1]$ is the selection intensity of the type, X. Modeling the role of a drug on a population committed to tumor regression/recurrence is then equivalent to shaping fitness functions based on the scientific understandings about the relation between different types of cells when a drug is on or off. In

order to complete the description of our model, we introduce some key concepts in the following two subsections.

1.3.1 Prisoner's dilemma game

A Prisoner's dilemma (PD) game is a two-player-game, originally framed in classical game theory by M. Flood and M. Dresher while working at the RAND Corporation in 1950. What makes this game a *dilemma* game, in the context of classical game theory, is that rational decisions to maximize their own payoff leads them to choose a strategy that instead provides them with a lower payoff than they would have gained if they chose the alternative. Later, the game was used in an iterated form to capture the essence of the emergence of cooperation [21, 38, 39, 42, 44, 55]. Being hard to be understood in the framework of classical game theory, this altruism is easily seen in nature, especially in animal worlds. For example, in some species, it is often seen that one gives an alarm for their peers when it encounters a predator in order to let them hide while exposing itself to danger. It is also seen in global climate-change that all countries take advantage from maintaining a stable climate, but any single country often hesitates to regulate CO_2 emission, thinking of maintaining this behavior as being more beneficial to itself than it would be if all countries decided to reduce CO_2 emission. This scenario has been dubbed 'the tragedy of the commons'. Achievable altruism has been deeply studied in evolutionary theory with the variety of generalization from iteration to the number of strategies.

In a classical Prisoner's dilemma (PD) two-player-game, each player can choose to cooperate (C) or defect (D) in playing a game each round. Given a 2×2 payoff matrix

$$M = \begin{array}{c} \\ C \\ D \end{array} \begin{array}{c} \begin{array}{cc} C & D \end{array} \\ \begin{pmatrix} R & S \\ T & P \end{pmatrix} \end{array} = \begin{array}{c} \\ C \\ D \end{array} \begin{array}{c} \begin{array}{cc} C & D \end{array} \\ \begin{pmatrix} 3 & 0 \\ 5 & 1 \end{pmatrix} \end{array}, \tag{1.28}$$

each receives R when both cooperate whereas each receives P when both defect. When two players with different strategies encounter, a cooperator receives S and a defector receives T. What makes this game in (1.28) a Prisoner's dilemma game is *the Prisoner's dilemma inequality*:

$$T > R > P > S. \tag{1.29}$$

Under this assumption, all rational players will end up playing D since it gives a higher compensation in either cases when a partner cooperates or defects. This is called a Nash equilibrium. However, they would have received a higher payoff, R, each if they cooperated. Any single combination of R, S, T, and P that satisfies the inequality in (1.29) defines a Prisoner's dilemma game, but the canonical choice is when $R = 3$, $S = 0$, $T = 5$ and $P = 1$ as given in (1.28).

In evolutionary game theory, strategies are interpreted as genotypes which are selected and passed to the next generation by natural selection depending on their frequencies in a population. Consider a infinite population of cooperators (C) and defectors (D). Let x_C be the frequency of cooperators and x_D that of defectors, then we have $x_C + x_D = 1$. Letting the selection intensities, w^C and w^D, of C and D be equal to 1 so that the payoff matrix, A, has the most influence on the fitness functions defined similarly to (1.11) but in continuous way, the fitness functions, f^C and f^D, are given by

$$\begin{aligned} f^C &= (M\vec{x})_1 = 3 \cdot x_C + 0 \cdot x_D, \\ f^D &= (M\vec{x})_2 = 5 \cdot x_C + 1 \cdot x_D, \end{aligned} \tag{1.30}$$

where $\vec{x} = (x_C, x_D)^\intercal$. Then the averaged fitness function, $< f >$, in the entire population becomes

$$< f >:= \vec{x}^\intercal M\vec{x} = 3x_C^2 + 5x_C x_D + x_D^2 \tag{1.31}$$

and it is straightforward to show that $< f >$ has the minimum value, 1.

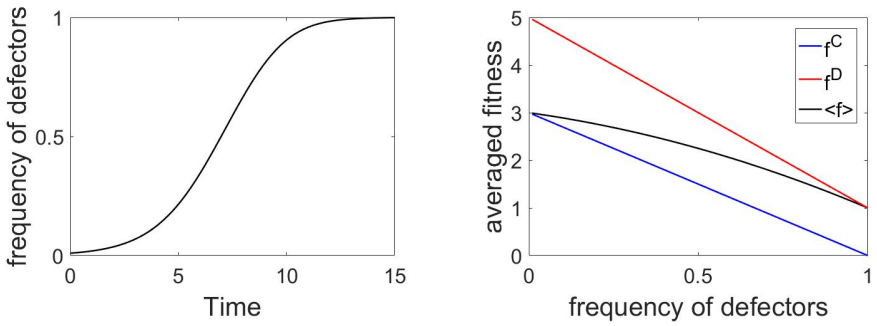

(a) (b)

Figure 1.1: Defectors (D) playing a Prisoner's dilemma game outcompete cooperators (C), grow in a S-shaped Gompertzian curve, and eventually saturate the entire population, eventually reaching a sub-optimal state according to the adjusted replicator system. For simulation, we set $R = 3$, $S = 0$, $T = 5$ and $P = 1$. (a) Initially nonzero defector subpopulations with the proportion, 0.01, keeps increasing over time in a S-shaped curve and eventually saturating the entire population; (b) The averaged fitness function, $< f >$, is unfortunately minimized at that evolutionarily stable strategy, D, meaning that $x_D = 1$ is an asymptotically stable but sub-optimal state.

Employing the adjusted replicator equation in (1.4) gives rise to

$$\dot{x}_C = -\frac{(1 + x_C)(1 - x_C)x_C}{< f >} \tag{1.32}$$

which implies that the deterministic system has fixed points at $x_C = 0, 1$. It is easy to check that $x_C = 0$ is asymptotically stable. Figure 1.1 illustrates that the proportion of defectors in an infinite population, that initially takes only 1% of the total population, increases along a S-shaped *Gompertzian curve* and reaches plateaus at 1 [27], but the averaged fitness function, $< f >$ is minimized at $x_C = 0$ being equal to 1. It is this Gompertzian growth law that makes the PD game useful as a tumor growth model. In fact, the system is driven to the stable homogeneous state of purely defectors whenever there initially exists the nonzero number of defectors, but that is a sub-optimal state. These two characteristics (Gompertzian growth and sub-optimal fitness) allow us to adopt a PD game for describing interactions between healthy and cancerous cells in our model by letting healthy cells be cooperators and cancer cells defectors.

1.3.2 Cost of resistance and competitive release

As mentioned earlier, one main factor that makes chemotherapy challenging is tumor recurrence followed by the initial tumor regression due to adaptive ability of a population, leading it to form resistance to a drug. This chemo-resistance is often explained by the ecological mechanism of *the competitive release* that was originally termed by J. H. Connell in [11] in 1961. The phenomenon unfolds when two species compete for a limited resource, with one species out competing the other, thereby suppressing the growth of the weaker species (i.e. the one with lower fitness). When a change in the environment occurs that kills the dominating species, it releases the weaker one from the competition, thereby allowing it to grow. For competing cancer cells, in the absence of chemotherapy, the dominant population are the chemo-sensitive cells (higher fitness), and the sub-dominant ones are the chemo-resistant ones (lower fitness due to the cost of resistance). With chemotherapy, the sensitive cells are mostly killed off, which releases the resistant cells from the competition and allows them to grow, rendering the tumor resistant. Though this term had been supported later by a lot of *in vivo* experiments mainly in the field of chemical ecology, cancer can also be modeled based on this notion in order to describe the chemotherapeutic response onto a population of healthy, sensitive and resistant cells.

It is known that resistant cells to a drug as well as sensitive cells typically exist even before chemotherapy is carried out as a result of pre-existing mutations. Typically, however, resistant cells are present in a population only in small numbers due to *the cost of resistance*: it is inherently expensive for cancer cells to maintain resistance. In other words, resistant cancer cells pay a fitness cost in the form of lowering their reproductive success. It has been demonstrated in laboratory experiments that resistant cells are less fit and less flourishing than sensitive cells in the absence of chemotherapy [8, 13, 20]. The application of chemotherapy, however, then lowers the fitness of the sensitive cell population, and the resistant cells begin to flourish. We will adopt these two notions to model the chemotherapeutic resistance of a tumor population.

1.3.3 Fitness landscape

We quantify the previous notions in our choice for the payoff matrix, A, in (1.25) to shape fitness landscape of all types of cells together with drug concentration. We let the concentration, $0 \leq C(t) \leq 1$, of a drug, which is a function of time indicating the drug intensity rather than the absolute amount, enter the cell population through selection functions, w^H, w^S and w^R, in a following way:

$$\begin{aligned} w^H(t) =& w_0, \\ w^S(t) =& w_0(1 - C(t)), \\ w^R(t) =& w_0, \end{aligned} \tag{1.33}$$

where w_0 is a constant which we will set equal to 1 for computational convenience since it can be scaled out without changing qualitative features. This definition in (1.33) allows the selection functions of all types to be time-dependent functions and quantitatively establishes that the concentration function, $C(t)$, becomes a controller of the system. When it is turned on, it lowers the fitness of the sensitive cell population, leaving the others unchanged.

A Prisoner's dilemma game is an adequate model to describe the relations between healthy cells and cancerous cells in a way that under no chemotherapy, healthy cells are cooperators whereas cancerous cells are defectors since it possesses two important features when it is interpreted by the replicator system in the evolutionary game theory perspective: (i) initially nonzero portion of defectors eventually saturates the entire population, and (ii) that asymptotically stable homogeneous state of defectors is sub-optimal. Thus we impose the payoff matrix, A, to satisfy the Prisoner's dilemma inequalities in (1.29) such that

$$a_{21} > a_{11} > a_{22} > a_{12}, \tag{1.34}$$

$$a_{31} > a_{11} > a_{33} > a_{13}, \tag{1.35}$$

where (1.34) defines a PD game between healthy cells and sensitive cells whereas (1.35) defines a PD game between healthy cells and resistant cells.

In addition, having a higher fitness, sensitive cells are abundant under no treatment though a small number of resistant cells are present. However, when a drug is delivered, it lowers the fitness of the sensitive cell population which, in turn, allows the resistant population to flourish (competitive release). In other words, the delivery of a drug, which is an artificial interference to a population, plays the role of catalyst for the proliferation of resistant cells by lowering the fitness of sensitive cells, releasing their competing agents (resistant cells), and allowing those resistant cells to use more resources, proliferate and eventually survive. These features, that are termed as the cost of resistance and the competitive release, convince us to adopt a PD game for interactions between sensitive cells and resistant cells where in the absence of treatment, resistant cells are cooperators whereas sensitive cells are defectors. We design the payoff matrix, A, to satisfy the following prisoner's dilemma inequality

$$a_{23} > a_{33} > a_{22} > a_{32} \tag{1.36}$$

as well as

$$a_{21} > a_{31} \tag{1.37}$$

to guarantee that sensitive cells have a higher fitness than resistant cells at all time, that is, regardless of the distribution of a population when chemotherapy is absent. Also, the fact that a drug administration at a high dose causes sensitive cells to be less fit than resistant cells is reflected by requiring that the fitness function, f^R, of resistant cells is greater than the fitness function, $f^S|_{C(t)\approx 1}$, of sensitive cells under a constant high concentration. Knowing from (1.33) and (1.27) that the fitness of sensitive cells is almost

equal to the background fitness, which is set to be 1, when the constant high chemo-dose is nearly equal to 1, this is obtained if we further set

$$a_{31}, a_{32}, a_{33} \geq 1 \tag{1.38}$$

with all three not being equal to 1 simultaneously.

For two drug model, we will design the fitness of all types in an analogous manner based on PD games, the cost of resistance and competitive release by letting drug concentration functions enter through selection functions. This will be discussed further in Chapter 4.

1.4 Structure of the thesis

In a finite population evolutionary game theory, what has received great attention by researchers are the state that a single mutant successfully enters a homogeneous population and the state that that single mutant survives and eventually takes over the whole population. The former is termed as *invasion* and the later is termed as *fixation*. Between two, what distinguishes a stochastic process from a deterministic system in modeling a co-evolving population is the fixation since it quantifies a chance of observing a new scenario driven by natural selection which would not be seen if it is modeled by the replicator system assuming an infinite population. Many researchers have devoted effort to finding either fixation probability or fixation time with many different stochastic models, resulting in fruitful analytical results.

In Chapter 2, we briefly go through the derivation of the exact formula of fixation probability for stochastic processes with 2 strategies. In classical evolutionary game theory assuming an infinite population, *the evolutionary stable strategy (ESS)* is well established as a state that survives and persists, hence is of great interest. However, this concept underwent modification in a finite population and we mention this evolutionary stable strategy (ESS_N) in a finite population, which is defined in terms of both fixation probability and invasion. We also refer to both one well-known approximation to *the rate of evolution*,

which is the multiplication of fixation probability and population size, under weak selection, and how the definition of ESS_N is sharpened with the use of this approximation. We point out that this approximation, in the form of the truncated Taylor expansion with the degree of 1, is only valid under an extraordinarily narrow weak selection window with the example of repeated Prisoner's dilemma game, and precisely give the upper threshold of those weak selection. We also show that the regular linear Taylor approximation becomes a better approximation over those limited region of weak selection. Moreover, we suggest a global approximation to the rate of evolution using *Bernstein polynomial*, which is defined on the whole selection interval, and explains its efficiency on a strong selection limit.

In Chapter 3, we adopt the frequency-dependent Moran process model with three strategies in order to model the role of single drug chemotherapy acting on a finite population of healthy (H), sensitive (S) and resistant (R) cells, all participating in tumor development. We shape the fitness functions of cells as discussed in section 1.3.3. Knowing that the fixation probability for the Moran process with three strategies does exist but is, so far, only expressed as a solution to a linear system, proved by E. M. Ferreira and A. G. M. Neves in [15], where the coefficient matrix is order of $O(N^4)$ for the population size N, we numerically compute fixation probability at $|\Lambda_N|$ many points distributed in phase space. Visualizing these fixation probabilities as N increases, we show how the stochastic version of competitive release converges to the basins of attraction for the adjusted replicator equation. Moreover, as a second part, *the adaptive chemotherapy schedule* associated with the adjusted replicator equations, developed in [36] but with the regular replicator equations, is applied to the stochastic Moran process to examine the chemotherapeutic response. It is obvious that applying this chemotherapy schedule to the stochastic process will fail in trapping the wiggly trajectory in a closed loop though it is designed to do for the expected deterministic system. It is for the randomness, driven by the finite population size, leads not only one single realization but also the averaged system of many realizations to settle on a neighborhood instead of the exact initial state after each evolutionary cycle. We quantify how badly this schedule works or how fast its use on the

Moran process is not justified as increasing the number of cycle. We later evaluate this adaptive schedule in terms of tumor volume, that is quantified as a sum of cancerous cells, by comparing it to the standard clinical approaches that have the same amount of the total dose of toxin: the maximum tolerated dose schedule (MTD) and the low-dose metronomic schedule (LDM).

In Chapter 4, we generalize Chapter 3 by introducing an additional drug, where the two drugs act asymmetrically, meaning that they have different response rates. Following [30], we equip our model with a drug interaction parameter, $-1 \leq e \leq 1$, in order to distinguish antagonistic ($e < 0$), additive ($e = 0$) and synergistic ($e > 0$) drug interactions from each other. We consider a finite population that is composed of sensitive (S) cells to both drugs, a group of cells (R_1) that are sensitive to drug 1 but resistant to drug 2, and a group of cells (R_2) that are sensitive to drug 2 but resistant to drug 1. Shaping the fitness functions of these three types of cancer cells analogously to but relatively more complex than that of a single drug model, the evolution of a population of cancer cells is modeled by the Moran process with three strategies. After we develop an adaptive chemotherapy schedule associated with the adaptive replicator equations for each drug interaction case that use up the similar total dose of toxin from both drugs, we apply each schedule to the Moran process. For the evaluation of these schedules, we separately adopt the tumor-growth model, which is the nonlinear deterministic differential equation, to describe tumor volume. With these two models, we study how successfully the adaptive chemotherapy schedule associated with the adjusted replicator dynamic works and how long the application of this chemotherapy can be justified, just as done in Chapter 3. Evaluation of this adaptive two drug schedule is then made either across or within drug interactions by comparing it to two standard clinical approaches such as MTD and LDM having the same total dose.

Finally in Chapter 5, we will discuss future potential research directions which would generalize our models in several important ways.

Chapter 2

Fixation probability for Moran processes with two strategies

Begun by M. A. Nowak *et al.* in modeling a finite population that play 2×2 game with the frequency-dependent Moran process, *fixation* has been intensively studied from finding its probability to finding the time that the underlying stochastic process takes until its occurrence, across many stochastic processes [2, 29, 40, 51, 56]. Fixation refers to a state that a single (or, in general, a finite number of) mutant is favored by selection replacing resident subpopulations and eventually takes over the entire population. The reason why this concept attracted many researchers is that this is what makes stochastic processes distinguished from deterministic models and what quantifies the randomness driven by finiteness in population size. For example, as shown in [51] for a 2×2 game, the Moran process for a finite population drives eight selection scenario whereas the deterministic replicator system for an infinite population leads to four selection ones, and those extended categorization was made based on fixation probability. Also, the well-established concept, *evolutionary stability*, in an infinite population was modified by M. A. Nowak *et al.* in [40] by introducing fixation probability as an extra condition besides the original invasion condition when adopting this concept into a finite population.

2.1 Fixation probability and evolutionary stability

Fixation probability has an exact formula for a 2×2 game though complex, and it was obtained by exploiting that $1-$ dimensional Moran process with two strategies can be considered as a random walk on a subset of $\mathbb{R}$ and using well-known ready-to-use theorems. In fact, the closed form is available for any birth-and-death processes as well as the Moran process. However, in general, the Moran process with d many strategies is not a random walk in $\mathbb{R}^{d-1}$ when $d \geq 3$, and this makes the computation challenging for a higher dimension. As far as we know, E. M. Ferreira and A. G. M. Neves were the first who recently proved the existence of the fixation probability for $d = 3$, and they represented it as a solution to a system of linear equations by formalizing the fixation probability as a solution of discretized $2-$dimensional Dirichlet problem for the Laplace equation in [15] in 2020. We will discuss more about it in the next chapter, but for a while we mainly focus on the fixation probability for the Moran process with two strategies in this chapter.

2.1.1 Computation of fixation probability

Consider the Moran process with two strategies, A and B, for a finite population of size N, all interacting equally likely each other and receiving a payoff according to the payoff matrix M in (1.1). We define a state of the Moran process by the number, i, of cells in the subpopulation, A, $i = 0, 1, \cdots, N$. For each i, let ρ_i^A be the probability that i mutants of type A replace all $B-$mutants and take over the population, and similarly ρ_i^B for B. Since all states of the Moran process are transient, the stochastic system eventually achieves the homogeneity of a population in either all A's or all B's, leading to $\rho_i^B = 1 - \rho_i^A$. Thus it is sufficient to compute ρ_i^A for a 2×2 game. We will use ρ_i^A and ρ_i interchangeably for convenience.

If mutation is not allowed, the Moran process with two strategies has two absorbing states, $i = 0$ and $i = N$, at which fixation probability is complete as follows:

$$\begin{aligned} \rho_0 &= 0, \\ \rho_N &= 1. \end{aligned} \tag{2.1}$$

For an intermediate states, $i = 1, \cdots, N-1$, the state can have a jump only to either $i+1$ or $i-1$ besides staying unchanged. Each jump is made at a probability, T_i^+ and T_i^-, respectively. Then it allows to have a following recurrence relation in terms of fixation probability, ρ_i, and transition probabilities, $T_i^{\pm}$:

$$\rho_i = T_i^- \rho_{i-1} + T_i^0 \rho_i + T_i^+ \rho_{i+1}, \tag{2.2}$$

where the probability, T_i^0, that the stochastic system remains unchanged is equal to $T_i^0 = 1 - T_i^+ - T_i^-$.

Defining variables, $\phi_i := \rho_i - \rho_{i-1}$ and $\lambda_i := T_i^-/T_i^+$, the equation (2.2) is re-written:

$$\begin{aligned} \phi_1 &= \rho_1, \\ \phi_{i+1} &= \lambda_i \phi_i \end{aligned} \tag{2.3}$$

for $i = 1, \cdots, N-1$, and this is equivalent to

$$\phi_{i+1} = \rho_1 \prod_{k=1}^{i} \lambda_i. \tag{2.4}$$

Summing (2.4) over i gives rise to $\sum_{i=1}^{N} \phi_i = (\rho_1 - \rho_0) + (\rho_2 - \rho_1) + \cdots + (\rho_N - \rho_{N-1}) = \rho_N - \rho_0 = 1$ and it leads to

$$\rho_1 = \frac{1}{1 + \sum_{j=1}^{N-1} \prod_{k=1}^{j} \lambda_k}. \tag{2.5}$$

Using the same summation of (2.4) but up to as less number of terms as desired, it implies $\rho_i = \rho_1(1 + \sum_{j=1}^{i-1}\prod_{k=1}^{j}\lambda_k)$, and the general fixation probability, ρ_i, of A starting from the state, i, is driven as follows:

$$\rho_i = \frac{1 + \sum_{j=1}^{i-1}\prod_{k=1}^{j}\lambda_k}{1 + \sum_{j=1}^{N-1}\prod_{k=1}^{j}\lambda_k} \tag{2.6}$$

with equating $\sum_{j=1}^{i-1}\prod_{k=1}^{j}\lambda_k$ to 0 when $i = 1$.

The derivation of fixation probability in (2.6) has not made use of the underlying stochastic process except for that it is a birth-and-death process so that a state can move at most by ± 1 in one time step. For this reason, the expression in (2.6) is valid for any $1-$dimensional birth-and-death processes with no mutation assumption. We end this subsection by specifying this fixation probability for the Moran process for the later use. From (1.12), the variable, $\lambda_i := T_i^-/T_i^+$, can be explicitly written in terms of fitness functions of A and B for the Moran process, and the fixation probability in (2.6) is nothing but

$$\rho_i = \frac{1 + \sum_{j=1}^{i-1}\prod_{k=1}^{j} f_k^B/f_k^A}{1 + \sum_{j=1}^{N-1}\prod_{k=1}^{j} f_k^B/f_k^A}. \tag{2.7}$$

2.1.2 Evolutionarily stable strategy in a finite population

Corresponding to the Nash equilibrium, which is a strategy with which no plyer improves its reward by switching to another, in classical evolutionary game theory, one of the main interests in evolutionary game theory is to find a strategy, pure or mixed, persistent to natural selection through time in a coevolutionary population. Such strategy is what is called *an evolutionarily stable strategy (ESS)*, originally invented by M. Smith in [46, 47, 48, 49]. Assuming an infinite population, ESS is a strategy that for an infinitesimally large population playing this strategy, an infinitesimally small population playing a different strategy is

not able to invade into the nearly homogeneous population. Precisely in a 2×2 game with a payoff matrix M in (1.1), a strategy, B, is said to be evolutionarily stable if either

$$(i) d > b \quad \text{or} \tag{2.8}$$

$$(ii) d = b \quad \text{and} \quad a < c. \tag{2.9}$$

This condition is made by letting the fitness of the subpopulation, A, smaller than that of B when the population is nearly composed of individuals of type B, so that natural selection opposes the spread of infinitesimally small fractions of A in infinitely large populations of B.

As evolutionary game theory developed and the needs for more realistic models describing a finite coevolving population arose, this concept of evolutionary stability had been challenged to be adopted to a finite population. D. Foster and P. Young suggested a new concept of stability, which they called *stochastically stable equilibrium (SSE)*, for a stochastic system that is designed using the Wiener process added to the deterministic replicator equations in [17] in 1990. By defining SSE as a long-run viability, they convinced that attractors in dynamical system are not sufficient to be an alternative due to the dependence of the limiting behavior of the system on the initial distribution. In fact, they defined SSE to be a state at which the stochastic system asymptotically stays within its small neighborhood with a positive probability as the stochastic effects decreases, where the decreased effects is measured as the shrinking variance of the Wiener process.

Recognizing that a single mutant, successfully invaded a resident population, is possibly able to take over the entire finite population, M. A. Nowak *et al.* modified the concept of EES, that M. Smith had suggested, in [40] in a way that selection opposes both invasion and fixation, and began to be widely used

in this field. Denoting it by ESS_N, a strategy, B, is said to be evolutionarily stable in a finite population of size N for a 2×2 game in (1.1) if followings are satisfied:

$$(i) b(N-1) < c + d(N-2), \tag{2.10}$$

$$(ii) \rho_1^A < \frac{1}{N}. \tag{2.11}$$

The condition in (2.10) is equivalent to $f_1^A < f_1^B$ and guarantees that selection opposes A invading a resident population of B whereas the condition in (2.11) describes that A is not favored taking over the entire population by natural selection. The quantity, $\frac{1}{N}$, in (2.11) is the fixation probability of A when the selection is absent for both types such that the coevolutionary population evolves exclusively under the neutral drift. Knowing $\lambda_k = 1$ in (2.5) under $w^A = w^B = 0$, this quantity is easily computed, and we denote it by $\rho_1^{w=0}$ to specify no selection intervention.

2.2 Local approximation to fixation probability under weak selection

In Darwinian evolution theory, all species of organisms competing each other for the same limited resources survive and reproduce being favored by the natural selection if fitter, where how fitter is slightly differentiated from each other compared to the neutral drift. For this reason, the weak selection limit got a great attention, and this is where abundant analytical results were obtained. Fixation probability for a birth-and-death process has an exact formula for a 2×2 game, but its complexity drove many researchers to consider an approximation instead under weak selection. For a two-player-game in (1.1), one well-known local approximation to *the rate of evolution*, $N\rho_1$, which is multiplying the fixation probability by

the population size, was suggested in [40] in the form of the first order truncated Taylor expansion with the shared selection $w := w^A = w^B$ as follows:

$$N\rho_1^A \approx \frac{1}{1-(\alpha N-\beta)w/6}, \tag{2.12}$$

where $\alpha = a + 2b - c - 2d$ and $\beta = 2a + b + c - 4d$. We denote the rational function of w in the right hand side of (2.12) by Γ_N or by $\Gamma_N(w)$ to specifically the independent variable, w.

2.2.1 Equivalence of stochastic processes under weak selection

Using the local approximation in (2.12) or equivalently

$$\rho_1^A \approx \frac{1}{[1-(\alpha N-\beta)w/6]N} \tag{2.13}$$

under weak selection, the second condition of ESS_N in (2.11) for a finite population is sharpened, and the definition of ESS_N under weak selection in Section 2.1.2 is replaced by:

$$(i) b(N-1) < c + d(N-2), \tag{2.14}$$

$$(ii) \alpha N < \beta. \tag{2.15}$$

M. A. Nowak *et al.* in [40] linked the second condition to an unstable internal fixed point of a coordination game, which is defined with two constraints, $a > c$ and $b < d$. According to the replicator equations, this game has an internal equilibrium, $x^* := \frac{d-b}{a-b-c+d}$ such that the deterministic system is driven to the homogeneous state of all B's whenever the initial frequency of A is less than x^* whereas it is attracted by

$x = 1$ (all A's) if the initial proportion of A exceeds x^*. It is straightforward that for a large but finite N, the inequality (2.15) is equivalent to $a + 2b < c + 2d$, and this can be re-written in terms of x^* as

$$x^* > 1/3. \tag{2.16}$$

Surprisingly, this says that the A mutant is opposed replacing the resident population B by the natural selection if the frequency of A is higher than $1/3$ whereas favored otherwise. This is what is termed as a '$1/3$ *law*', and it is the key condition that is used to show the equivalence of any two stochastic processes.

The '$1/3$ law' for the Moran process was derived by M. A. Nowak *et al.* in [40] in 2004, and to this model the equivalence of the Wright-Fisher model in [25], of the local update process in [57], of the Fermi process in [58, 61], and of the generalized Moran process in [1] were shown in the sense that all of these processes hold the '$1/3$ law' under weak selection, where its derivation for the Moran process exploits the local approximation to fixation probability in (2.13). In fact, '$1/3$ law' was proven in [28] to be valid for any processes under weak selection as long as it is in the domain of Kingman's coalescence, and all the stochastic processes mentioned earlier belong to this set, thus being equivalent to each other. However, the violation of '$1/3$ law' was also discussed when the extra condition, $Nw >> 1$, is introduced in [57], and when the fixation probability is approximated by a Taylor expansion with a higher degree than 1 in [61].

We end this subsection by discussing the relationship between the tradition ESS for an infinite population and ESS_N for a finite population under the weak selection limit with two extreme cases of population size. For $N = 2$, the conditions, (2.14) and (2.15), for ESS_N reduce simply to $b < c$, and it implies that

ESS_N is a neither necessary nor sufficient condition for ESS, referring to (2.8) and (2.9). On the other hand, when N is finite but large, the conditions, (2.14) and (2.15), are re-written by

$$(i) b < d, \tag{2.17}$$

$$(ii) x^* < 1/3, \tag{2.18}$$

meaning that ESS_N is a sufficient but not necessary condition for ESS. In summary, ESS_N recovers the traditional ESS as N increases, and this is compatible with the fact that a stochastic process converges to the deterministic (adjusted) replicator equations in the increase of N.

2.2.2 Too limited validity of the local approximation

Despite of the height of its fame as a local approximation under weak selection, the approximation, Γ_N, in (2.12) to the rate of evolution, $N\rho_1$, in the form of the linear truncated Taylor expansion has its validity on an extraordinarily small subinterval of $[0, 1]$. In fact, it is limited from above and the upper threshold varies depending on the population size, N. This limited validity is due to the fact that for each N the local approximation, $\Gamma_N(w)$, is a rational function in selection, w, and this takes negative values on the majority part of the whole interval $[0, 1]$ of selection, being inappropriate to be used in approximating a positive function. Taking that the rate of evolution, $N\rho_1$, is a positive function and ranges 0 to N into account, an approximation is acceptable at least if it shares the same range, $[0, N]$. Forcing $0 \leq \Gamma_N \leq N$ gives rise to an upper threshold of w whenever $\alpha N - \beta > 0$:

$$w \leq \frac{6(N-1)}{(\alpha N - \beta)N}. \tag{2.19}$$

Denoting the right hand side of (2.19) by TRS_N, we note that the upper threshold, TRS_N, is order of $O(1/N^2)$ and it shrinks to 0 as N increase if $\alpha > 0$.

In order to see how ineffective the local approximation, Γ_N, is, we come back to a Prisoner's dilemma game defined for two players in (1.28) with the Prisoner's dilemma inequality in (1.29). First, we note that the strategy, D, is an evolutionarily stable strategy for both a finite and infinite population. Recalling (2.8) and (2.9), it is obvious that D is an evolutionary stable strategy for an infinite population since $P > S$. For a finite population modeled by the Moran process, it is straightforward to obtain (2.10), and we consider the factor, λ_k, of products in (2.6) for the second condition of ESS_N in (2.11). For the Moran process, we have $\lambda_k = f_k^D / f_k^C$, and in the strongest selection temperature for both A and B it is equivalent, for a PD game, to

$$\lambda_k = \frac{Tk + P(N-k-1)}{R(k-1) + S(N-k)}. \tag{2.20}$$

Using the PD inequality in (1.29), it is easy to check $\lambda_k > 1$ and it implies that $\rho_1^C < \frac{1}{N}$, meaning that a C mutant is opposed by selection replacing D and taking over the resident D populations. As a result, D is also an evolutionarily stable strategy for a finite population. Thus, it is hard to understand the emergence of cooperation if a PD game is played only one time. For this reason a repeated PD game for a finite/infinite number of times was studied extensively in the field of both classical and evolutionary game theory with the desire for the descriptive paradigm of the emergence of cooperation.

In a repeated PD game, players choose a strategy between C and D each round and a series of strategies during the set number of times establishes a strategy for this game. For example, *"Always cooperate (ALLC)"* is a strategy that a player cooperates all the time whereas *"Always defect (ALLD)"* is a strategy with which a player joins a game by defecting all the time. Obviously, a player with $ALLD$ outcompetes another with $ALLC$, receiving a higher payoff each round. In fact, $ALLD$ is a strict Nash equilibrium. Besides these, one strategy of direct reciprocity for a repeated PD game is what is known to be *Tit-For-Tat (TFT)*, with which a player cooperates at the first round and does whatever its opponent did in the previous round from the second round. In other words, a player with TFT is just as generous as the opponent is but never forgives once the opponent betrays. This strategy, TFT, was first invented by A. Rapoport and

won the iterated PD game tournament held by R. Axelrod in 1984 [3] though it was only the best among those of the participants. Later, the winner was replaced by a strategy taking a probability into account, called *Generous Tit-For-Tat (GTFT)*, and a player with $GTFT$ forgives with a positive probability and keeps cooperating even if an opponent defected in the previous round.

We consider an iterated PD game with the strategies, TFT and $ALLD$, during n rounds. Then the payoff matrix between TFT and $ALLD$ is as follows:

$$\begin{array}{c} \\ TFT \\ ALLD \end{array} \begin{array}{c} \begin{array}{cc} TFT & \quad ALLD \end{array} \\ \begin{pmatrix} nR & S+(n-1)P \\ T+(n-1)P & nP \end{pmatrix} \end{array}. \tag{2.21}$$

It is straightforward in an infinite population that $ALLD$ is an ESS in an infinite population since nP is always greater than $S+(n-1)P$ for all n since $S<P$. However, if $nR>T+(n-1)P$ is additionally assumed, or equivalently

$$n > \frac{T-P}{R-P}, \tag{2.22}$$

then TFT also becomes an ESS. The condition, (2.22), is established by forcing each TFT-individual to receive a higher expected payoff, nR, than the expected payoff, $T+(n-1)P$, that each $ALLD$-individual receives when TFT is abundant in a population. With this extra condition that requires a large enough number of repetition of a PD game, the invasion of infinitesimally small $ALLD$-subpopulation is opposed by selection to an infinitesimally large TFT-subpopulation. In this homogeneous state of all TFT's, all individuals cooperate and the ultimate piece is achieved since no one defects in a population, and this supports the emergence of cooperation in an infinite population.

We now turn our gear to a finite population under weak selection, particularly on $[0, 0.01]$. Unlike being an ESS in an infinite population, the strategy, $ALLD$, is no longer an ESS_N for almost every N under

weak selection. In order to specify the critical value of the population size over which the evolutionarily stability of B is not guaranteed under weak selection, we consider two conditions in (2.14) and (2.15). The condition in (2.14) is satisfied if $ALLD$ has a higher expected fitness than TFT when there is only one TFT mutant in a population, which can be written as $f_1^{TFT} < f_1^{ALLD}$. Assuming the shared selection strength, $w := w^{TFT} = w^{ALLD}$, for TFT and $ALLD$, it is then equivalent to show:

$$[S + (n-1)P](N-1) < T + (n-1)P + nP(N-2), \tag{2.23}$$

and this is rearranged to

$$(P - S)(N-2) + (T - S) > 0. \tag{2.24}$$

The Prisoner's dilemma inequality in (1.29) allows the inequality in (2.24) to hold for all $N \geq 2$. Hence, selection opposes a single TFT mutant invading the resident $ALLD$ population for all N. In fact, this invasion inability of a single A-individual to the B-populations holds regardless of selection strength as long as TFT and $ALLD$ share the same selection strength. On the other hand, the fixation condition in (2.14) is equivalent to

$$[nR + 2S - T - (n-1)P]N < 2nR + S + T - 2(n+1)P \tag{2.25}$$

under weak selection. With the choice of parameters, $T = 5$, $R = 3$, $P = 1$, $S = 0$ and $n = 10$, (2.25) leads to $N < 43/14$. Selection favors a single TFT mutant taking over the entire population for all N but $N = 2$ and $N = 3$. Thus the strategy, $ALLD$, is not an ESS_N if $N \geq 4$ under weak selection, and this is the new scenario that the deterministic system does not result.

Recall that the fixation condition in (2.14) of ESS_N is obtained from adopting the local approximation, Γ_N, in (2.12) to the rate of evolution, $N\rho_1^A$, under weak selection. For the numerical purpose, we plot the

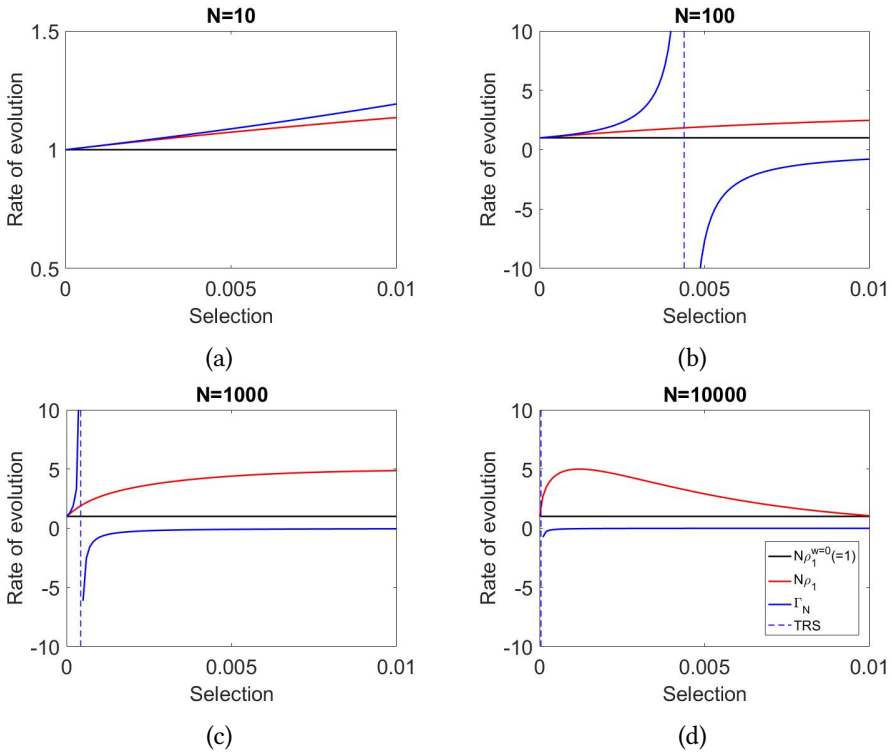

Figure 2.1: The local approximation, Γ_N, in (2.12) to the rate of evolution, $N\rho_1$, of a single TFT mutant under weak selection has limited validity with the upper threshold of selection strength, TRS, which is order of $O(N)$ for the repeated Prisoner's dilemma game between TFT and $ALLD$. (Parameters $T = 5$, $R = 3$, $P = 1$, $S = 0$ and $n = 10$ in all panels) (a) $N = 10$, $TRS = 0.05567010$; (b) $N = 10^2$, $TRS = 0.00437730$; (c) $N = 10^3$, $TRS = 0.00042946$; (d) $N = 10^4$, $TRS = 0.00004287$

exact value, $N\rho_1^{TFT}(= N\rho_1)$, in red line together with its approximation, Γ_N, in blue line for the repeated Prisoner's dilemma game under weak selection, precisely on $[0, 0.01]$, for $N = 10, 10^2, 10^3, 10^4$ with the choice of $T = 5$, $R = 3$, $P = 1$, $S = 0$ and $n = 10$ (Fig.2.1). Comparing to the rate of evolution, $N\rho_1^{w=0}(= 1)$ (black solid line), in the random drift case, $N\rho_1$ in Fig.2.1 shows that the fixation of TFT is favored by selection under all weak selection on $[0, 0.01]$ for all $N = 10, 10^2, 10^3, 10^4$ though how fast a TFT mutant takes the entire population depends on the total population size, N. However, more importantly, the well-known approximation, Γ_N, that performs well on $[0, 0.01]$ for an extraordinarily small population size such as $N = 10$ becomes an invalid estimate on an increasing subinterval of $[0, 0.01]$ as N increases since Γ_N approximates $N\rho_1$ by a negative number once w passes the vertical asymptote. The exact upper threshold, TRS_N (blue dashed line), of weak selection below which the use of Γ_N is

acceptable was computed for each N in (2.19) and is also added to Figure 2.1. It is clearly shown that TRS_N shifts towards 0 as N increases, making Γ_N work on a too tight window on which the regular linear Taylor expansion performs even better.

2.3 Bernstein approximation: global approximation to fixation probability

As seen in the previous section, the local approximation, Γ_N, to the rate of evolution, $N\rho_1$, is often used under weak selection though it has limited validity, particularly for a large N. However, unlike the one in [56] for the Fermi process using the fact that its fitness function is designed to cover any nonnegative selection strength, none of global approximations on $[0, 1]$ for the Moran process has been discussed so far. We suggest one global approximation by using the Bernstein polynomial that was originally constructed by S. Bernstein in [4] in 1912 and used to prove Weierstrass approximation theorem, which states that a continuous function on a closed interval can be uniformly approximated by a series of polynomials.

Given a function, $f(x)$, defined on the closed interval, $[0, 1]$, *the Bernstein polynomial of degree d of the function $f(x)$* is defined by:

$$\sum_{k=0}^{d} f(\frac{k}{d})\binom{d}{k}x^k(1-x)^{d-k}. \tag{2.26}$$

Denoting (2.26) by $B_d(f)$, it is proven that if f is continuous on $[0, 1]$, then $B_d(f)$ converges uniformly to f on $[0, 1]$ as $d \to \infty$ with an error bound:

$$\mid f(x) - B_d^f(x) \mid \leq (1 + \frac{1}{4}d^{-2})\omega(f; d^{-1/2}), \tag{2.27}$$

where the modulus, $\omega(f, d^{-1/2})$, of continuity of f is defined by

$$\omega(f, d^{-1/2}) = \sup_{x,y\in[0,1],|x-y|<\delta} \{\mid f(x) - f(y) \mid\}. \tag{2.28}$$

Expanding the formula in (2.26), it is easy to check that $B_d(f)$, which is a linear combination of polynomials of degree at most d, is the weighted average of functions $x, x^2, \cdots, x^d$. From its construction, obtaining the global approximation, $B_d(f)$, precisely requires to know $d+1$ many function values at selection values, $w = \frac{k}{d}$, $k = 0, 1, \cdots, d$, that equally partition the interval, $[0,1]$, into d subintervals whereas getting the local approximation, Γ_N, is based on the stronger differentiability condition of $N\rho_1$ but at only one location $w = 0$.

For a finite population of individuals playing a two-player game defined in (1.1), we denote by r_i the rate of evolution, $N\rho_i$, for $i = 1, \cdots, N-1$. Then this approximation object, $N\rho_i$, can be globally approximated on $[0,1]$ by the Bernstein polynomials in (2.26) as follow:

$$B_d(r_i; w) := \sum_{k=0}^{d} r_i(\frac{k}{d}) \binom{d}{k} w^k (1-w)^{d-k}. \tag{2.29}$$

Furthermore, if the finite population is modeled by the Moran process, then it presumes that all entries of a payoff matrix are positive since it otherwise brings in a negative transition probability. This positiveness guarantees that the fitness functions in (1.11) for the Moran process are continuous on $[0,1]$, and so is ρ_i in (2.7). This completes the continuity of r_i, and we have that for each i, $B_d(r_i)$ uniformly converges to r_i as $d \to \infty$.

We visit again the repeated Prisoner's dilemma game between TFT and $ALLD$, defined in (2.21), where this game is repeated more than $\frac{T-P}{R-P}$ times to guarantee that selection opposes invasion of $ALLD$ into a homogeneous TFT-population, having the emergence of cooperation in mind. In order to model a finite population playing this game by the Moran process, it is necessary to assume that all entries of

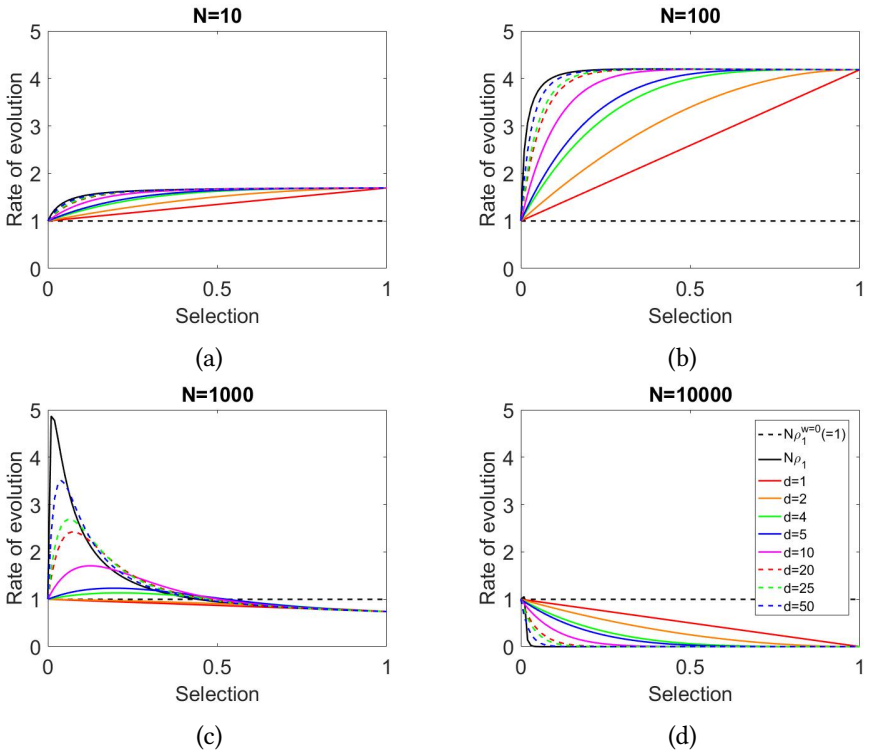

Figure 2.2: The Bernstein polynomials, $B_d(r_1)$, of degree, d, approximates the rate of evolution, $r_1 := N\rho_1$, in (2.12) in the whole region of selection strength, being more accurate with the increase of d. For simulation, we choose parameters, $T = 5$, $R = 3$, $P = 1$, $S = 0$ and $n = 10$, in all panels for the repeated Prisoner's dilemma game between TFT and $ALLD$. (a)$N = 10$. Both r_1 and $B_d(r_1)$ are increasing function on $[0, 1]$ being greater than the rate of evolution, $r_1^{w=0} := N\rho_1^{w=0}$, under the neutral drift. Selection favors TFT replacing $ALLD$ for all selection strength; (b) $N = 10^2$. The same interpretation as for $N = 10$ is made but with a higher rate of evolution; (c) $N = 10^3$. Selection favors TFT replacing $ALLD$ for weak selection while it does not for strong selection according to either the exact or approximate functions with $d > 1$; (d) $N = 10^4$. Selection opposes TFT replacing $ALLD$ for all selection strength according to the approximation $B_d(r_1)$ for all d, however, it does not if selection is extraordinarily weak according to the exact function.

(2.21) are positive to allow the whole range of selection for this selection dynamics. Using the Prisoner's dilemma inequality in (1.29), it is equivalent to

$$\begin{aligned} P > 0, \\ S + (n-1)P > 0. \end{aligned} \tag{2.30}$$

With the choice, $T = 5$, $R = 3$, $P = 1$, $S = 0$ and $n = 10$, the inequalities in (2.30) are satisfied and the uniform convergence of the Bernstein polynomial, $B_d(r_i)$, to the rate of evolution of a single TFT-mutant is implied for this repeated Prisoner's dilemma game. With this selection of parameters, we plot the Bernstein approximation, $B_d(r_1)$, with a set of degrees, $d = 1, 2, 4, 5, 10, 20, 25, 50$, for each $N = 10, 10^2, 10^3, 10^4$ along with both the exact function of $N\rho_1$ in black solid line and the rate of evolution, $N\rho_1^{w=0}(= 1)$, under the neutral drift in black dashed line (Fig.2.2). For each N, it is clearly seen that $B_d(r_1)$ generally better approximates r_1 as d increases and it is also supported by the reduced error, $|B_d(r_i) - r_i|$ (Fig.2.3). When $N = 10^4$, $N\rho_1$ is nearly equal to 0 on the majority of selection except for weak selection on which it slightly increases near $w = 0$ and is followed by a sudden drop to almost 0. On the other hand, all the Bernstein polynomials, $\{B_d(r_1)\}_d$, take the value, 1, at $w = 0$ and they monotonically decrease to 0 as w increases though the higher d, the faster decrease. These approximations lead us to interpret that a single TFT-mutant is opposed by selection replacing the $ALLD$-mutants regardless of selection intensity whereas it is implied by the exact function, $N\rho_1$, that selection opposes the fixation of TFT on $[0, 1]$ but on an extraordinarily small weak selection window.

This interpretation is compatible with the fact that the deterministic adjusted replicator system has a bistability for this game so that the system is driven to all $ALLD$'s if the initial frequency of TFT does not exceeds a critical proportion. Precisely, assuming the same nonzero selection intensity for TFT and $ALLD$, the deterministic system is driven to TFT as long as $f^{TFT} > f^{ALLD}$, where $f^{TFT} - f^{ALLD}$ for this game is given by

$$\begin{aligned} f^{TFT} - f^{ALLD} &= [nRx + (S + (n-1)P)(1-x)] - [(T + (n-1)P)x + nP(1-x)] \\ &= [(n(R-P) - (T-P)) + (P-S)]x - (P-S) \end{aligned} \tag{2.31}$$

with $x := x^{TFT}$ denoting the frequency of TFT in an infinite population. Using the Prisoner's dilemma inequality and the assumption on the number of iteration in (2.22), both $(n(R-P)-(T-P))+(P-S)$ and $P-S$ are positive, and we have $f^{TFT} > f^{ALLD}$ if and only if

$$x > \frac{P-S}{n(R-P)-(T-P))+(P-S)} =: \hat{x} \tag{2.32}$$

and we denote the internal equilibrium by $\hat{x}$. Our choice of parameters gives rise to $\hat{x} = \frac{1}{17}$. The initial state, $i = 1$, in a finite populations with $N = 10^4$ corresponds to the state, $x_0 = 10^{-4}$, in an infinite population. The initial state, x_0, is definitely less than $\hat{x}$, and it leads the deterministic system to all $ALLD$'s by (2.32). Noting that the adjusted replicator equation is the asymptotic system of the Moran process in the large population size limit, it implies that for a finite but large population selection is not likely to favor a single TFT-mutant taking over the entire population if the initial proportion of TFT is less than the critical value, $\hat{x} = 1/17$. This is what is shown in Figure.2.2d. Every Bernstein approximation, $B_d(r_1)$, of any degree is strictly less than $N\rho_1^{w=0}(=1)$ for all $w \neq 0$, meaning that selection opposes the fixation of TFT. However, things interesting take place with the exact function, $N\rho_1$, on an absolutely tiny interval including $w = 0$. On that extremely small window, selection slightly favors TFT replacing $ALLD$, and this is a new feature that is driven by stochasticity from the finite population size and was not captured by the deterministic system.

This new feature continues on a wider weak selection interval as N decreases due to the stronger stochasticity. When $N = 10^3$, r_1 is greater than 1 on weak selection, $[0, 0.43)$, whereas it is less than 1 on strong selection, $(0.43, 1]$. Thus, the fixation of TFT is reached with the extended weak selection intensity with this smaller population size, $N = 10^3$, compared to that with $N = 10^4$ (Fig.2.2c). This can be similarly translated by $B_d(r_1)$ as long as $d > 2$ so that $B_d(r_1)$ crosses the horizontal line of $N\rho_1(=1)$, with the more accurate interpretation for a higher d. Eventually, when N becomes as small as $N = 10$ or

$N = 10^2$, we observe that selection favors the saturation of TFT, though the rate is higher with $N = 10^2$, according to either r_1 and $B_d(r_1)$.

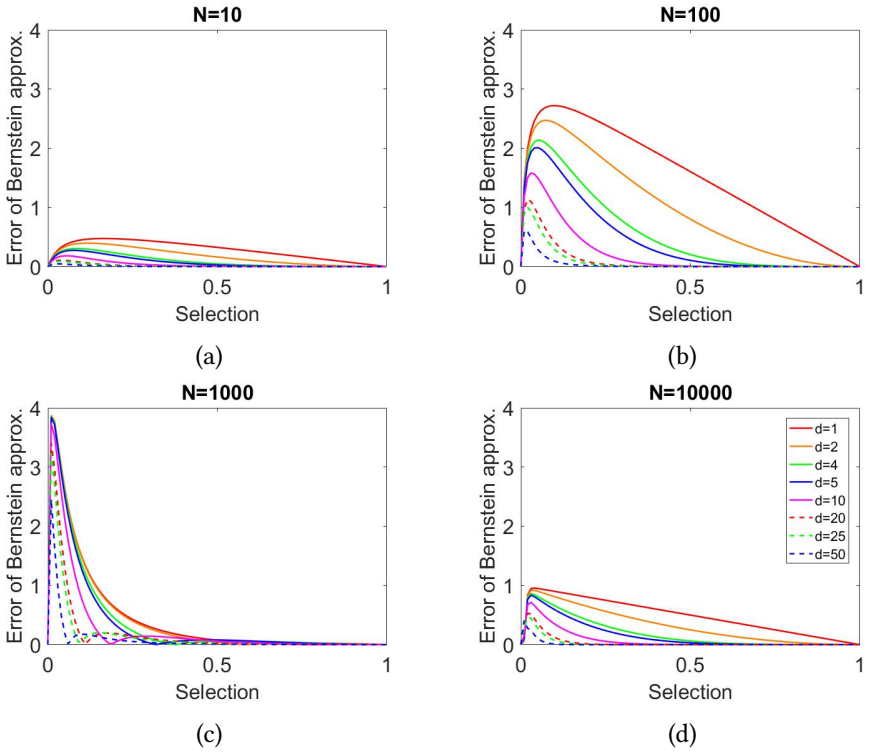

Figure 2.3: The error, produced by the Bernstein polynomial, $B_d(r_1)$, in approximating the rate of evolution, $r_1 = N\rho_1$, is reduced as much as desired by increasing the degree, d, for each N although a relatively higher degree is required for an intermediate value of N. Despite of its universality as a global approximation on $[0, 1]$, it does not behave well particularly under weak selection, producing a relatively high error. (Parameters $T = 5$, $R = 3$, $P = 1$, $S = 0$ and $n = 10$ in all panels) (a)$N = 10$; (b) $N = 10^2$; (c) $N = 10^3$; (d) $N = 10^4$

In summary, the Bernstein polynomial, $B_d(r_1)$, plays the role of a global approximation to the rate of evolution, $r_1 = N\rho_1$, on $[0, 1]$. Its performance improves as d increase for each N so that the error can be reduced as much as desired, and the major refinement is achieved for strong selection. However, the weakness of this approximation is on weak selection, especially near $w = 0$, where it produces a relatively bigger error compared to that on strong selection intensity. Despite of this bigger error near $w = 0$, this error is overall smaller for either a small or a large population size, as shown in Figure 2.2a and Figure 2.2d. On the other hand, the error remains big near $w = 0$ even with a higher degree for an intermediate value of N, particularly for N at which selection dynamic for fixation changes at some mild selection strength in

$(0, 1)$ as shown in Figure 2.2c. In fact, the numerical simulation for the repeated Prisoner's dilemma game with the same choice of parameters results that the regular linear Taylor expansion outperforms both the Bernstein approximation, $B_d(r_1)$, and the local approximation, Γ_N, on the weak selection window over which Γ_N is valid with the constraint in (2.19).

Chapter 3

Stochastic single drug chemotherapy model

For our stochastic single drug chemotherapy model for a finite population with health, sensitive and resistant cells by the Moran process, we specify the payoff matrix, A, in (1.25) satisfying (1.34)-(1.38) as follows:

$$A = \begin{array}{c} \\ H \\ S \\ R \end{array} \begin{array}{c} \begin{array}{ccc} H & S & R \end{array} \\ \begin{pmatrix} 3 & 1.5 & 1.5 \\ 4 & 2 & 2.8 \\ 3.9 & 1 & 2.2 \end{pmatrix} \end{array} \tag{3.1}$$

Each state, (i, j), of the Moran process represents a population with i healthy cells, $N - i - j$ sensitive cells and j resistant cells, and it is assigned to a lattice point in a phase space that is $2-$simplex, S_2. Each vertex of the phase space represents a homogeneous population and is denoted by its type, and at a point in each side of S_2 the population consists of only two types of subpopulations. $i-$numbering goes next to the side, $\overline{HS}$, and $j-$numbering lies on the bottom of the side, $\overline{SR}$ (Fig.3.1).

For example, When $N = 10$, there are 66 distinct states, and 30 of them consist of less than three distinct subpopulations and they are assigned to boundary points (black dots in Fig.3.1) in S_2. The remaining states correspond to the population with no vanishing subpopulations and they are mapped to interior points (red dots in Fig.3.1).

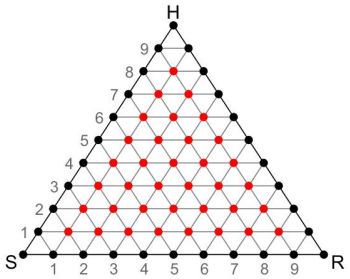

Figure 3.1: The space set, Λ_N, of the Moran process with H, S and R is indicated as dots in the phase space, S_2, when $N = 10$. Each state, $(H, S, R) = (i, N - i - j, j)$, is assigned to a lattice point in S_2, where i-numbering goes next to the side, $\overline{HS}$, and j-numbering lies on the bottom of the side, $\overline{SR}$.

The space set, Λ_N, defined in (1.24), has exactly $\frac{(N+1)(N+2)}{2}$ elements, and more precisely this set is a disjoint union of a set of $\frac{(N-2)(N-1)}{2}$ interior points and a set of $3N$ boundary points. The number of interior points is order of $O(N^2)$ whereas the number of boundary points is order of $O(N)$. The points gradually expand as N increases and the state space of an infinite population, which we denote by Λ_∞, eventually fills in the whole $2-$simplex, S_2 (Fig.3.2). Letting x_H and x_R the frequencies of healthy cells and resistant cells, a state, $(H, S, R) = (x_H, 1 - x_H - x_R, x_R) \in \Lambda_\infty$ of the deterministic system is assigned to the point in S_2 that is distant away from $\overline{SR}$ by x_H and from $\overline{SH}$ by x_R.

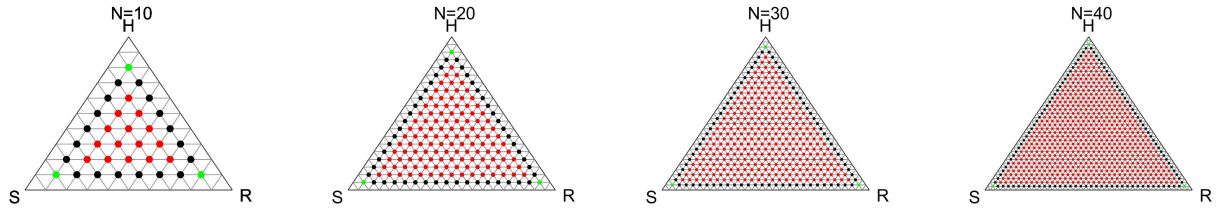

(a) (b) (c) (d)

Figure 3.2: The space set, Λ_N, of the Moran process with H, S and R gets denser in the phase space, S_2, with the increase of the population size, N. For each N, $|\Lambda_N|$ is order of $O(N^2)$, being equal to $\frac{(N+1)(N+2)}{2}$. (a) $N = 10$, $|\Lambda_N| = 66$; (b) $N = 20$, $|\Lambda_N| = 231$; (c) $N = 30$, $|\Lambda_N| = 496$; (d) $N = 40$, $|\Lambda_N| = 861$

Since the Moran process is a discrete-time and finite-space Markov chain that each type of subpopulations changes its size by at most 1 in one time step, a state, (i, j), only moves to one of its neighboring 6 lattice points in a phase space or stays remained, each with a certain probability. This microscopic probabilistic movement defines the Moran process with three strategies to be a random walk in Λ_N, not in $\mathbb{R}^2$.

Define $T_{i,j}^{XY}$ to be the transition probability at (i,j) that the number of X subpopulations increases by 1 whereas the number of Y subpopulations decreases by 1, where $X, Y \in \{H, S, R\}$. For example, recalling that a state is determined by the number of H and R subpopulations, $T_{i,j}^{HS}$ is the transition probability that the state, (i,j), moves to $(i+1,j)$ in one time step. Let $T_{i,j}^{cons}$ be the probability that the system at the state, (i,j), stays remained in one time step. Then all, not necessarily zero, 7 transition probabilities are given by:

$$
\begin{aligned}
T_{i,j}^{HR} &= \frac{if_{i,j}^{H}}{N_{i,j}^{w}} \cdot \frac{j}{N}, \\
T_{i,j}^{HS} &= \frac{if_{i,j}^{H}}{N_{i,j}^{w}} \cdot \frac{N-i-j}{N}, \\
T_{i,j}^{RH} &= \frac{jf_{i,j}^{R}}{N_{i,j}^{w}} \cdot \frac{i}{N}, \\
T_{i,j}^{RS} &= \frac{jf_{i,j}^{R}}{N_{i,j}^{w}} \cdot \frac{(N-i-j)}{N}, \\
T_{i,j}^{SH} &= \frac{(N-i-j)f_{i,j}^{S}}{N_{i,j}^{w}} \cdot \frac{i}{N}, \\
T_{i,j}^{SR} &= \frac{(N-i-j)f_{i,j}^{S}}{N_{i,j}^{w}} \cdot \frac{j}{N}, \\
T_{i,j}^{cons} &= 1 - (T_{i,j}^{HR} + \cdots + T_{i,j}^{SR}),
\end{aligned}
\tag{3.2}
$$

where the weighted population size, $N_{i,j}^{w}$, is defined by $N_{i,j}^{w} = if_{i,j}^{H} + (N-i-j)f_{i,j}^{S} + jf_{i,j}^{R}$ and the expected fitness functions, $f_{i,j}^{X}$, are defined by the equation in (1.27) with the time-dependent selection functions in (1.33). Then the Moran process with H, S and R eventually evolves according to an initial state and these transition probabilities in (3.2).

Together with the stochastic Moran process, we also consider the deterministic adjusted replicator equations for an infinite population playing the same game in (3.1) since this is the asymptotic system of the Moran process in the large population size limit and hence we may have an intuition for the dynamics

driven by the Moran process for a finite populations with a large population size. The adjusted replicator dynamic is governed by the following equations:

$$\begin{aligned} \dot{x_H} &= \frac{f^H - < f >}{< f >} x_H, \\ \dot{x_S} &= \frac{f^S - < f >}{< f >} x_S, \\ \dot{x_R} &= \frac{f^R - < f >}{< f >} x_R, \end{aligned} \tag{3.3}$$

where the expected fitness functions at $\vec{x} := (x_H, x_S, x_R)^\intercal$ are given, with the time-dependent selections functions in (1.33), by:

$$\begin{aligned} f^H &= 1 - w^H + w^H (A\vec{x})_1, \\ f^S &= 1 - w^S + w^S (A\vec{x})_2, \\ f^R &= 1 - w^R + w^R (A\vec{x})_3. \end{aligned} \tag{3.4}$$

It is analytically proven that when a constant chemo dose is administered over time, the system has asymptotically stable states: $(x_H, x_S, x_R) = (0, 1, 0)$ whenever $C(t) < \frac{1}{3}$ and $(x_H, x_S, x_R) = (0, 0, 1)$ whenever $C(t) > \frac{1}{2}$. The sensitive populations dominate the total population for constant low dose chemotherapy whereas the system is led to the all resistant populations for constant high dose chemotherapy regardless of an initial distribution. A low chemo dose acts as a main tool to remove the competing agents, resistant cells, helping sensitive cells proliferate in a population by making the environment beneficial for them. Similarly, a high chemo dose allows resistant cells to win in a competition with sensitive cells and eventually take over the whole population. That is, the chemo dose plays the role of controller of the deterministic system, causing the competitive release between sensitive cells and resistant cells.

For an intermediate value of $C(t)$, the system has bistability to cancerous states, and the initial state determines its fate to either S or R. In other words, the proportion of area of states in a phase space

eventually converging to the all S state is equal to 1 for $C < \frac{1}{3}$, and it starts gradually decreasing in the increase of $C(t)$ and finally reaches 0 for $C > \frac{1}{2}$. The proportion of area of states in a phase space being attracted to the all R state is exactly the reverse increasing on $[0, 1]$. Moreover, the adjusted replicator system has an internal fixed point

$$\left(\frac{3(48C+47)}{2(32C+13)} - \frac{7}{2}, \frac{48C+47}{4(32+13)}, \frac{9}{2} - \frac{7(48C+47)}{4(32C+13)}\right) \tag{3.5}$$

for $\frac{19}{48} < C < 0.625$, and the system spirals out from this internal fixed point.

3.1 Fixation probability for the Moran process with three strategies

In this section, we want to examine how the stochasticity driven by the finiteness of population size distorts the adjusted replicator dynamics in terms of fixation probability. In other words, the question is to study at what probability the Moran process with three strategies leads the finite population to be fixated at the all sensitive populations when it stats at (i, j), and similarly to the all resistant populations. To this end, we denote by $\pi_{i,j}^X$ the fixation probability to $X \in \{H, S, R\}$ at the state (i, j). We will drop X in $\pi_{i,j}^X$ when the specification of type is not needed. At a boundary state, a population has at most two different types of cells and the revival of the eliminated type never happens since no mutation is assumed in our model. Thus, the further evolution since the arrival at a boundary state is then described by the Moran process with two strategies, for which the fixation probability is ready to be used in (2.6). Thus the question reduces to finding the fixation probability only at interior states, for instance, at all colored dots in Figure 3.2.

At an interior point, $(i,j) \in int(\Lambda_N) := \{(i,j) | 1 \leq i \leq N-2, 1 \leq j \leq N-2, i+j \leq N-1\}$, we have a following recursion in terms of the fixation probability, $\pi_{i,j}$, and transition probabilities in (3.2):

$$\begin{aligned}(1 - T^{cons}_{i,j})\pi_{i,j} =& T^{HR}_{i,j}\pi_{i+1,j-1} + T^{RH}_{i,j}\pi_{i-1,j-1} + T^{HS}_{i,j}\pi_{i+1,j} \\ &+ T^{SH}_{i,j}\pi_{i-1,j} + T^{SR}_{i,j}\pi_{i,j-1} + T^{RS}_{i,j}\pi_{i,j+1}.\end{aligned} \tag{3.6}$$

Using the lexicographic order, $r(i,j)$,

$$\begin{gathered}(1,1),(1,2),\cdots,(1,N-2), \\ (2,1),(2,2),\cdots,(2,N-3), \\ \cdots, \\ (N-3,1),(N-3,2), \\ (N-2,1),\end{gathered} \tag{3.7}$$

we assign to each state, $(i,j) \in int(\Lambda_N)$, the order:

$$r(i,j) = \frac{(i-1)(2N-2-i)}{2} + j. \tag{3.8}$$

Equating $\pi_{i,j}$ to $\pi(r(i,j))$, the recursion in (3.6) is re-written in a matrix form:

$$EX = F, \tag{3.9}$$

where E is a $\frac{(N-1)(N-2)}{2} \times \frac{(N-1)(N-2)}{2}$ square matrix and

$$X = [\pi(r(1,1)), \pi(r(1,2)), \cdots, \pi(r(N-2,1)]^T \tag{3.10}$$

is a $\frac{(N-1)(N-2)}{2} \times 1$ column vector. Note that all elements of X are the fixation probabilities, $\pi_{i,j}$'s, at $(i,j) \in int(\Lambda_N)$, listed using the order $r(i,j)$ in (3.8), and the elements in the $r(i,j)^{th}$ row of E are precisely determined by the transition probabilities to either its surrounding six states such as $(i \pm 1, j)$, $(i, j \pm 1)$, $(i \pm 1, j \mp 1)$ or the same state, (i,j). The entries of F are completely determined by the fixation probabilities at the boundary states. By solving the linear system $EX = F$ in (3.9), we may compute the fixation probability on $int(\Lambda_N)$. The proof and the detailed explanation for the idea of getting the fixation probability for the Moran process with three strategies can be found in [15]. We do not go over it but we will numerically study the stochastic effect of a finite population on asymptotic dynamics using this findings.

In order to see a local effect, we fix a state with the proportion, $(H,S,R) = (0.8, 0.1, 0.1)$, where healthy cells are abundant in a total population. At this state, we numerically compute the fixation probabilities to H, S or R when chemotherapy is administered at a constant dose in $[0,1]$ (Fig.3.3). Unlike what is analytically shown that the adjusted replicator dynamics has two attracting state, S or R, depending on the constant drug concentration, the Moran process evolves and may eventually reach any one of homogeneous states, H, S, R, with a nonzero probability for any value of $C(t)$, particularly for a small N.

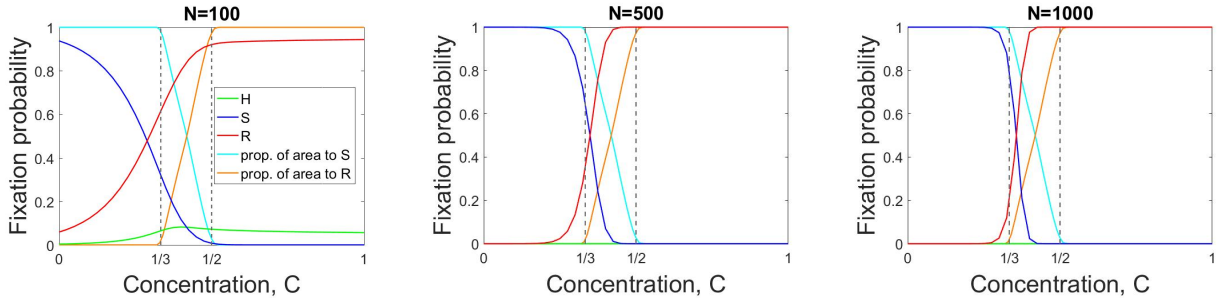

Figure 3.3: Local fixation probability for the Moran process at the state, $(H,S,R) = (0.8, 0.1, 0.1)$, approaches the proportion of area for the basin of attraction by the adjusted replicator dynamics as the population size, N, increases although unexpected features such as fixation to H are observed for a small N. (a) $N = 100$; (b) $N = 500$; (c) $N = 1000$

The stochasticity introduced to a finite population by its size allows the stochastic system to have nonzero fixation probability to H as well as to either S or R. For example, in Figure 3.3a, the fixation probability to H (green line) at the state, $(0.8, 0.1, 0.1)$, for $N = 100$ is overall 10% beating the fixation probability to S (blue line) for some $1/3 < C < 1/2$, with which the adjusted replicator dynamic is asymptotically driven to either all sensitive state or all resistant state depending on the drug intensity. However, for a fixed such C, this fixation probability to H at this state tends to decrease as N increase and the fixation to H seems almost impossible when N reaches 500. That is, this new scenario, that is not expected by the adjusted replicator dynamic, such as the absorption of the system to H is captured with a small N, but it disappears shortly with the increase of N. Also, on $[1, 1/3]$, the fixation probability to R (red line) is nonzero and increases, eventually reaching nearly 0.5 around $C = \frac{1}{3}$ for $N = 100$. However, the adjusted replicator system converges to the all sensitive states for $C < \frac{1}{3}$ regardless of the initial distribution, and the area of the basin of attraction to R is in fact equal to zero (orange). Similarly, with the increase of N, the fixation probability to R decreases to zero for each C on $[0, \frac{1}{3}]$, and it numerically supports the convergence of the Moran process to the adjusted replicator system again. For comparison, the proportion of areas on which attraction to either S or R is reached by the adjusted replicator system is presented along with the fixation probabilities in each panel of Figure 3.3.

All of these is literally the universal property throughout all states in a population though the fixation probability was examined at one state with the proportion, $(0.8, 0.1, 0.1)$. We will now focus on the global fixation probability by fixing some values of C's instead: $C(t) \equiv 0.29, 0.37, 0.45, 0.53$. For a while, we point out numerical constraint on the size of a population for the computation of global fixation probabilities. In order to numerically compute the fixation probability at all states requires to solve the linear system in (3.9), where the coefficient matrix, E, has the size, $\frac{(N-1)(N-2)}{2} \times \frac{(N-1)(N-2)}{2}$.

However, the matrix, E, is sparse of which each row has at most 7 nonzero elements since the Moran process with three strategies is able to change its current state, (i, j), to one of 6 nearby states, $(\pm i, j)$,

$(i, \pm j)$, $(\pm i, \mp j)$, or to stay unchanged at (i, j) in one time step. In fact, the $r(i, j)$th row of E, where (i, j) corresponds to a red dot in Figure 3.2, has exactly 7 nonzero elements, the row corresponding to a black dot has 5 nonzero elements, and the row corresponding to a green dot has 3 nonzero elements. This sparsity helps to reduce the question to solving the linear equation in terms of the sparse matrix of E, where the number of elements of the sparse matrix, E, is order of $O(N^2)$ while it is order of $O(N^4)$ for the full matrix, E. For a numerical solution, we use an iterative method, the least squared method (*lsqr*), with the error tolerance, 10^{-6}. This setting allows us to obtain the global fixation probability for N up to $2,000$ in a reasonable computation time. The computation time dramatically increases in N and it successfully computed the numerical global fixation probability for $N = 2,000$ within a day, but it fails during a week for $N = 2,500$.

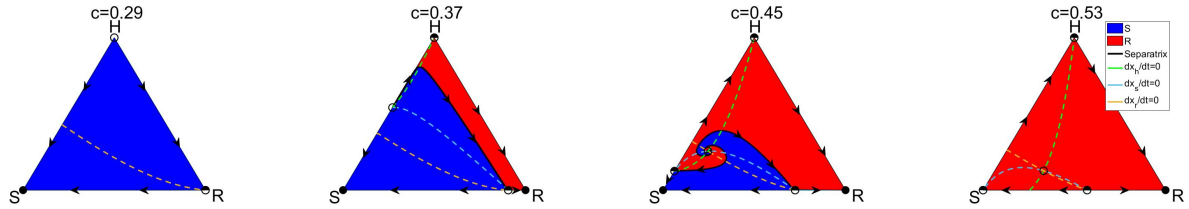

(a) (b) (c) (d)

Figure 3.4: The basins of attraction by the adjusted replicator dynamics with constant chemo concentration, $C := C(t)$, shows the smooth transition from the global attraction by S to the global absorption to R with the increase of C, describing the competitive release of resistant subpopulations with high chemotherapy concentration. The system experiences bistability to S or R for an intermediate value of C. (a) $C \equiv 0.29$; (b) $C \equiv 0.37$; (c) $C \equiv 0.45$; (d) $C \equiv 0.53$

For the purpose of comparison with the Moran process, we investigate the basin of attraction by the adjusted replicator dynamics with $C = 0.29, 0.37, 0.45, 0.53$ with which the different key dynamics are shown (Fig.3.4). The basin of attraction to S and R are respectively depicted in blue and red regions. The asymptotically dominant subpopulation of type S with $C \equiv 0.29$ starts reducing its attraction region with the increase of C. The basin of attraction to R with $C \equiv 0.37$ gradually expands its region from states with fewer sensitive cells in a population towards the all sensitive state with $C \equiv 0.53$. We indicate the separatrix in a black solid line for each C. Meanwhile, the deterministic system has an internal fixed point

with the proportion, $(0.2555, 0.6259, 0.1186)$, with $C \equiv 0.45$ from which the system spirals out. In fact, this internal fixed points exists for all C such that $\frac{19}{28} < C < 0.625$.

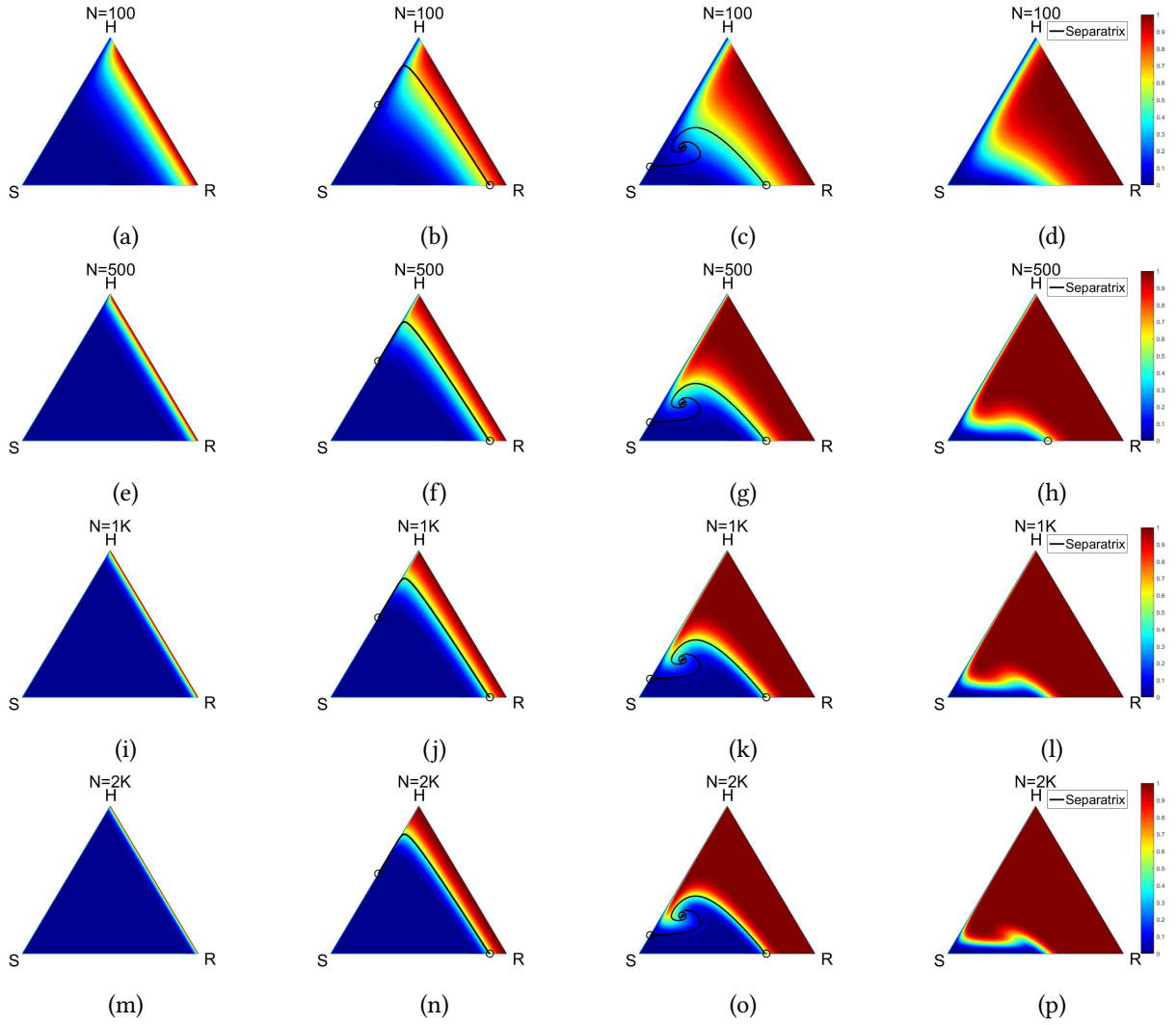

Figure 3.5: Fixation probability to R for the Moran process with constant chemotherapy concentrations, $C := C(t)$, shows the stochastic version of the competitive release of the resistant cells with high concentration for each population size, N. For a fixed C, each region in a phase space with either a high or a low probability respectively approaches the basin of attraction to either R or S by the adjusted replicator system as N increases. (a) $C \equiv 0.29$, $N = 100$; (b) $C \equiv 0.37$, $N = 100$; (c) $C \equiv 0.45$, $N = 100$; (d) $C \equiv 0.53$, $N = 100$; (e) $C \equiv 0.29$, $N = 500$; (f) $C \equiv 0.37$, $N = 500$; (g) $C \equiv 0.45$, $N = 500$; (h) $C \equiv 0.53$, $N = 500$; (i) $C \equiv 0.29$, $N = 1000$; (j) $C \equiv 0.37$, $N = 1000$; (k) $C \equiv 0.45$, $N = 1000$; (l) $C \equiv 0.53$, $N = 1000$; (m) $C \equiv 0.29$, $N = 2000$; (n) $C \equiv 0.37$, $N = 2000$; (o) $C \equiv 0.45$, $N = 2000$; (p) $C \equiv 0.53$, $N = 2000$

In Figure 3.5, the fixation probability to R at every state is described in a way that blue indicates the fixation to R never happens whereas red indicates that the fixation surely occurs. With $C \equiv 0.29$, the

Moran process has no chance to reach the fixation to R at the majority of states, but the system at states where sensitive cells are rare in a population evolves and the resistant cells finally dominate the entire population with a high probability for a small population size $N = 100$ (Fig.3.5a). As expected, the region of positive fixation probability to R gradually shrinks as N increases to $N = 2,000$ (Fig.3.5a,3.5e, 3.5i, 3.5m). When $C \equiv 0.37$, the area of states in which the fixation probability to R is reached with a high probability is near the side, $\overline{HR}$, where there are relatively a small number of sensitive cells in a population. This region is included in the basin of attraction to R of the adjusted replicator dynamics, colored in red in Figure 3.4b, for each N. It expands towards the separatrix, and the area with non zero fixation probability to R gets sharper and sharper around the separatrix in the increase of N (Fig.3.5b, 3.5f, 3.5j, 3.5n). When $C \equiv 0.45$, as the adjusted replicator system has an internal fixed point from which the system spirals out, the Moran process also shows that the high and low probability of the fixation to R is obtained in each side of the basin boundary, and the region of the neutral fixation probability gets narrower around the basin boundary as N increase (Fig.3.5c, 3.5g, 3.5k, 3.5o). With $C \equiv 0.53$, the almost sure fixation to R in the total phase space is hardly met even when a population size is as big as $N = 2000$, however, the region where the fixation is certainly attained gets enlarged towards the state, S, in the increase of N (Fig.3.5d, 3.5h, 3.5l, 3.5p).

The fixation probability to R for the Moran process overall shows the asymptotically similar patterns to the basins of attraction to R by the adjusted replicator dynamics for a large N for each $C(t) \equiv 0.29, 0.37, 0.45, 0.53$. Thus it is rarely reached at a state outside the basin boundary though it is still possible at a low probability depending on the mixture of the subpopulations. However, when the population size is small so that the stochasticity is strong, somewhat different dynamic from the deterministic system is seen mainly around the basin boundary with $C \equiv 0.37, 0.45$.

3.2 Single drug adaptive control

Setting the chemotherapy concentration, $C := C(t)$, constant in time, it was found that the adjusted replicator system has two attractor states depending on the constant value of the chemo concentration C. With the choice of $C(t) \equiv 0$, the trajectories of the adjusted replicator dynamics starting at states near the all healthy state show their eventual convergence to the all sensitive state in a phase space. In fact, the basin of attraction to S is the whole region of a phase space except for two states: the all healthy state and the all resistant state. When $C(t) \equiv 0.7$, the trajectories of the deterministic system starting at the states near the equilibrium, $\left(0, \frac{9C-3}{4C+2}, \frac{5-5C}{4C+2}\right) = (0, 0.6875, 0.3125)$, show that the system is driven to the all resistant state, and this absorption is made at all state but both S and R (Fig.3.6). More interestingly, overlapping these two families of dynamics with two different constant chemo concentrations produce several closed loops (Fig.3.6c). By scheduling a chemotherapy as a step function between $C(t) \equiv 0$ and $C(t) \equiv 0.7$, it is possible to permanently trap the deterministic system in a closed loop and prevent it from the absorption to a cancerous state as under a constant chemo dose. We pick, for numerical experiment, one closed loop and denote the intersection near the S corner by P and the intersection near the line, $\overline{HR}$, by Q, where $P = (0.04, 0.9, 0.06)$ and $Q = (0.53, 0.11, 0.36)$ (Fig.3.7a).

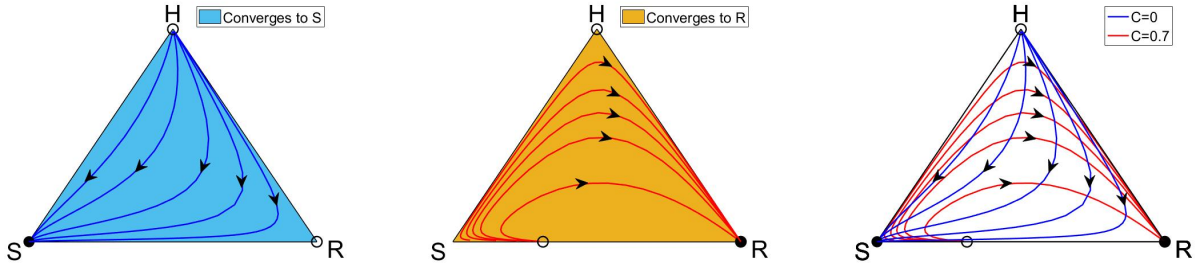

(a) (b) (c)

Figure 3.6: Deterministic trajectories describe the evolutionary stable states (ESS) of the adjusted replicator system for different constant chemotherapy values. (a) Under $C(t) \equiv 0$, the competitive release of the sensitive subpopulations, S, to drug drives all trajectories to the S corner. (b) Under $C \equiv 0.7$, the competitive release of the resistant subpopulations R to drug drives all trajectories to the R corner. (c) Trajectories with two different constant chemotherapy combinations overlap at different times and generate a closed loop.

In order to design a chemotherapy schedule precisely, let T_{PQ} be the time it takes that the point, P, evolves by the adjusted replicator equations and reaches the point, Q, and let T_{QP} be the time that the system takes to get from Q to P. Administering a high chemo $C(t) \equiv 0.7$ during T_{PQ} unit time, the adjusted replicator system starting at point P moves along the red line arriving at Q. Then, turning the chemo off for T_{QP} unit time, the point Q is driven by the system back to the point P along the blue line (Fig. 3.7a). We call the time, $T_{PQ} + T_{QP}$, that it takes to return to the initial state one evolutionary cycle. The evolutionary cycle varies with the choice of two states and thus the chemo schedule needs to be carefully designed with the deep investigation of the patient's medical status in the clinical purpose. Also for the later use, we call the time, T_{PQ} or T_{QP}, a half evolutionary cycle. In our deterministic model, each half cycle is $T_{PQ} = 19.36$ and $T_{QP} = 12.56$ and hence one evolutionary cycle is equal to 31.92 unit time.

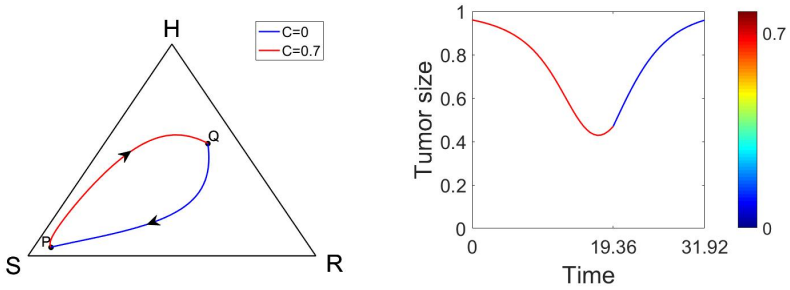

(a) (b)

Figure 3.7: Switching chemotherapy on and off at adequate times traps a trajectory associated with the adjusted replicator system within a closed loop. (a) The system, that starts at P, moves along a red line and arrives at Q when the high chemo dose, $C(t) \equiv 0.7$, is continuously administered during $T_{PQ} = 19.36$ unit time. When chemo is turned off during further $T_{QP} = 12.56$ unit time, it returns to the initial point, P, eventually generating a closed loop, PQP; (b) The tumor volume is controlled with the use of the adaptive schedule for an evolutionary cycle, experiencing tumor regression and recurrence.

Continuing this chemotherapy schedule, what is called an adaptive schedule, for infinitely many evolutionary cycles, the adjusted replicator system starting at P returns back to P every $T_{PQ} + T_{QP}$ unit time. In addition, the initially high volume of tumor decreases for T_{PQ} since the high chemo helps to remove the sensitive cells in a population at the beginning, however, the drug administration during longer than necessary period results in the regrowth of tumor slightly before it reaches T_{PQ}. After turning the

chemo off, the tumor volume keeps increasing and finally recovering the initial tumor volume when one evolutionary cycle is over (Fig.3.7b). Using the adaptive schedule for multiple cycles causes the tumor size to oscillate and be controlled by preventing the system from the absorption to either S or R corners.

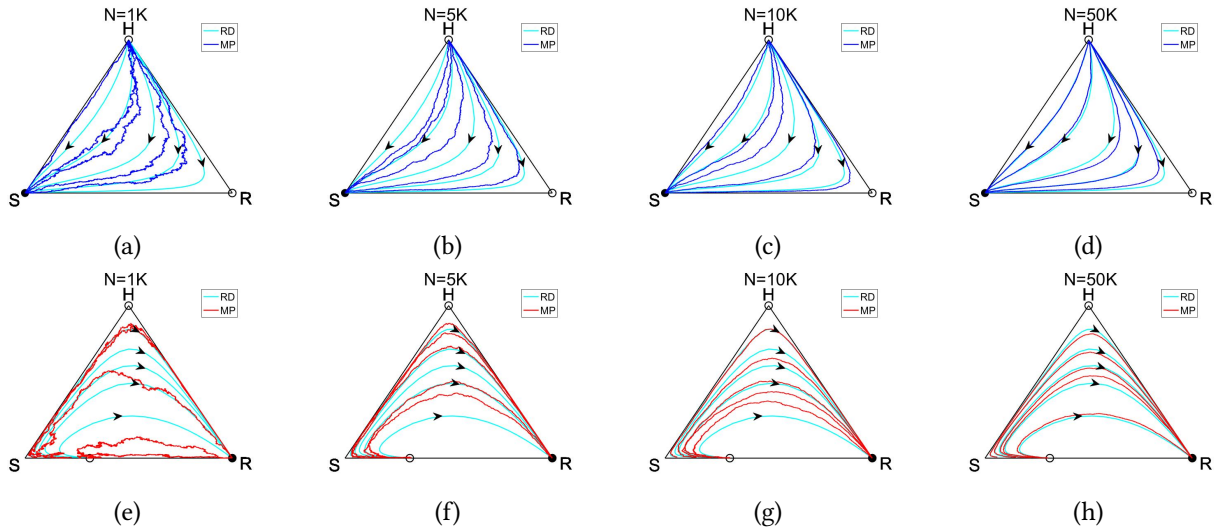

Figure 3.8: Realizations of multiple trajectories associated with the Moran process under administration of a constant chemotherapy show the ability of the stochastic system to behave similarly to what the adjusted replicator dynamics drive, getting closer as the population size increases. The Moran process, starting at a state near the corner H with $C(t) \equiv 0$ (blue wiggled lines), possibly evolves and attains the homogeneous population of all S for each N, having smoother trajectories as N increases and finally being similar to the deterministic trajectory (light blue line). Similarly, the Moran process starting at a state near the fixed point $(0, 0.6875, 0.3125)$ (red wiggled lines) is able to be driven to the state R with $C(t) \equiv 0.7$ for each N. (a) $C(t) \equiv 0$, $N = 1K$; (b) $C(t) \equiv 0$, $N = 5K$; (a) $C(t) \equiv 0$, $N = 10K$; (a) $C(t) \equiv 0$, $N = 50K$; (e) $C(t) \equiv 0.7$, $N = 1K$; (f) $C(t) \equiv 0.7$, $N = 5K$; (g) $C(t) \equiv 0.7$, $N = 10K$; (h) $C(t) \equiv 0.7$, $N = 50K$

We will apply this adaptive schedule to the Moran process with H, S, R and see if how badly our model behaves for one evolutionary cycle. To this end, we first investigate the stochastic trajectory against the deterministic trajectory in a phase space with the use of a constant chemo schedule for $N = 1K$, $5K$, $10K$, $50K$, where the stochastic movement is determined by the transition probabilities in (3.2). We are able to find one realization of the Moran process starting at a state near the H corner and achieving the fixation to S with no chemo administered for each N. One realization of the Moran process starting at a state near the fixed point, $(0, 0.6875, 0.3125)$, and eventually converging to R with the constant use of a drug $C(t) \equiv 0.7$ is also obtained. For both constant drug schedules, the stochastic trajectories get

wiggled around the deterministic trajectories and become smoother and smoother in the increase of N finally being similar to the deterministic ones for a large N (Fig.3.8).

However, it is just one realization of the Moran process as an example and a stochastic system can only be understood in terms of its distribution in general. Recalling the relation in (1.17) between the evolution step, τ, for the Moran process and the evolution time, t, for the deterministic adjusted replicator system through which the convergence of the Moran process to the deterministic system is driven, we simulate $1,000$ individual Moran processes all starting at P during the half evolution steps, $T_{PQ} \cdot N$, with $C(t) \equiv 0.7$ and indicate the terminal points of all realizations as red dots for each $N = 1K, 5K, 10K$ and $50K$ (Fig.3.9).

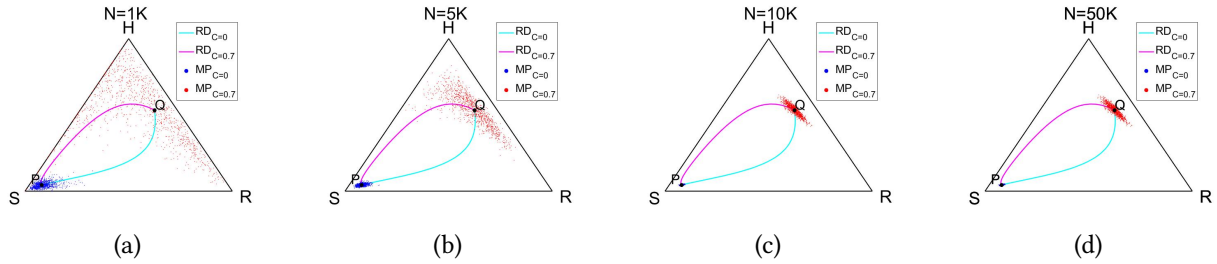

(a) (b) (c) (d)

Figure 3.9: The spread of the distribution of points around Q (or P) for $1,000$ realizations of the stochastic Moran process gets denser and demonstrates the shrunken randomness as the population size increases when each realization is under the administration of a constant chemo schedule $C(t) \equiv 0.7$ (or $C(t) \equiv 0$) during half an evolutionary cycle, T_{PQ} (or T_{QP}), since its exact start at P (or Q). (a) $N = 1K$; (b) $N = 5K$; (c) $N = 10K$; (d) $N = 50K$

It is obvious that they form a distribution near the point, Q, at which the deterministic ends its half cycle starting from P, and the deviation becomes smaller in the increase of N getting denser around Q. When they are plotted in the SR coordinate system, the mean frequency, μ_S, of the sensitive subpopulations at the terminal points around Q for $1,000$ realizations approaches the proportion of S at Q, which is precisely equal to 0.11 (Fig.3.10a-3.10d). It means that as N increase, the mean frequency μ_S, which is the sample mean, becomes a less biased estimator for the proportion of S at Q. The mean frequency, μ_R, of the resistant subpopulations around Q also becomes a more accurate estimator for the frequency of R at the state, Q, being equal to 0.36. One thing notable from the distribution in SR coordinate system is that

the deviation in the direction of R is in general smaller than in the direction of S for each N though both are getting smaller in the increase of N, and it is because the expected deterministic system diverges near P moving towards H and then eventually towards R with $C \equiv 0.7$ while it converges to S with $C \equiv 0$ as shown in Figure 3.6. When the terminal points around Q are plotted in the principal axis coordinate system, we see that not only both the semi-major and the semi-minor axis decrease in N but also it forms a multi Gaussian distribution for a large N (Fig.3.10e-3.10h).

We separately simulate $1,000$ individual Moran process all starting at Q during the evolution steps, $T_{QP} \cdot N$, with $C(t) \equiv 0$ and indicate the terminal points of each realization in blue dots. It shows the similar pattern that the first half cycle with $C(t) \equiv 0.7$ results in terms of the shrinking distribution. The mean frequency, μ_S, of the sensitive subpopulations at the terminal points of the$1,000$ realizations of the Moran process around P converges to the frequency of S at P being equal to 0.9 while the mean frequency, μ_R, of the resistant subpopulations around P approaches the proportion of R at P being equal to 0.06 as N increases. However, unlike that the terminal points from the first half evolutionary cycle are more widely distributed along the S axis in the SR coordinate system, the end pints from the second half cycle are equally likely distributed along both axes, and it is because the expected deterministic system converges to S under $C(t) \equiv 0$ (Fig.3.10i-3.10p). In addition, when they are plotted in the principal axis coordinate system, we see that the multi Gaussian-like distribution is achieved with the smaller N compared to the first half evolution cycle, and both the semi-major and the semi-minor axis are apparently smaller for each N.

Now, we extend the evolution steps from a half evolutionary cycle up to the full one cycle, $(T_{PQ} + T_{QP}) \cdot N$. It means that we apply the adaptive chemotherapy schedule associated with the deterministic system to the Moran process in the following way: each realization of the Moran process starts at P under a high constant chemo dose, $C(t) \equiv 0.7$, during $T_{PQ} \cdot N$ evolution steps, and once it reaches a neighborhood of Q in the last step, we turn the high chemo off and the Moran process evolves from that neighborhood

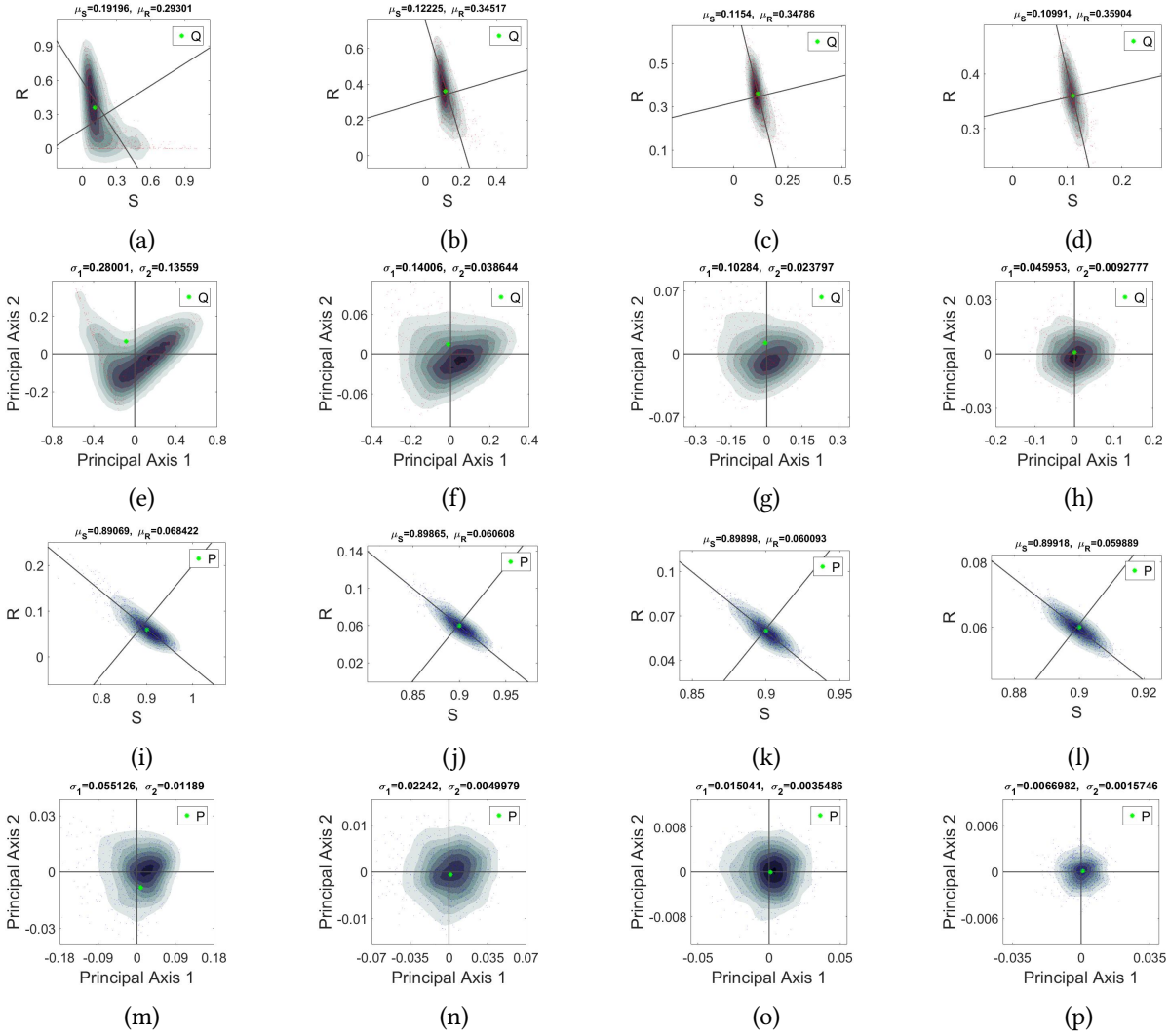

Figure 3.10: The spread of the distribution of points in the principal axis coordinate system for $1,000$ realizations of the Moran process is, for a large population size, characterized as a multi Gaussian distribution around Q (or P) when each realization is under the administration of a constant chemo schedule $C(t) \equiv 0.7$ (or $C(t) \equiv 0$) during half an evolutionary cycle, T_{PQ} (or T_{QP}), since its exact start at P (or Q). The mean frequency, μ_S (or μ_R), of the sensitive (or resistant) subpopulations around the point, P (or Q), converges to the proportion of S (or R) as N increases, with the decreasing semi-major axis, σ_1, and semi-minor axis, σ_2. (a) $N = 1K$, $\mu_S = 0.1920$, $\mu_R = 0.2930$; (b) $N = 5K$, $\mu_S = 0.1223$, $\mu_R = 0.3452$; (c) $N = 10K$, $\mu_S = 0.1154$, $\mu_R = 0.3479$; (d) $N = 50K$, $\mu_S = 0.1099$, $\mu_R = 0.3590$; (e) $N = 1K$, $\sigma_1 = 0.2800$, $\sigma_2 = 0.1356$; (f) $N = 5K$, $\sigma_1 = 0.1401$, $\sigma_2 = 0.0386$; (g) $N = 10K$, $\sigma_1 = 0.1028$, $\sigma_2 = 0.0238$; (h) $N = 50K$, $\sigma_1 = 0.0460$, $\sigma_2 = 0.0093$; (i) $N = 1K$, $\mu_S = 0.8907$, $\mu_R = 0.0684$; (j) $N = 5K$, $\mu_S = 0.8987$, $\mu_R = 0.0606$; (k) $N = 10K$, $\mu_S = 0.8990$, $\mu_R = 0.0601$; (l) $N = 50K$, $\mu_S = 0.8992$, $\mu_R = 0.05989$; (m) $N = 1K$, $\sigma_1 = 0.0551$, $\sigma_2 = 0.0119$; (n) $N = 5K$, $\sigma_1 = 0.0224$, $\sigma_2 = 0.0050$; (o) $N = 10K$, $\sigma_1 = 0.0150$, $\sigma_2 = 0.0035$; (p) $N = 50K$, $\sigma_1 = 0.0067$, $\sigma_2 = 0.0016$

during $T_{QP} \cdot N$ evolution steps, which expectedly arrive near P. According to the convergence of the system, it is expected that for a large N, this return is achievable with a high probability, however, it is

hard to occur in a small population due to the strong stochasticity though not impossible. We show one example of the stochastic trajectory with a small population of size, $N = 50$, along the lattice together with the deterministic trajectory in a phase space when a drug is administered according to the adaptive chemotherapy schedule.

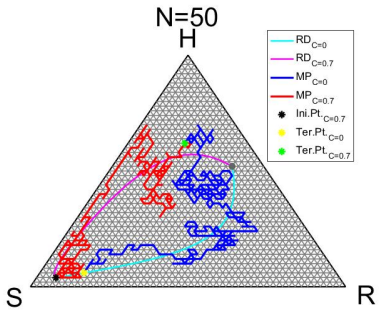

Figure 3.11: The stochastic trajectory of one realization of the Moran process under the administration of the adaptive chemotherapy, associated with the adjusted replicator dynamics, develops a random walk along a lattice in a phase space, S_2. The adaptive schedule is able to prevent the stochastic system from the saturation of cancer cells, even in a small population with $N = 50$. Starting at $P = (0.04, 0.9, 0.06)$ (black dot), it moves along the lattice (red line) and reaches a neighborhood (green dot) of $Q = (0.53, 0.11, 0.36)$, during T_{PQ} evolution time. Turning off the chemo at that green dot, the stochastic system evolves (blue line) and eventually reaches a neighborhood (yellow dot) of the initial point, P, during T_{QP}.

The strong stochasticity allows the trajectory of the Moran process starting at P under $C(t) \equiv 0.6$ to jump back and forth around the deterministic trajectory along the lattice in a phase space and terminates its movement at a point far away from Q. However, it is also the strong stochasticity that leads the terminal point with $C(t) \equiv 0.7$ to a point near P after $T_{QP} \cdot N$ evolution steps under $C(t) \equiv 0$ preventing the system from the absorption to a cancerous state. Again, it is one realization and we simulate $1,000$ realizations of the Moran process under the adaptive chemo schedule to understand it in distribution with $N = 10K$ and $50K$, and see how large N enables the stochastic system to resume its initial state after one evolutionary cycle with a high probability.

The distribution of the points near Q shows the similar pattern that $1,000$ realization of the Moran process during the first half cycle results since it is just one another sample of the same size. However, the distribution of the points near P after the full one cycle is more broad compared to the case during the

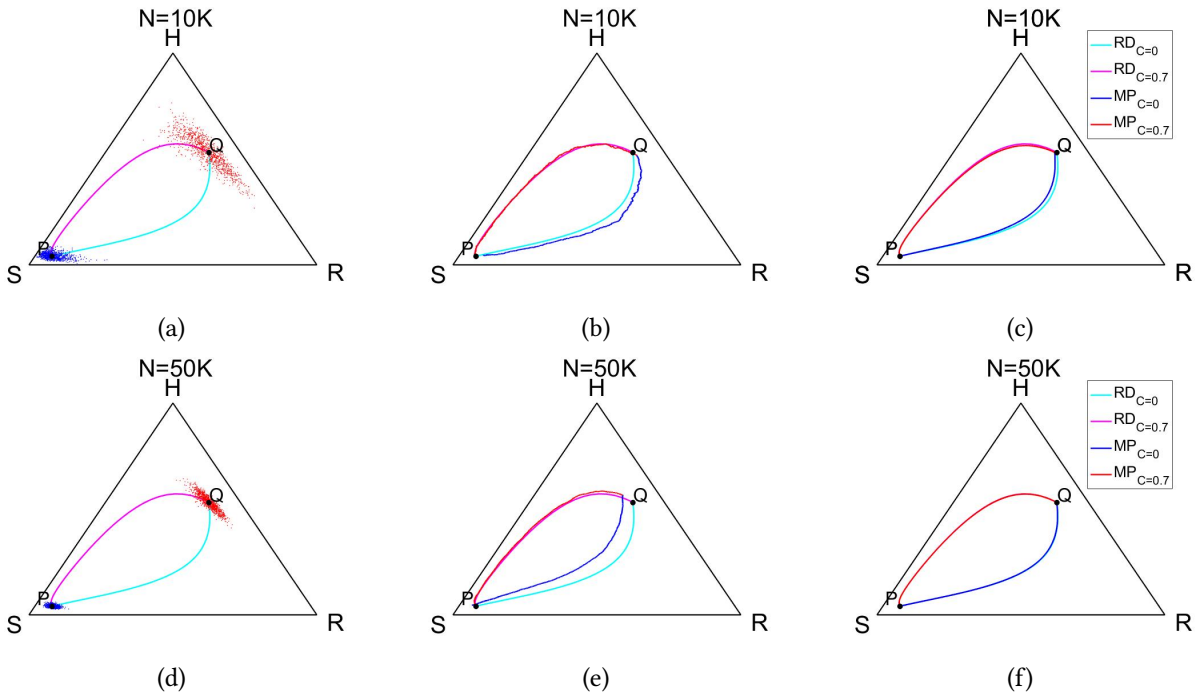

Figure 3.12: The averaged trajectory of $1,000$ realizations of the Moran process under the adaptive schedule, associated with the adjusted replicator system, during one evolutionary cycle ($T_{PQ} + T_{QP} = 31.92$ unit time) fits the corresponding deterministic trajectory for a large population size. The Moran process is likely to return nearly to the initial state with a high probability for a large N even though the spread of the distribution of the points near Q is still wide. (a) the distribution of the points associated with the adaptive chemo schedule for $N = 10K$; (b) the trajectory of one single realization of the Moran process with $N = 10K$; (c) the averaged trajectory of $1,000$ realizations of the Moran process with $N = 10K$; (d) the distribution of the points for $N = 50K$; (e) the trajectory of one single realization with $N = 50K$; (f) the averaged trajectory with $N = 50K$

second half evolutionary cycle shown in Figure 3.9 for each N (Fig. 3.12a, 3.12d). It is obviously because each realization starts at one of red dots near Q for the second half cycle under the adaptive chemo schedule unlike it starts at the exact point, Q, for Figure 3.9, and this drives the system to settle down at a point further away from P resulting in a broad distribution around. Clearly, the distribution around the initial state P is of the greater interest due to the fact that the randomness works in a cooperative way so that the system fallen far away from Q after the first half evolution cycle might be able to end its evolution near the state P in the end of the full one round.

Thus, we will investigate the distribution only around the initial point when it comes to the full evolution cycle or longer. The distribution of points around P in the SR coordinate system particularly when

$N = 50K$ shows the deviation in either direction is equally likely forming a multivariate Gaussian distribution with the mean frequency, $\mu_S = 0.8973$, of the sensitive subpopulations and the mean frequency, $\mu_R = 0.06125$, of the resistant subpopulations (Fig.3.13). These play the role of the estimators for the proportion, 0.9, of S and the proportion, 0.06, of R at the state, P, being less accurate compared to the case with the half evolutionary cycle discussed in Figure 3.9.

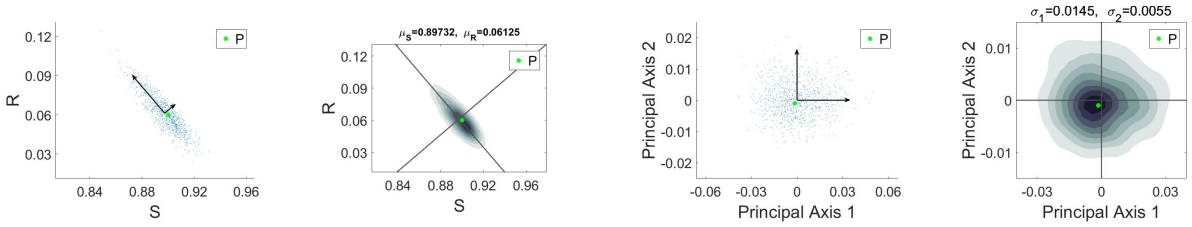

(a) (b) (c) (d)

Figure 3.13: The spread of the distribution of points for $1,000$ realizations of the stochastic Moran process with $N = 50K$ is characterized as a multivariate Gaussian distribution, centered nearly at the initial point, P, when each realization is under the administration of the adaptive schedule during one evolutionary cycle ($T_{PQ} + T_{QP} = 31.92$ unit time). As shown in the SR and the principal axis coordinate system, the deviation is equally likely to each other in either directions. (a) the distribution of the points around P in the SR coordinate system; (b) the kernel density distribution in the SR coordinate system; (c) the distribution of the points in the principal axis coordinate system; (d) the kernel density distribution in the principal axis coordinate system

We also show the whole trajectory of the Moran process under the adaptive schedule for one evolutionary cycle in Figure 3.12. One realization of the process moves closely to the closed loop around the points, P and Q, for each N while the trajectory passes the point, Q, during the first half cycle with $N = 10K$ but it does not reach close enough Q with $M = 50K$ (Fig.3.12b, 3.12e). However, the averaged trajectory of the Moran process with $N = 50K$ definitely shows the closer fit to the deterministic trajectory (Fig.3.12c, 3.12f). This implies that the adaptive chemo schedule helps the stochastic system recover the initial state after one evolutionary cycle at a high probability for a large N.

3.3 Single drug adaptive control for multiple evolutionary cycles

Now, we want to continue applying this adaptive chemotherapy schedule to the Moran process but during multiple evolutionary cycles, and see how early the recovery of the approximate initial state is broken for a large population. To be precise, the Moran process initially starting at P evolves under the adaptive chemo schedule for one evolutionary cycle and arrives at a point in the neighborhood of P. Then at that terminal state of the first cycle, we turn the chemo on again to start the second round of the adaptive chemo schedule for the next evolutionary cycle, and continue doing these steps for a few more rounds. That is, the process in the current round starts at the terminal state in the previous round for one evolutionary cycle. This is a natural extension of the application of the adaptive schedule to the Moran process, but it is not straightforward or easy to answer the question due to the facts obtained from its expected system.

The adjusted replicator system is sensitive in the initial state as well as in the chemotherapy concentration: initially close two points can have completely different fate at the end under the same constant chemo schedule, particularly either if they are located across the basin boundary for a fixed C such that $\frac{1}{3} < C < \frac{1}{2}$ or if they are in the neighborhood of an unstable fixed point of the system. Also the basin boundary of the deterministic system experiences the smooth transition in a phase space as the constant drug concentration, C, which acts as a parameter, increases from $1/3$ to $1/2$. Hence the system starting at a fixed initial state can be lead to a different homogeneous state with a slight change in C if the change causes the initial point to be located on the other side of the basin boundary. For these reasons and with the randomness of the stochastic system added, the fate of the Moran process in the following round is indeterminate even though the Moran process under the adaptive schedule returns close enough to the initial state in the current round.

Here, we consider the adaptive schedule during 4 cycles for the numerical experiment with $N = 10K$ and $50K$. The stochastic trajectory during the first, second, third and fourth round is plotted in a red, green, blue and pink line, respectively while the deterministic trajectory is shown in light blue in Figure

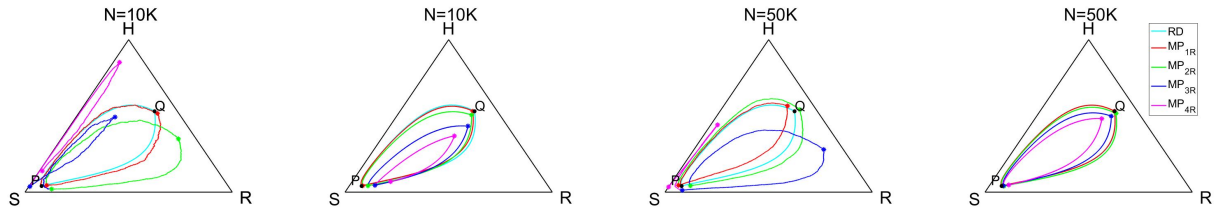

(a) (b) (c) (d)

Figure 3.14: For each N, the averaged trajectory of $1,000$ realizations of the stochastic Moran process shows that the saturation of cancer cells can be delayed until the 4th evolutionary cycle when each realization evolves under the administration of the adaptive schedule, associated with the adjusted replicator system, during 4 evolutionary cycles since its exact start at P, although the tightness of the the averaged stochastic trajectory to the deterministic one lasts shorter with a smaller population size. (a) the trajectory of one single realization for the Moran process with $N = 10K$; (b) the averaged trajectory of $1,000$ realizations for the Moran process with $N = 10K$; (c) the trajectory of one single realization with $N = 50K$; (d) the averaged trajectory with $N = 50K$

3.14. Also, we mark the terminal point in each round in the starred shape, colored accordingly. One realization of the Moran process starting at P under the adaptive schedule with $N = 10K$ shows that it moves along the red line in the first round as expected by the deterministic system (light blue line) and arrives at the red point near P before it terminates its life at the all sensitive state (Fig.3.14a). The second round starts at that red point near P, and it moves along the green line being off the expected trajectory and returns to the green point near P in the end of the second round. The third round starts at the red point near P, and it arrives at the blue point near P after moving along the blue line. Unfortunately, the blue point at which the third round ends represents the state where one subpopulation is rare in the total population, and it possesses a high potential that the system is driven to the $\overline{SH}$ line where the population is composed of only two subpopulations of the type, S and H. Once it enters a state of two subpopulations, the continuation of the adaptive chemo schedule eventually causes the system to converge to a cancerous state.

A similar scenario is shown in the single realization of the Moran process with $N = 50K$ (Fig.3.14c). It moves closely around the closed loop associated with the deterministic system up to the second round, however, it starts being far off the expected orbit and finally ends at the pink point near P at the end of the

fourth round. Then it is from now on laid in the similar situation to the end of the third round in Figure 3.14a with $N = 10K$.

Nevertheless, it is not that disappointing to apply the adaptive chemo schedule when the averaged trajectory for $1,000$ realizations of the Moran process is taken into account. On average, the adaptive schedule keeps cancerous cells from fixating the total population for 4 evolutionary cycles. The Moran process starting at P with $N = 10K$ under the adaptive schedule approximately re-attains the initial state P in the end of each round though it becomes further and further from P as the number of rounds increases and it does not behave similarly to the deterministic system from the third round (Fig.3.14b). However, the distance from P to the averaged point in the end of each round gets smaller as N increases, and it results that the Moran process behaves similarly to the deterministic system in its trajectory much longer (Fig.3.14d).

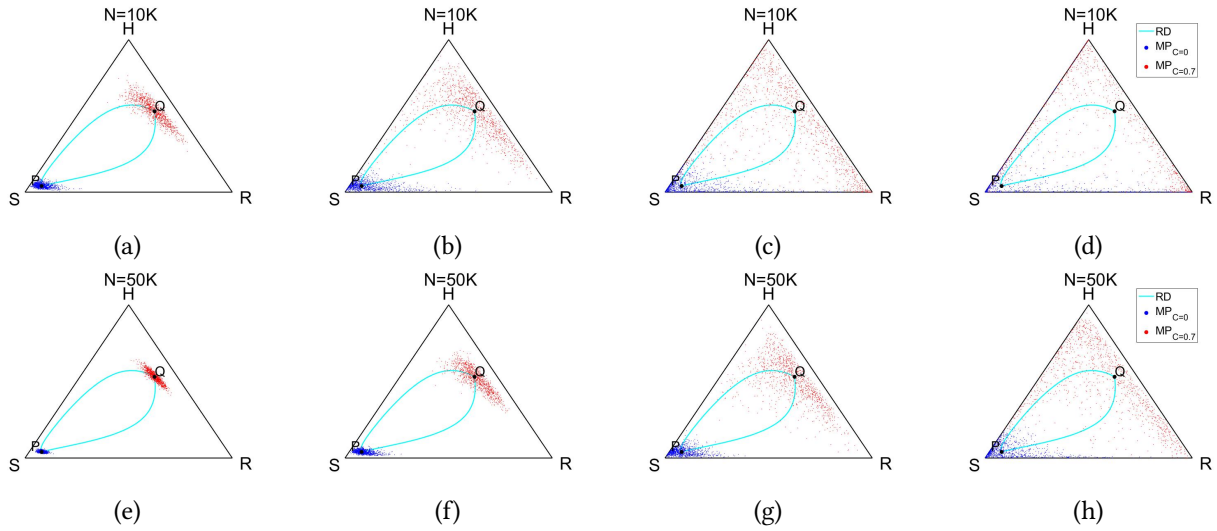

Figure 3.15: The spread of the distribution of terminal points (blue dots) around P in each round for $1,000$ realizations of the stochastic Moran process becomes wider as the number of rounds increases when each realization evolves under the administration of the adaptive schedule, associated with the adjusted replicator system, during 4 evolutionary cycles since its exact start at P. (a) $N = 10K$, round 1; (b) $N = 10K$, round 2; (c) $N = 10K$, round 1; (d) $N = 10K$, round 4; (e) $N = 50K$, round 1; (f) $N = 50K$, round 2; (g) $N = 50K$, round 1; (h) $N = 50K$, round 4

In fact, the points near P for $1,000$ realizations of the Moran process in the end of each round are distributed wider and wider as the number of rounds increases for each $N = 10K$ and $50K$ (Fig.3.15).

Obviously, the relatively thick cluster around P is maintained in each round with $N = 50K$ compared to $N = 10K$. Finally, the cluster around P starts blurry from the third round with $N = 10K$ and in the fourth round with $N = 50K$ (Fig.3.15). As they lose clustering around P, many of them end their 4 rounds of evolution near the all sensitive state meaning that the fixation of S eventually reached with a high probability.

This becomes more apparent to see when the points are plotted in the SR coordinate system. For $N = 50K$, the range of the distribution of S and R are equally likely up to the last round (Fig.3.16). However, they get more clustered towards the point $(1, 0)$ in the SR coordinate system as the number of rounds increases, where $(1, 0)$ represents the all sensitive state. Finally they are no longer clustered around P in the last round and it means that the sensitive mutants finally fixates the total population with a high probability after 4 evolutionary cycle. Also, the multivariate Gaussian distribution is already broken in the third round, and both the semi-major and the semi-minor axis keeps increasing in the number of rounds.

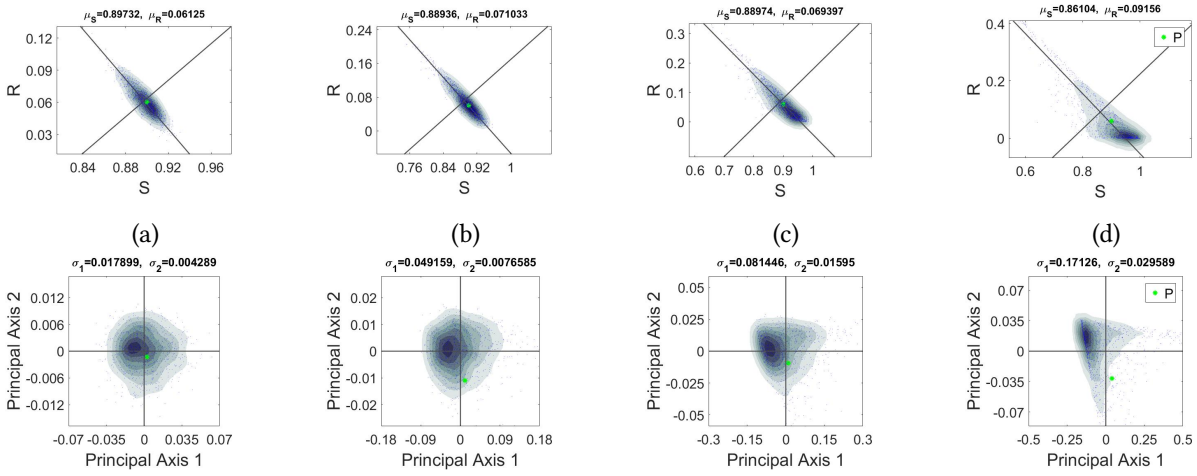

Figure 3.16: As the number of rounds increases, the spread of the distribution of points around P for $1,000$ realizations of the stochastic Moran process for $N = 50K$ becomes centered towards the homogeneous sensitive state and immediately looses the multivariate Gaussian-like distribution, where each realization evolves under the administration of the adaptive schedule, associated with the adjusted replicator system, during 4 evolutionary cycles since its exact start at P. (a) round 1; (b) round 2; (c) round 3; (d) round 4; (e) round 1; (f) round 2; (g) round 3; (h) round 4

Extending the number of the evolutionary cycles up to 8 rounds, we clearly see the overall increase of these values in the number of rounds for each $N = 10K$ and $50K$ while they are overall smaller with $N = 50K$ due to the thicker cluster around P (Fig.3.17). Fitting the discrete data in the log-log plot shows the power-law dependence of the semi-major (minor) axis on the number of rounds. Precisely, the fitted curve for the semi-major (minor) axis of the distribution of the points around P for $1,000$ Moran processes starting at P as a function of the number of rounds in the log-log scale is following: for $N = 10K$

$$\begin{aligned} \sigma_1 &\sim 0.0505 \cdot n^{1.3269}, \\ \sigma_2 &\sim 0.0071 \cdot n^{1.8753}, \end{aligned} \tag{3.11}$$

and for $N = 50K$

$$\begin{aligned} \sigma_1 &\sim 0.0149 \cdot n^{1.8519}, \\ \sigma_2 &\sim 0.0025 \cdot n^{2.0424}, \end{aligned} \tag{3.12}$$

where σ_1 is the semi-major axis, σ_2 is the semi-minor axis, and n is the number of rounds.

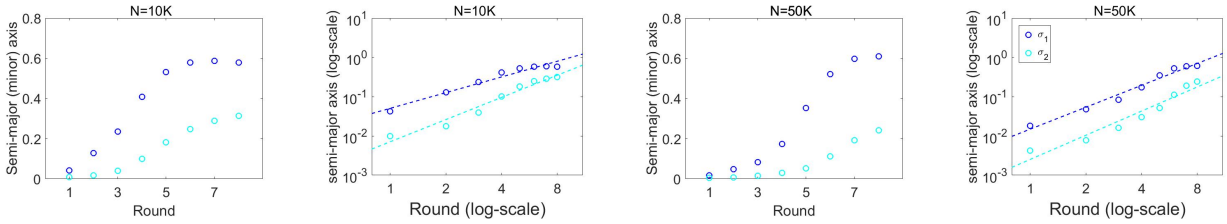

(a) (b) (c) (d)

Figure 3.17: The semi-major (and -minor) axis of the distribution of the points around P at the end of each evolutionary cycle for $1,000$ realizations of the Moran process overall increases in the number of rounds, showing the power-law dependency, where each realization evolves under the administration of the adaptive schedule associated with the adjusted replicator system during 8 evolutionary cycles since its exact start at P. (a) $N = 10K$; (b) $N = 10K$, the log-log fit; (c) $N = 50K$; (d) $N = 50K$, the log-log fit

3.4 Comparison of adaptive single drug chemotherapy schedule with standard clinical approaches

Among several clinical chemotherapy schedules, we consider two frequently used standard schedules: the maximum tolerated dose schedule (MTD) and the low-dose metronomic schedule (LDM). The former is the highest dose of a drug by which any significantly unacceptable side effects are not produced while the later is the low dose of a drug that is continuously given for a finite time. We compare the effectiveness of the adaptive chemotherapy schedule to those standard clinical chemo schedules in terms of either the prevention ability of the system from converging to a cancerous state or the control ability of its induced tumor size.

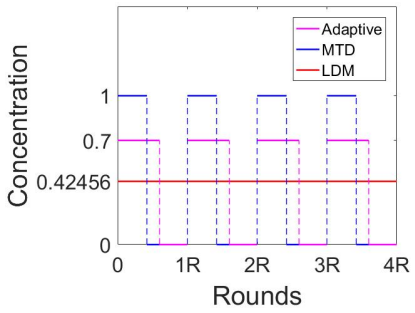

Figure 3.18: Two standard clinical approaches, the maximum tolerated schedule (MTD) and the low-dose metronomic schedule (LDM), are designed in order to have the same total dose as the adaptive chemotherapy schedule associated with the deterministic replicator system has during 4 rounds. In each cycle of the length, 31.92, MTD delivers a drug at the highest concentration during the first 13.552 unit time, followed by no chemo until the end of each cycle. On the other hand, a drug is continuously delivered during the whole cycles at as low concentration as 0.42456 for LDM.

For our comparison, each chemo schedule is subject to having the same total dose over a finite time. For a drug concentration function, $C(t)$, defined on $[0, T]$ for $T > 0$, the total dose, $D(T)$, delivered during T unit time is defined by

$$D(T) := \int_0^T C(t)dt. \tag{3.13}$$

Let $C^{\text{Adaptive}}(t)$, $C^{MTD}(t)$ and $C^{LDM}(t)$ be the drug concentration functions of the adaptive, MTD and LDM schedules, respectively, at time, t. We assume that

$$\int_0^T C^{\text{Adaptive}}(t)dt = \int_0^T C^{\text{MTD}}(t)dt = \int_0^T C^{\text{LDM}}(t)dt, \tag{3.14}$$

where $T = T_{PQ} + T_{QP} = 31.92$ for the numerical purpose. Then it is straight forward that the highest dose is delivered until 13.552 unit time followed by no drug administration until a cycle ends for MTD, and the constant dose as low as $C^{LDM}(t) \equiv 0.42456$ is continuously administered during 31.92 unit time, the whole cycle, for LDM to have same total dose each other in one evolutionary cycle. These schedules are to be repeated as many times as the number of the evolutionary cycles increases (Fig.3.18).

As shown in Figure 3.14, the adaptive schedule works effectively for 4 rounds by turning chemo on and off at adequate times, delaying the competitive release and inhibiting the fixation of cancerous cells in a population. For a denser population, the trajectory was better controlled on average, tightly moving around the closed loop associated with the deterministic system during longer evolutionary cycles. Define a tumor size as the sum of frequencies of cancerous cells, that is, the sum of sensitive cells and resistant cells. Note that a tumor size is a function in time ranging on $[0, 1]$ where 0 indicates healthy state with no tumor cells in a population while 1 indicates that no hope expected since a population is merely composed of sensitive and resistant cells.

Then, the tumor size under the adaptive schedule is well controlled on average during 4 cycles never reaching 1, the full tumor state. In our model, since the Moran process starts at P where the dominant cells are of the sensitive type, the tumor size at the state, P, is as big as 0.96. As drug is administered at a high dose for $T_{PQ} \cdot N$ evolution steps on the Moran process with $N = 50K$, starting at P, in the beginning of each cycles, tumor size reduces nearly about 0.5 with the slight increase at the end. This slight increase in tumor size origins from the resistance to drug as a result of a long drug administration

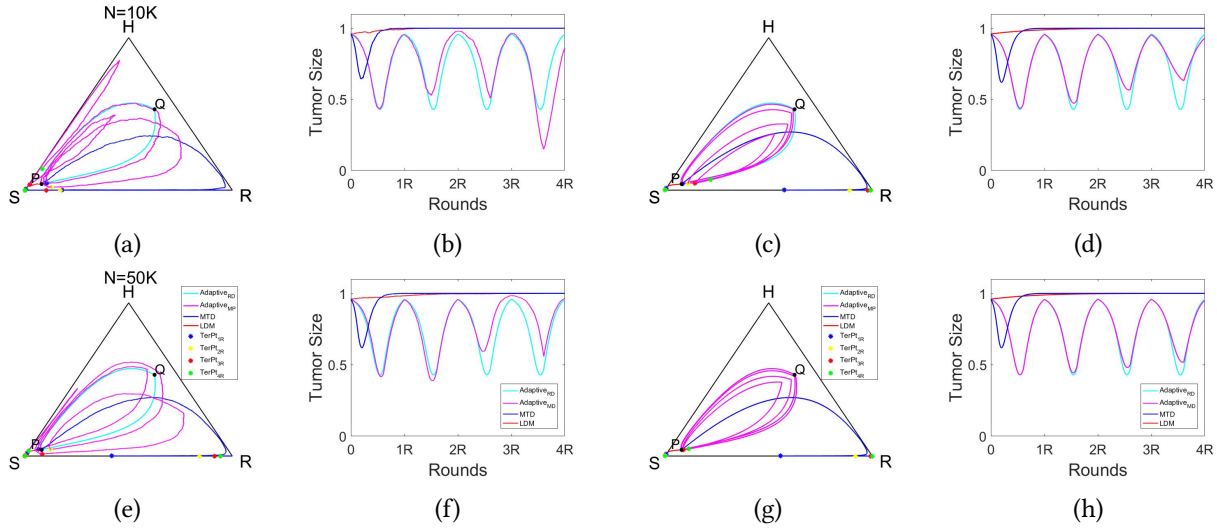

Figure 3.19: The adaptive chemotherapy schedule associated with the replicator system is compared to the standard clinical approaches, MTD and LDM, in order to demonstrate its efficiency in terms of delaying the time of saturation of tumor cells, which is attained before the first round ends under either MTD or LDM schedules. The adaptive schedule beats the other two standard clinical chemo schedules since not only it prevents the system from converging to a cancerous state and but also the tumor size is thus controlled for 4 rounds on average. (Each of $1,000$ realizations of the Moran process evolves under the administration of the adaptive schedule, MTD or LDM independently during 4 evolutionary cycles since its exact start at P.) (a) $N = 10K$, one single realization; (b) $N = 10K$, the tumor size associated with the single trajectory; (c) $N = 10K$, the averaged trajectory; (d) $N = 10K$, the tumor size associated with the averaged trajectory; (e) $N = 50K$, one single realization; (f) $N = 50K$, the tumor size associated with the single trajectory; (g) $N = 50K$, the averaged trajectory; (h) $N = 50K$, the tumor size associated with the averaged trajectory

causing the re-growth of tumor. When chemo is shortly turned off, tumor size keeps increasing and almost recovers the full tumor state in $T_{QP} \cdot N$ evolution steps. It is true that the tumor size consequently increases on average compared to when the chemo just starts being turned off. However, the composition of the population totally changes to the mostly sensitive cells so that it is ready to sensitively react to a drug. As the second cycle begins, the tumor size undergoes down and up in the similar pattern on average, and continues until the last round (Fig.3.19h).

On the other hand, the two standard clinical approaches show hopeless results for a large N. The maximum tolerated dose schedule shortly drives the system to states where the resistant cells are abundant by immediately causing the resistance to a drug and bringing the re-growth of tumor. After the chemo is turned off, the tumor size finally reaches its full volume and the system permanently enters the state

where a healthy cell no longer exists even in the end of the first evolutionary cycle. Later, the control of the chemo dose just changes its state between the more sensitive and the more resistant, but the tumor size never reduces eternally on average. The low-dose metronomic schedule does not seem to be a promising method to attempt to cure a caner once a patient's state is already full of cancer cells, that the initial point P represents in our model. According to the adjusted replicator dynamics, the population starting at P is likely to end up being the all sensitive with the constant concentration, $C(t) \equiv 0.42456$, because P is located in the basin of attraction to S. Thus, the Moran process starting at P is more likely to converge to S with a higher probability as N increases. It implies that not only the adaptive schedule but also the clinical approach must be applied after carefully investigating the patient's state.

We summarizing this section by presenting the effectiveness of the adaptive schedule for the Moran process starring at P during 4 evolutionary cycles. In order to quantify the efficacy, we define that one realization of the Moran process starting at P successfully ends its evolution during 4 evolutionary cycles if it neither gains the full tumor volume on the way nor has over 99% sensitive cells in the end.

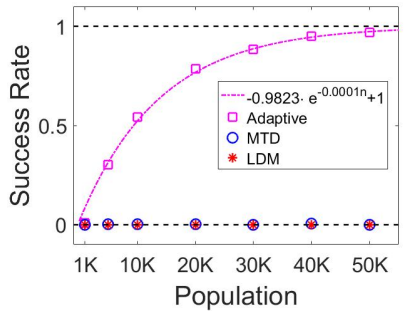

Figure 3.20: Among $1,000$ realizations of the Moran process, the rate that it is well controlled and returns back nearly to the initial state, neither gaining the full tumor volume nor having over 99% sensitive cells after 4 evolutionary cycles, is computed under the adaptive, MTD or LDM chemo schedules independently. The adaptive chemo schedule obviously is superior than other two schedules, having the nearly full rate when $N = 50K$, while MTD has an extraordinarily small but positive success rate up to the 3 rounds.

Then we see that the adaptive schedule works better for each N since it has the highest rate compared to the clinical standard schedules (Fig.3.20). Also, as N increases, its success approximately increases in the form of an exponential function in N:

$$-0.9823 \cdot e^{0.0001 \cdot N} + 1, \tag{3.15}$$

where N is the population size. However, LDM unfortunately brings no positive fate to the population even when the population is small, suggesting the different approach if the patient is at the state, P. The maximum tolerated dose is also not promising at this state with nearly zero chance. When the population size is bigger than $20K$, it shows no chance with $1,000$ realizations, however, that results in a small being smaller than 10% but positive probability that the system is successfully not driven to a cancerous state for a small N.

Chapter 4

Stochastic two drug chemotherapy model

In the previous chapter, we studied the single drug chemotherapeutic response to a finite population of competitively interacting healthy, sensitive and resistant cell when modeled by the Moran process. In general, many clinical approaches use more than one toxin simultaneously. Drugs may interact in a way that they result in a greater cumulative effect than the combined individual effects from the multiple independent drug use. On the other hand, drug mixture may cause a consequently smaller effect than the summed individual effects. The former is termed as *synergism* whereas the later as *antagonism*, where *additivity* refers to the individual summation of the effects from the independent drug uses. Both synergism and antagonism have been studied and quantified for about a century since the ignition by C. I. Bliss in [5] in 1939, and more recently in [9].

In this thesis, we adopt the drug interaction parameter, $e \in [-1, 1]$, quantified by Y. Ma and P. K. Newton in [30] in a way that $e < 0$ indicates antagonistic drug interactions, $e = 0$ refers to the additive interactions, and $e > 0$ stands for synergistic interactions. We model two drug chemotherapeutic response by the Moran process in a similar spirit to the single drug model, however, what makes these two models distinguishable is the drug interaction parameter, e. In this framework, synergism is considered the most promising drug interactions to cure cancer in the sense that it kills as many cancer cells using a smaller amount of toxins as drugs in isolation would do as a sum with a higher amount of dose. However, drug

administration continuously changes fitness of cells in all type in a coevolving population, and scheduling chemotherapy based on a track of distribution of all cell types seems to be more realistic in controlling tumor volume.

4.1 S, R_1, R_2 multi drug model

The model that we employ is the Moran process with all cancerous cells of three different types: (i) sensitive cancer cells (S) that are sensitive to both drug 1 and drug 2, (ii) resistant cancer cells (R_1) that are sensitive to drug 1 but resistant to drug 2, and (iii) resistant cancer cells (R_2) that are sensitive to drug 2 but resistant to drug 1. We let $C_i(t)$ be the concentration of drug i, $i = 1, 2$, in time, t, ranging from 0 and 1 with an additional condition, $C_1(t) + C_2(t) \leq 1$, for all t. These concentration functions together with the drug interaction parameter, e, enters though selection functions, $w^X, X \in \{S, R_1, R_2\}$, and distorts the fitness functions as follows:

$$\begin{aligned} w^S(t) &= w_0(1 - C_1(t) - C_2(t) - eC_1(t)C_2(t)), \\ w^{R_1}(t) &= w_0(1 - C_1(t)), \\ w^{R_2}(t) &= w_0(1 - C_2(t)), \end{aligned} \tag{4.1}$$

where w_0 is constant that scales out and is set to be equal to 1 for the computational purpose. Similarly to the equation in (1.33), the selection function of sensitive cells is defined to be inversely proportional to the concentration, $C_i(t)$, of whatever drugs to which they act sensitively, in the additive drug interaction case. The value of e in (4.1) accounts for a greater or smaller cumulative effects for synergism and antagonism, compared to the sum of single effects from independent drug use. Thus, for a fixed e, the concentration functions, $C_i(t)$, act as controllers of the stochastic system and allow us to schedule chemotherapy on the purpose of controlling tumor growth with the allowance of acceptable tumor increase.

Then these selection functions shapes the fitness landscape, defined similarly as in (1.27) but with $X \in \{S, R_1, R_2\}$, with the payoff matrix where i counts the number of S subpopulations whereas j counts the number of R_2 subpopulations. We assume a pairwise Prisoner's dilemma game for three subpopulations with a 3×3 payoff matrix, A:

$$A = \begin{array}{c} \\ S \\ R_1 \\ R_2 \end{array} \begin{array}{c} \begin{array}{ccc} S & R_1 & R_2 \end{array} \\ \begin{pmatrix} a_{11} & a_{12} & a_{13} \\ a_{21} & a_{22} & a_{23} \\ a_{31} & a_{32} & a_{33} \end{pmatrix} \end{array}. \tag{4.2}$$

Considering the cost of resistance and the competitive release, S cells are set to be defectors while R_i's are cooperators, just as in the single drug model with H, S and R. Also, it is obviously more interesting to let each pair of R_1 and R_2 individuals play an asymmetric game, and we design the payoffs between R_1 and R_2 in a way that R_1 cells are dominant subpopulations in a long term according to the adjusted replicator dynamics. Thus the payoff matrix, A, for S, R_1 and R_2 are assumed to satisfy the Prisoner's dilemma inequalities:

$$\begin{aligned} a_{21} < a_{11} < a_{22} < a_{12}, \\ a_{31} < a_{11} < a_{33} < a_{13}, \\ a_{32} < a_{22} < a_{33} < a_{23} \end{aligned} \tag{4.3}$$

with the extra conditions that enables sensitive cells to have a higher expected fitness than that of each resistant cells:

$$\begin{aligned} a_{13} > a_{23}, \\ a_{13} > a_{33}. \end{aligned} \tag{4.4}$$

In addition, noting that the selection-dependent expected fitness function, $f_{i,j}^X$, is equal to 1 when $w^X = 0$, we force all entries of A, which correspond to payoffs that resistant cells receives, to be bigger than the background fitness, 1, so that it allows the competitive release of resistant cells when the sum of two drugs is intense and the fitness of sensitive cells are as little as 1:

$$\begin{aligned} &a_{21}, a_{22}, a_{23} \geq 1, \\ &a_{31}, a_{32}, a_{33} \geq 1. \end{aligned} \tag{4.5}$$

For the numerical purpose, we specify the payoff matrix, A, that is assumed to satisfy the inequalities in (4.3) - (4.5) as follows:

$$A = \begin{array}{c} \\ S \\ R_1 \\ R_2 \end{array} \begin{array}{c} \begin{array}{ccc} S & R_1 & R_2 \end{array} \\ \begin{pmatrix} 2 & 2.8 & 2.8 \\ 1.5 & 2.1 & 2.3 \\ 1.5 & 1.8 & 2.2 \end{pmatrix} \end{array}. \tag{4.6}$$

For each (i, j), the Moran process can change its state into 6 neighborhood in Γ_N, defined in (1.24), in one time step, besides the inactivity at the current state. Each transition probabilities are as follows:

$$\begin{aligned} T_{i,j}^{SR_2} &= \frac{if_{i,j}^S}{N_{i,j}^w} \cdot \frac{j}{N}, \\ T_{i,j}^{SR_1} &= \frac{if_{i,j}^S}{N_{i,j}^w} \cdot \frac{N-i-j}{N}, \\ T_{i,j}^{R_2S} &= \frac{jf_{i,j}^{R_2}}{N_{i,j}^w} \cdot \frac{i}{N}, \\ T_{i,j}^{R_2R_1} &= \frac{jf_{i,j}^{R_2}}{N_{i,j}^w} \cdot \frac{(N-i-j)}{N}, \\ T_{i,j}^{R_1S} &= \frac{(N-i-j)f_{i,j}^{R_1}}{N_{i,j}^w} \cdot \frac{i}{N}, \\ T_{i,j}^{R_1R_2} &= \frac{(N-i-j)f_{i,j}^{R_1}}{N_{i,j}^w} \cdot \frac{j}{N}, \end{aligned} \tag{4.7}$$

and $T_{i,j}^{cons} = 1 - (T_{i,j}^{SR_2} + \cdots + T_{i,j}^{R_1R_2})$, where the weighted population, N^w, is defined by $N^w = if_{i,j}^S + (N-i-j)f_{i,j}^{R_1} + jf_{i,j}^{R_2}$. These microscopic probabilistic movement eventually determine the evolution of cancer cells.

In measuring tumor size, x_{tumor}, following the notation in [30], an independent important tool aside from the stochastic Moran process is the tumor-growth equation:

$$\dot{x_{tumor}} = (< f > -g)x_{tumor}, \tag{4.8}$$

where g is the constant background fitness, and $< f >$ is the averaged fitness in an infinite population. Precisely, letting $\vec{x} := (x_S, x_{R_1}, x_{R_2})^\intercal$ be the frequency vector of S, R_1, R_2 subpopulations, the averaged fitness f^X of X, $X \in \{S, R_1, R_2\}$ is given by:

$$\begin{aligned} f^S &= 1 - w^S + w^S(A\vec{x})_1, \\ f^{R_1} &= 1 - w^{R_1} + w^{R_1}(A\vec{x})_2, \\ f^{R_2} &= 1 - w^{R_2} + w^{R_2}(A\vec{x})_3 \end{aligned} \tag{4.9}$$

with $x_S + x_{R_1} + x_{R_2} = 1$. The nonlinear averaged fitness function, $< f >$, in the entire population is defined to be

$$< f >= f^S x_S + f^{R_1} x_{R_1} + f^{R_2} x_{R_2}. \tag{4.10}$$

First, we consider situation in which both drugs are constantly administered, and those two drugs are additive, that is, $e = 0$. We assume an infinite size of a population for a while in order to understand the expected dynamic, the adjusted replicator dynamic:

$$
\begin{aligned}
\dot{x_S} &= \frac{f^S - < f >}{< f >} x_S, \\
\dot{x_{R_1}} &= \frac{f^{R_1} - < f >}{< f >} x_{R_1}, \\
\dot{x_{R_2}} &= \frac{f^{R_2} - < f >}{< f >} x_{R_2}.
\end{aligned}
\tag{4.11}
$$

The system has a different set of the evolutionary stable states depending on the concentration combination of two drugs. It is numerically depicted in Figure 4.1 for three different constant chemotherapy combinations of drug 1 and drug 2. When no drug is delivered, that is, $C_1 = 0$ and $C_2 = 0$, the tumor saturates to the S corner regardless of the initial distribution of three subpopulations (Fig.4.1a). When $C_1 = 0.8$ and $C_2 = 0$, the high chemo dose of drug 1 causes the competitive release of the resistant subpopulations R_2 to drug 1 and all trajectories are driven to the R_2 corner (Fig.4.1b). Under $C_1 = 0$ and $C_2 = 0.8$, the competitive release and of the resistant subpopulations R_1 to drug 2 is caused as a result of administering high chemo dose of drug 2 and all trajectories are instead driven to the R_1 corner (Fig.4.1c).

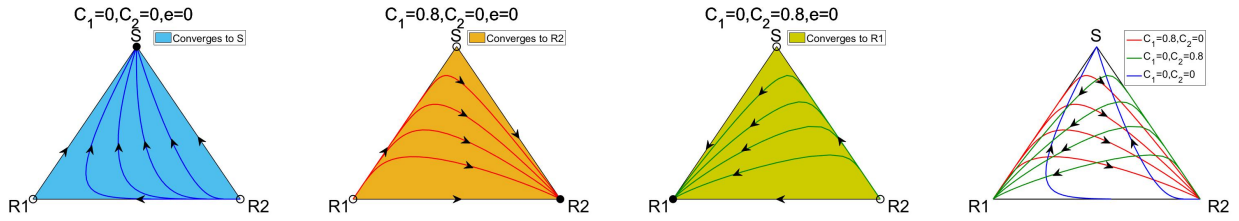

(a) (b) (c) (d)

Figure 4.1: Deterministic trajectories describe the evolutionary stable states (ESS) of the adjusted replicator system for different constant chemotherapy values with $e = 0$. (a) Under $C_1 = 0$ and $C_2 = 0$, the tumor saturates to the S corner regardless of the initial distribution of the three subpopulations. (b) Under $C_1 = 0.8$ and $C_2 = 0$, the competitive release of the resistant subpopulations R_2 to drug 1 drives all trajectories to the R_2 corner. (c) Under $C_1 = 0$ and $C_2 = 0.8$, the competitive release of the resistant subpopulations R_1 to drug 2 drives all trajectories to the R_1 corner. (d) Trajectories with three different constant chemotherapy combinations of drug 1 and drug 2 overlap at different times and generate a closed loop.

Knowing that the adjusted replicator dynamic is the limiting system of the Moran process, it is expected that the stochastic Moran process whose fate is determined by the transition probabilities in (4.7) shows

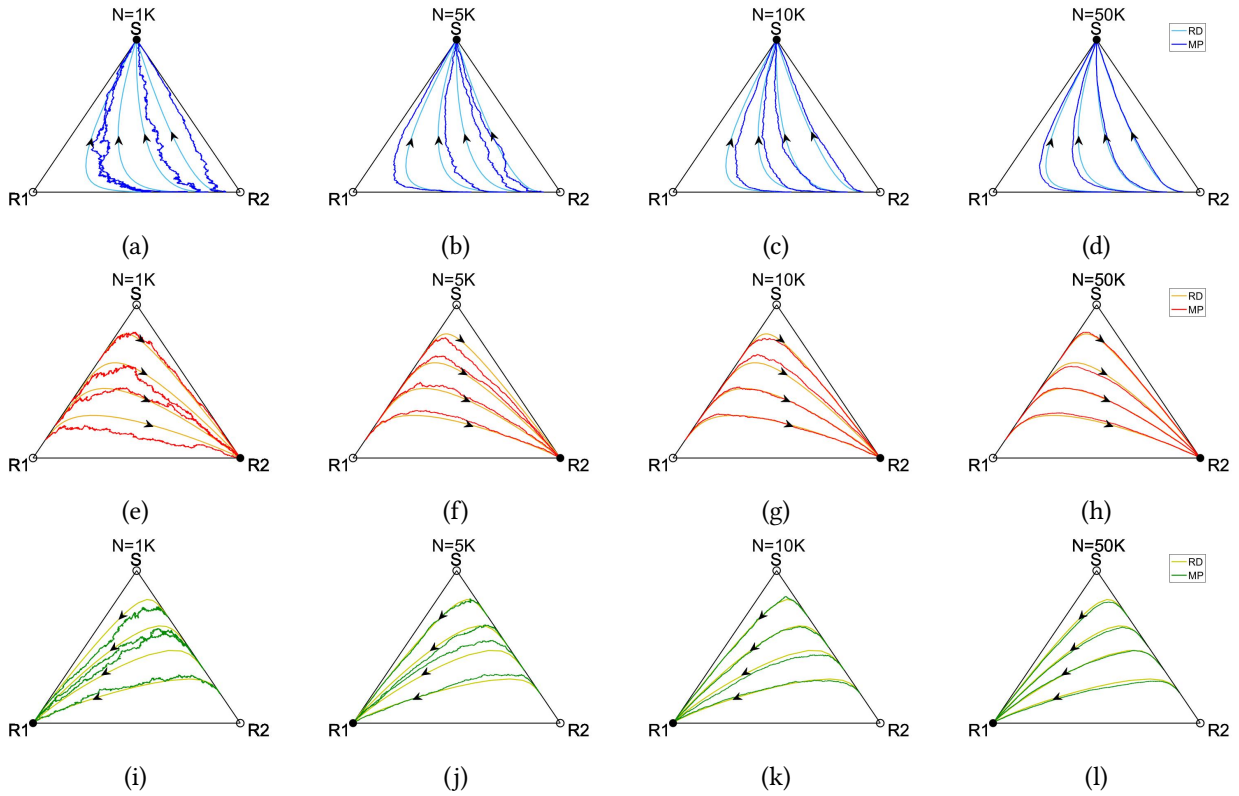

Figure 4.2: Realizations of multiple trajectories associated with the Moran process under administration of different constant chemotherapy combinations of drug 1 and drug 2 ($e = 0$) show the ability of the stochastic system to behave similarly to what the adjusted replicator dynamics drive, getting closer as the population size increases. For example, the Moran process, starting at a state near the corner R_2 with $C_1(t) \equiv 0, C_2(t) \equiv 0$ (blue wiggled lines), possibly evolves and attains the homogeneous population of all S for each N, having smoother trajectories as N increases and finally being similar to the deterministic trajectory (light blue line). (a) $C(t) \equiv 0$, $N = 1K$; (b) $C(t) \equiv 0$, $N = 5K$; (a) $C(t) \equiv 0$, $N = 10K$; (a) $C(t) \equiv 0$, $N = 50K$; (e) $C(t) \equiv 0.7$, $N = 1K$; (f) $C(t) \equiv 0.7$, $N = 5K$; (g) $C(t) \equiv 0.7$, $N = 10K$; (h) $C(t) \equiv 0.7$, $N = 50K$

more similar trajectory to the deterministic one as the population size increases for the same constant chemotherapy schedule of two drugs. According to the relation between the evolutionary step, τ, for the Moran process of size, N, and the evolution time, t, for the deterministic system as in (1.17), the number of steps that is under a chemotherapy schedule is determined. For example, a constant combination of drug 1 and drug 2 are administered during $t \cdot N$ steps for the stochastic Moran process if the same concentration of drugs are delivered for t unit time for the deterministic replicator system. One realization of the Moran process is presented in Figure 4.2 under three drug combinations of two drugs: (i) $C_1 = 0, C_2 = 0$, (ii)

$C_1 = 0.8, C_2 = 0$, or (iii) $C_1 = 0, C_2 = 0.8$ for each $N = 1K$, $5K$, $10K$ and $50K$. For a large $N = 50K$, it is relatively easy to find a stochastic trajectory that moves tightly to the deterministic trajectory for all three drug combinations. Each realization under $C_1 = 0, C_2 = 0$ often ends its journey at the S corner which is the evolutionary stable strategy of the deterministic system. It is true for the other two combinations. For a small N, it is not impossible to obtain a trajectory that moves as the deterministic trajectory does though it is wiggled and off the solid deterministic line and that arrives at the ESS of the deterministic system. However, it hardly takes place in general for as small N as $1K$ that the fixation to that ESS occurs with a positive probability for all drug combinations.

Moreover, overlapping figures, 4.1a, 4.1b and 4.1c, we see that trajectories with three different constant chemotherapy combinations of drug 1 and drug 2 intersect at different times and eventually generate a closed loop in a phase space (Fig.4.1d). On the numerical purpose, we fix $O(0.617, 0.321, 0.062)$, $P(0.44, 0.13, 0.43)$ and $Q(0.807, 0.051, 0.142)$, and consider a deterministic trajectory starting at O, governed by the replicator dynamic under an adaptive schedule. This chemotherapy schedule delivers drug 1 at the constant concentration, $C_1 = 0.8$, with no drug 2 for $T_{OP} := 6.933$ unit time, turns both drugs off for $T_{PQ} := 6.248$ unit time, and administers drug 2 at the constant concentration, $C_2 = 0.8$, with drug 1 missing for $T_{QO} := 6.324$ unit time successively (Fig.4.3a). We call the sum-up time, $T_{OP} + T_{PQ} + T_{QO} = 19.2653$, one evolutionary cycle, and use the term $1/3$ cycle to refer to each piece of time in a cycle for convenience.

As can be seen in the figure 4.3b, under this adaptive chemotherapy schedule the adjusted replicator system starting at O moves along a red line under $C_1 = 0.8$ and $C_2 = 0$ and arrives at P after T_{OP} unit time. Turning chemotherapy off at P, the system begins to have more sensitive cells in a population and reaches O, moving along a blue line, after T_{PQ} unit time since T_{OP}. Again turning chemotherapy on being under $C_1 = 0$ and $C_2 = 0.8$ at O, it finally evolves along a green line and reaches back O in T_{QO} unit time after $T_{OP} + T_{PQ}$, generating a closed loop, $OPQO$, for one evolutionary cycle. When no

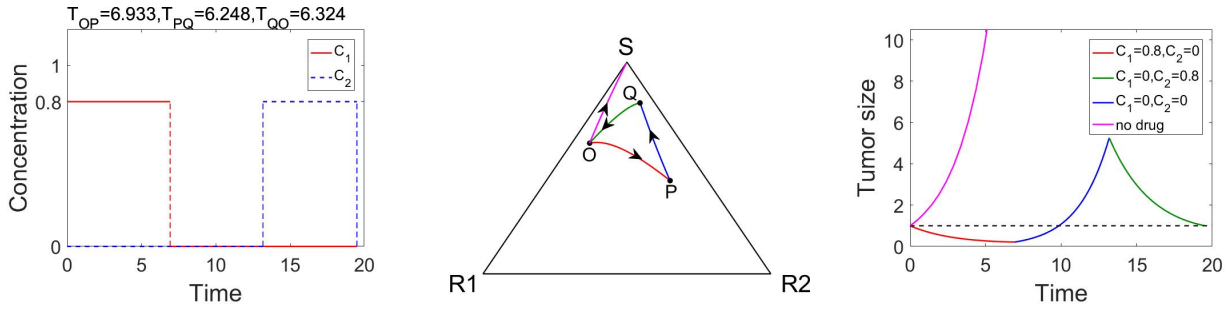

(a) (b) (c)

Figure 4.3: Switching constant chemotherapy combinations of two drugs ($e = 0$) on and off at adequate times traps a trajectory, associated with the adjusted replicator system, within a closed loop, controlling a tumor size. (a) OP: $C_1 = 0.8$, $C_2 = 0$ during $T_{OP} = 6.933$ unit time, PQ: $C_1 = 0$, $C_2 = 0$ during $T_{PQ} = 6.248$ unit time, QO: $C_1 = 0$, $C_2 = 0.8$ during $T_{QO} = 6.324$ unit time; (b) the trajectory treated according to the multi drug additive adaptive schedule and the untreated trajectory (pink) being driven to the S corner; (c) tumor size under untreated (pink) and the adaptive chemotherapy schedule. (For this numerical experiment, we take $g = 1.5519$.)

drug is administered, the system in the state O starts rapidly having more sensitive cells and sensitive cells nearly saturates in a population taking 99.56% within one evolutionary cycle (Fig.4.3b). It is then clear that if both drugs are administered according to the adaptive chemotherapy schedule for longer than 1 cycle, even when 2 cycles, the saturation of cancerous cells is preventable while it would if no drugs were delivered for the same time period.

The efficacy of the application of the adaptive chemotherapy schedule can be seen in terms of tumor volume that is given by the equation in (4.8). It is straightforward that the following equation of an exponential form solves that tumor-growth equation:

$$x_{tumor}(t) = x_{tumor}(0)\exp(\int_0^t (< f > -g) \quad dt). \tag{4.12}$$

Also, it is clear that the solution in (4.12) is T-periodic if g is set to be as follows:

$$g = \int_0^T (< f > -g) \quad dt. \tag{4.13}$$

For the simulation of our specific model with the payoff matrix, A, in (4.6), we set $T = T_{OP} + T_{PQ} + T_{QO}$ to be one cycle and $g = \int_0^T (< f > -g) \quad dt$ as in (4.13) so that the tumor volume returns back to the initial size after one evolutionary cycle when the adaptive chemotherapy schedule is applied. Using the *Euler* method to quantify g followed by some manual adjustment, such g turns out to be equal to 1.5519 for the additive drug interaction case. Setting the initial tumor size to be 1 for simplicity, we see that the first $1/3$ cycle with a high dose of drug 1 reduces the tumor size, the second $1/3$ cycle with no drug used allows the regrowth of tumor, and the last $1/3$ cycle with a high dose of drug 2 mitigates the cancerous condition and resumes the initial tumor size. Continuing the drug use repeatedly along with this adaptive chemotherapy schedule theoretically controls both the state of patients' condition by letting their corresponding deterministic trajectories trapped in a S, R_1, R_2 phase space and the tumor volume going through a series of decreases and an increase. This is a great advantage of designing a chemotherapy schedule compared to when it is untreated. In fact, the tumor size explosively increases if untreated, and the initial tumor size begin 1 reaches over 10 even in the first $1/3$ evolutionary cycle while it decreases reaching nearly 0 when the adaptive chemotherapy schedule is applied (Fig.4.3c).

4.2 Adaptive control of evolutionary cycles with additive multi drug schedule

Now we apply the adaptive chemotherapy schedule (Fig.4.3a) associated with the deterministic adjusted replicator dynamics to the Moran process for a few cycles, and observe for a large N how fast the stochasticity does not justify its application in an additive ($e = 0$) multi drug case by increasing the number of rounds. As seen in Figure 4.2 for constant drug use, the stochastic trajectory evolve around the deterministic trajectory and it is fixated to the corresponding ESS of the deterministic system with nonzero probability. However, it is just one realization and does not represent the overall behavior of the stochastic

process. Like we did in the previous chapter, we simulate $1,000$ realizations of the Moran process in order to understand its behavior through their distribution and their sample mean.

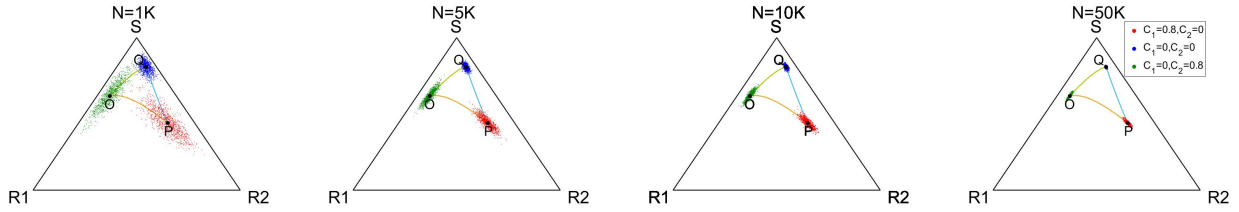

(a) (b) (c) (d)

Figure 4.4: The spread of the distribution of points around P (Q or O) for 1, 000 realizations of the stochastic Moran process gets denser and demonstrates the shrunken randomness as the population size increases when each realization is under the administration of a constant chemo combination $C_1(t) \equiv 0.8, C_2(t) \equiv 0$ ($C_1(t) \equiv 0, C_2(t) \equiv 0$ or $C_1(t) \equiv 0, C_2(t) \equiv 0.8$) with $e = 0$ during $1/3$ evolutionary cycle, T_{OP} (T_{PQ} or T_{QO}), since its exact start at O (P or Q). (a) $N = 1K$; (b) $N = 5K$; (c) $N = 10K$; (d) $N = 50K$

First, for each $N = 1K$, $5K$, $10K$ and $50K$, we apply the adaptive chemotherapy schedule to $1,000$ realizations of the Moran process of size N during $1/3$ evolutionary cycle when each starts at a given point, O, P or Q. The Moran process starting at O under a high constant drug 1 schedule, $C_1 = 0.8$ and $C_2 = 0$ during $T_{OP} \cdot N$ evolutionary steps ends its journey around the point P where the adjusted replicator system settles down after the first $1/3$ evolutionary cycle. Each of terminal points of $1,000$ realizations is indicated as a red dot and they form a cluster near P in Figure 4.4. Likewise, for the second $1/3$ evolutionary cycle, each starts at a fixed point P and evolves as untreated during $T_{PQ} \cdot N$ evolutionary steps. All of them arrives at a point near Q, forming a blue cluster around Q. For the third $1/3$ cycle, all the realizations start at Q and their destiny under a high constant drug 2 schedule, $C_1 = 0$ and $C_2 = 0.8$, is shaped around O as a green cloud. It infers that the tumor size at the last evolutionary step of each $1/3$ cycle driven by the Moran process would be more or less than one associated with the deterministic system (Fig.4.3c).

Obviously, all distributions around O, P and Q are more spread for a small N and they get more centered at the corresponding point as N increases. We zoom in all these clouds and plot them in the principal axis coordinate system (Fig.4.5). We observe that for each fixed constant chemotherapy schedule,

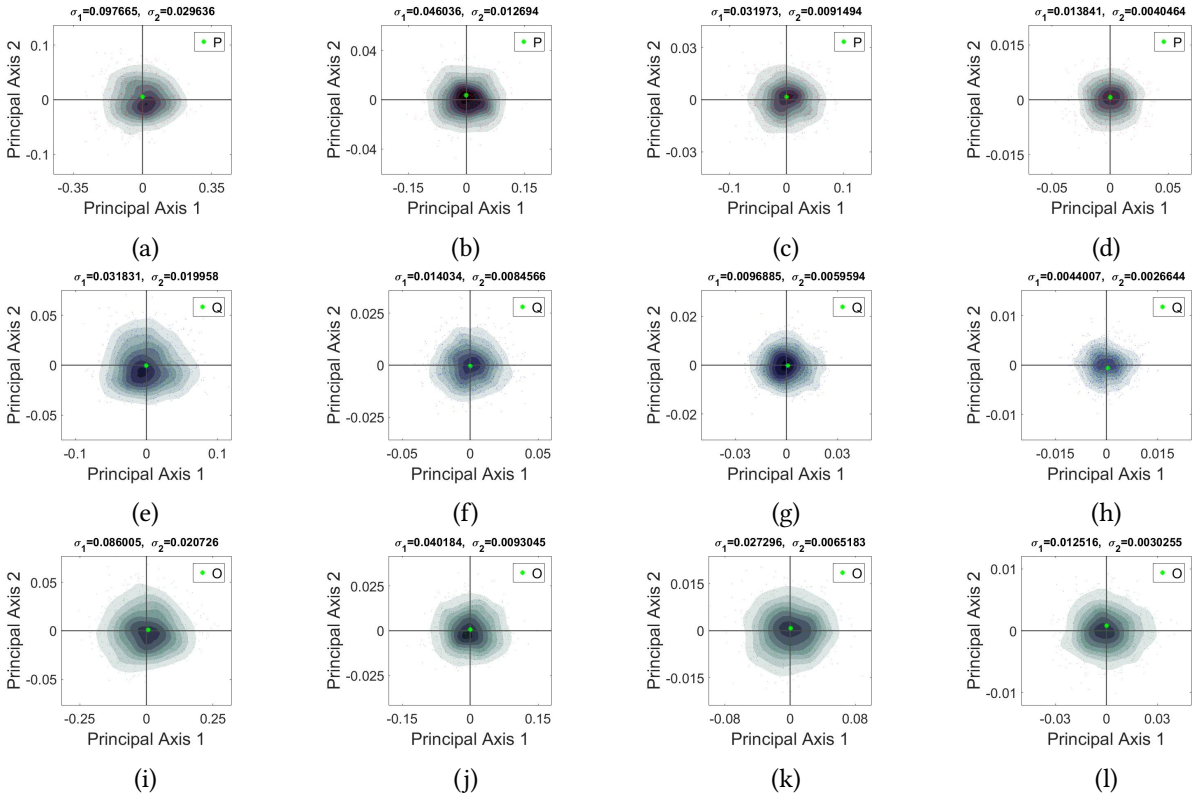

Figure 4.5: The spread of the distribution of points in the principal axis coordinate system for $1,000$ realizations of the Moran process is, for a large population size, characterized as a multivariate Gaussian distribution around P (Q or O) when each realization is under the administration of a constant chemotherapy combination $C_1(t) \equiv 0.8, C_2(t) \equiv 0$ ($C_1(t) \equiv 0, C_2(t) \equiv 0$ or $C_1(t) \equiv 0, C_2(t) \equiv 0.8$) with $e = 0$ during $1/3$ evolutionary cycle, T_{OP} (T_{PQ} or T_{QO}), since its exact start at O (P or Q). As the population size increases, both the semi-major axis, σ_1 and the semi-minor axis, σ_2, decrease. (a) $N = 1K$, $\sigma_1 = 0.0977$, $\sigma_2 = 0.0296$; (b) $N = 5K$, $\sigma_1 = 0.0460$, $\sigma_2 = 0.0127$; (c) $N = 10K$, $\sigma_1 = 0.0320$, $\sigma_2 = 0.0091$; (d) $N = 50K$, $\sigma_1 = 0.0138$, $\sigma_2 = 0.0040$; (e) $N = 1K$, $\sigma_1 = 0.0318$, $\sigma_2 = 0.0120$; (f) $N = 5K$, $\sigma_1 = 0.0140$, $\sigma_2 = 0.0085$; (g) $N = 10K$, $\sigma_1 = 0.0097$, $\sigma_2 = 0.0060$; (h) $N = 50K$, $\sigma_1 = 0.0044$, $\sigma_2 = 0.0027$; (i) $N = 1K$, $\sigma_1 = 0.0860$, $\sigma_2 = 0.0207$; (j) $N = 5K$, $\sigma_1 = 0.0402$, $\sigma_2 = 0.0093$; (k) $N = 10K$, $\sigma_1 = 0.0273$, $\sigma_2 = 0.0065$; (l) $N = 50K$, $\sigma_1 = 0.0125$, $\sigma_2 = 0.0030$

they are distributed following a multi Gaussian with the decreasing semi-major and semi-minor axes in the increase of N. More interestingly, the semi-major and semi-minor axis near Q are significantly small compared to those around either P or O, being approximately three times less. It is true that the expected deterministic system converges, for all three constant drug combinations, to S under $C_1 = 0, C_2 = 0$, R_2 under $C_1 = 0.8, C_2 = 0$, and R_1 under $C_1 = 0, C_2 = 0.8$. However, the expected terminal point around

Q after the second $1/3$ cycle is much closer to its ESS, the S corner, and it leads to the smaller semi-major (-minor) axis.

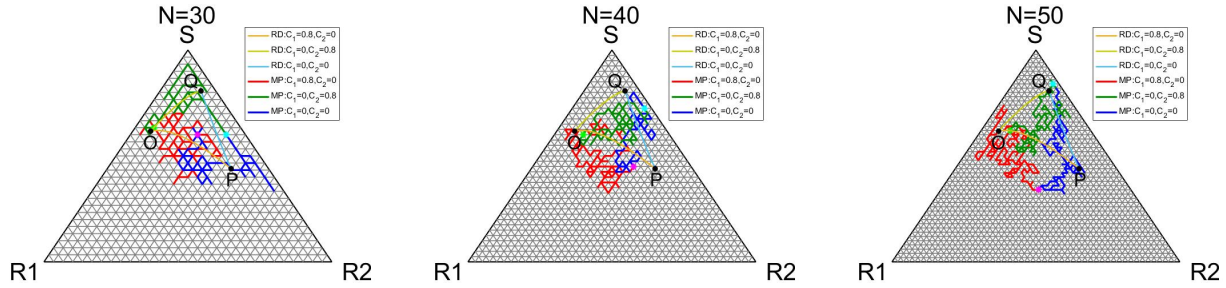

(a) (b) (c)

Figure 4.6: The stochastic trajectory of one realization of the Moran process under the administration of the additive adaptive chemotherapy, associated with the adjusted replicator dynamics, as in Figure 4.3a develops a random walk along a lattice in a phase space, S_2. The adaptive schedule is able to prevent the stochastic system from the saturation of cancer cells, even in a small population with $N = 30$. (a) $N = 30$; (b) $N = 40$; (c) $N = 50$

We now extend the $1/3$ cycle to one full cycle during which the adaptive chemotherapy schedule is applied to the Moran process who starts at O. All figures in the figure 4.6 visualize the random walk of the stochastic process along grids in a phase space for a small N as $N = 30$, 40 and 50. Iterating states of the process that starts at O under $C_1 = 0.8$ and $C_2 = 0$, it travels along red segments while either arriving one of the nearest 6 grid points or staying at the same point in one step, and it finally reaches a pink point after $T_{OP} \cdot N$ evolutionary steps. Turning both drugs off at that pink points drives the process to move along blue segments and arrive at a light blue point in $T_{PQ} \cdot N$ steps. When a high chemo schedule of drug 2 as $C_1 = 0$ and $C_2 = 0.8$ is constantly delivered, the light blue point initiate its move along a green line, terminating its journey at a light green point in $T_{QO} \cdot N$ steps. For these small N, the Moran process rarely return to the neighborhood of the initial point, O, with a high probability. However, with several trials, at least one realization that shows the approximate return to the original point under the adaptive chemotherapy schedule was made.

Increasing the population size, it is more likely that the trajectory of the stochastic process under the adaptive schedule is shaped tightly to the closed loop, $OPQO$, which the associated deterministic

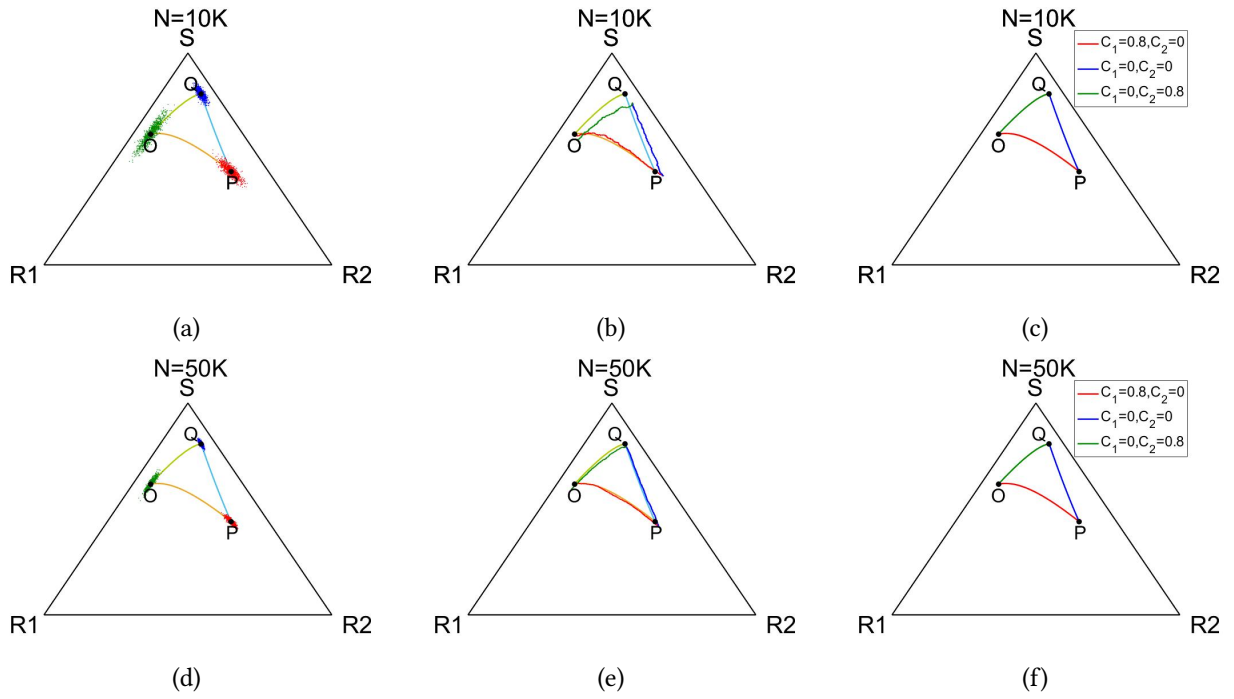

Figure 4.7: The averaged trajectory of $1,000$ realizations of the Moran process under the additive adaptive schedule, associated with the adjusted replicator system, during one round ($T_{OP}+T_{PQ}+T_{QO}=19.2653$ unit time) fits the corresponding deterministic trajectory for a large population size with $e=0$. The Moran process is likely to return nearly to the initial state with a high probability for a large N even though the spread of the distribution of the points near Q is still wide. (a) the distribution of the points associated with the adaptive chemo schedule for $N=10K$; (b) the trajectory of one single realization of the Moran process with $N=10K$; (c) the averaged trajectory of $1,000$ realizations of the Moran process with $N=10K$; (d) the distribution of the points for $N=50K$; (e) the trajectory of one single realization with $N=50K$; (f) the averaged trajectory with $N=50K$

system generates for one full evolutionary cycle, still being off from it. We examine how well or badly the adaptive schedule allows the stochastic system to resume its initial frequency after one evolutionary cycle for $1,000$ realizations of the Moran process. Each realizations starts at O and both the second and the third $1/3$ evolutionary cycles start at the point where their previous $1/3$ cycle ends. Our simulation of $1,000$ realizations of the Moran process is given with the population size $N=10K$ and $50K$ in Figure 4.7. For each N, each simulation starts at O and it proceeds under $C_1=0.8$ and $C_2=0$ for the first $1/3$ evolutionary cycle, arriving at one of red points near P (Fig.4.7a,4.7d).

At the red point, both drugs starts being taken off and it is led to one of blue points near O by no drug strategy at the end of the second $1/3$ cycle. The blue point is finally transferred to one of green point

near O under $C_1 = 0$ and $C_2 = 0.8$ after the last $1/3$ cycle. Indicating trajectories along grids under the different constant drug combinations in red, blue and green in order, the trajectory of one such realization is given in Figure 4.7b and the figure 4.7e for $N = 10K$ and $N = 50K$, respectively. Both stochastic trajectories are drawn around the deterministic trajectory, $OPQO$, though it fits better the closed loop, $OPQO$, with the bigger population size.

In order to understand the general behavior of the stochastic process with the fixed size, simulation of $1,000$ such independent Moran process is carried out and it produces the distribution of points around O, P and Q. It is obviously expected that the spread of the distribution of points is denser with the bigger population as can be seen in Figure 4.7a and Figure 4.7d. However, even with this bigger deviation in distribution when $N = 10K$, the averaged trajectories in Figure 4.7c of those $1,000$ realizations of the Moran process already well represents its limiting system.

One other thing to point out in Figure 4.7a and Figure 4.7d is when each of these is compared to Figure 4.4c and Figure 4.4d with the same population size. Points in Figure 4.7a and Figure 4.7d are more widely spread around Q and O. It is because, for example, the distribution of points near Q in Figure 4.4 is obtained when the adaptive chemotherapy schedule is applied to the Moran process that starts at the fixed point, P, in order to observe the short term influence during $T_{PQ} \cdot N$ evolutionary steps. However, Figure 4.7 is given with the more extended perspective that it is for understanding the longer term influence of the chemotherapy schedule, thus, the stochastic process that ends at one of red dots near P starts at that point for the next $1/3$ cycle instead of beginning at the exact point, P. This perturbation in the initial state for the second or the third $1/3$ cycle results in the greater deviation of the distribution of points around Q or O.

This is numerically better supported in terms of the semi-major (-minor) axis of the distribution of points around O when they are plotted in the principal axis coordinate system as shown in Figure 4.8. With $N = 10K$, the semi-major axis is equal to $\sigma_1 = 0.0273$ and the semi-minor axis is equal to $\sigma_2 = 0.0065$

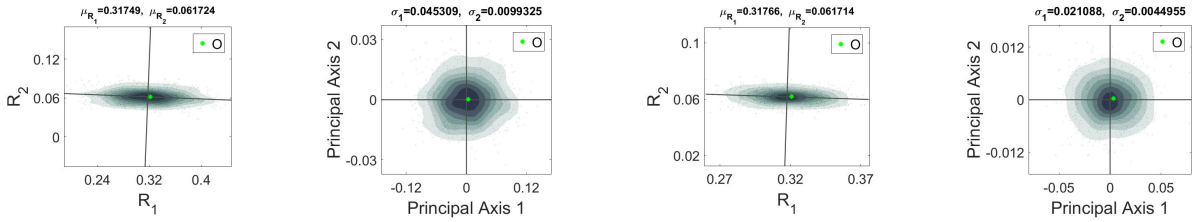

(a) (b) (c) (d)

Figure 4.8: The spread of the distribution of points for $1,000$ realizations of the stochastic Moran process is characterized as a multivariate Gaussian distribution, centered nearly at the initial point, O, when each realization is under the administration of the multi drug adaptive chemo schedule associated with the adjusted replicator dynamics during one round ($T_{OP} + T_{PQ} + T_{QO} = 19.2653$ unit time) with $e = 0$. The mean frequency, μ_{R_1} (or μ_{R_2}), of the subpopulation, R_1 (or R_2), around the point, O, converges to the proportion of R_1 (or R_2) as N increases, with the decreasing semi-major axis, σ_1, and semi-minor axis, σ_2. (a) $N = 10K$, $\mu_{R_1} = 0.3175$, $\mu_{R_2} = 0.0617$; (b) $N = 10K$, $\sigma_1 = 0.0453$, $\sigma_2 = 0.0099$; (c) $N = 50K$, $\mu_{R_1} = 0.3177$, $\mu_{R_2} = 0.0617$; (d) $N = 50K$, $\sigma_1 = 0.0211$, $\sigma_2 = 0.0045$

for the distribution of points near O when the third piece of the adaptive chemotherapy schedule is applied to the Moran process starting at Q as shown in Figure 4.5k while $\sigma_1 = 0.0453$ and $\sigma_2 = 0.0099$ at the end of the full one cycle of the adaptive schedule as in Figure 4.8b. It is true for $N = 50K$ that the deviation of the distribution of points at the end of one full cycle of the adaptive chemotherapy schedule is bigger than one in the last $1/3$ cycle due to the accumulated randomness in the initial points in the last two $1/3$ cycles.

Moreover, the distribution of points around O driven by the application of the adaptive chemotherapy schedule during one full evolutionary cycle closely follows the multi Gaussian centered closely to O (Fig.4.8b, 4.8d). In fact, the mean frequency, μ_{R_1}, of the R_1 subpopulations is equal to $\mu_{R_1} = 0.31749$ and the mean frequency, μ_{R_2}, of the R_2 subpopulations is equal to $\mu_{R_2} = 0.061724$ for $N = 10K$ while $\mu_{R_1} = 0.31766$ and $\mu_{R_2} = 0.061714$ for $N = 50K$ (Fig.4.8a,4.8c). Knowing the proportion of subpopulations, $(S, R_1, R_2) = (0.617, 0.321, 0.062)$, at O, it is shown that the center of the distribution is closely located to O with the reduced norm for the bigger population size. Furthermore, plotting the points in the R_1R_2 coordinate system shows that the R_1 axis almost coincides with the major principal axis and the R_2 axis with the minor principal axis, explaining that the continuous delivery of drug 2 in high concentration

in the last $1/3$ evolutionary cycle mostly forces the trade-off between the sensitive cells S and the resistant cells R_1 to drug 2.

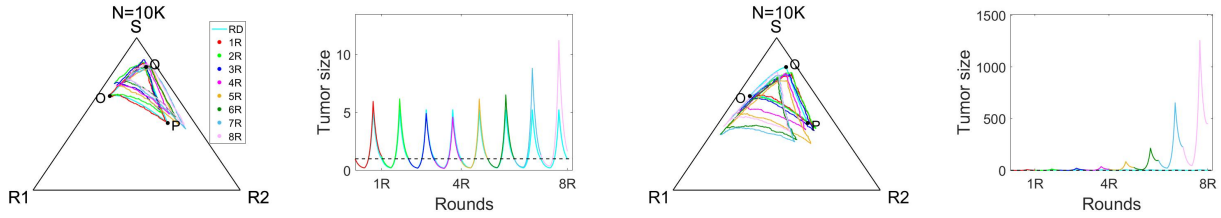

Figure 4.9: Two realizations of the stochastic Moran process of size $N = 10K$, starting at O and evolving under the adaptive chemo schedule during 8 rounds with $e = 0$, show a great difference in their tumor size as well as in their trajectories. (a) one realization; (b) corresponding tumor size to Figure 4.9a; (c) another realization; (d) corresponding tumor size to Figure 4.9c

We have just seen that the stochastic Moran process with as a big population size, N, as $N = 10K$ or $50K$ returns closely to the initial state on average in one evolutionary cycle of the adaptive chemotherapy schedule. It implies that the deduced tumor size using the tumor-growth equation in (4.8) is overall controlled undertaking a series of increases and decreases as the tumor size associated with the adjusted replicator system drops during the first $1/3$ cycle, rises up when untreated for the second $1/3$ cycle, and reduces during the third $1/3$ cycle, finally recovering the initial tumor size at the end of the one full evolutionary cycle. In order to answer the justification of the use of drugs according to the adaptive chemotherapy schedule, we continued this adaptation for 8 evolutionary cycles to the Moran process of the size $N = 50K$. It starts at O for the first round, and each round starts at the state where the previous round ends. For example, one realization of the Moran process starting at O terminates at one of green points at the end of one evolutionary cycle, which we call a round interchangeably. Then, the second round starts at that point instead of the exact point, O, and the following round begins in the same manner.

Two realizations of such application to the Moran process of size $N = 10K$ whose trajectories do not converge to any of cancerous states within 8 cycles are presented in Figure 4.9. Figure 4.9a and Figure 4.9c show that their trajectories maintain a triangle-like shape in each cycle without being fixated to a

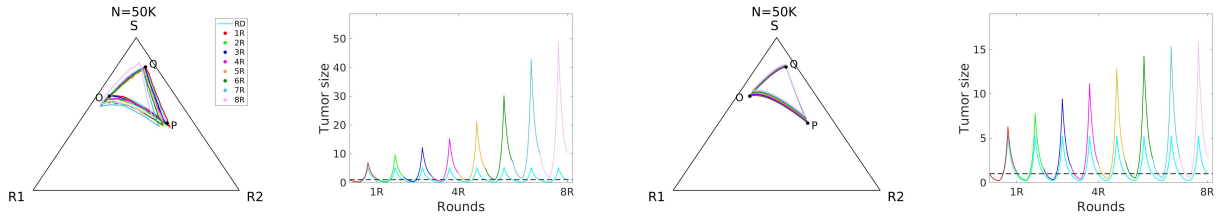

Figure 4.10: $1,000$ realizations of the stochastic Moran process with size $N = 50K$ show that the saturation of cancer cells can be delayed until the end of 8th round when each realization evolves under the administration of the multi drug adaptive chemo schedule, associated with the adjusted replicator system, with $e = 0$ during 8 rounds since its exact start at O. (a) one realization; (b) tumor size corresponding to Figure 4.10a; (c) the averaged trajectory of $1,000$ realizations; (d) the averaged tumor size corresponding to Figure 4.10c

cancerous state though they closely evolve around the deterministic trajectory, $OPQO$, only up to first a few rounds. Nonetheless, the tumor size associated with Figure 4.9a does not have a monotonically increasing maximum value of each cycle and gets doubled in the 7th round while one associated with Figure 4.9d incredibly soaks being over 500 in the same round. Likewise, each realization of the stochastic process results in apparently different dynamic and understanding stochastic process in distribution is needed.

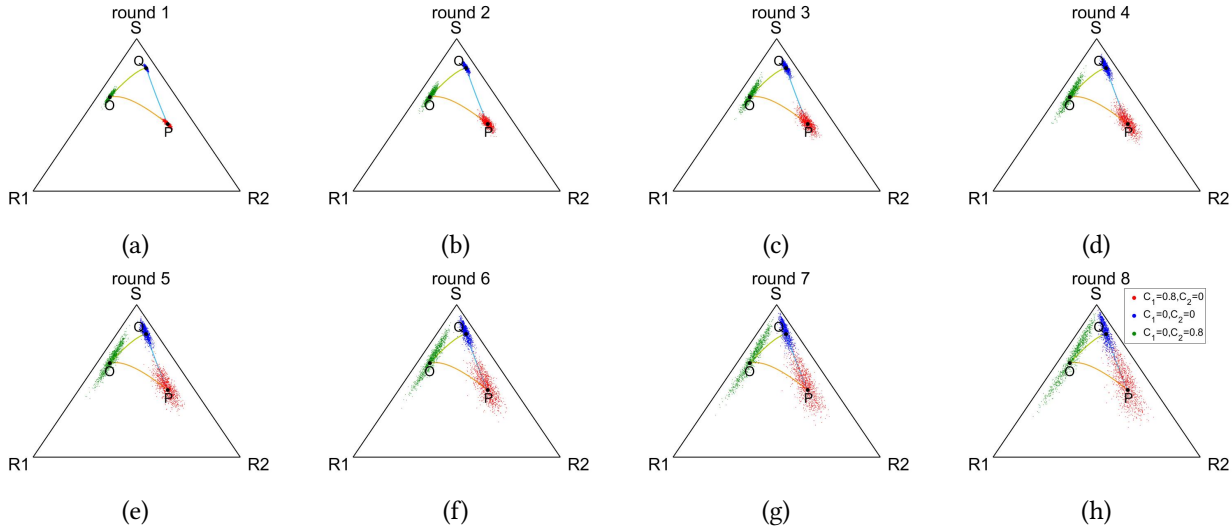

Figure 4.11: The spread of the distribution of terminal points (green dots) around O in each round for $1,000$ realizations of the stochastic Moran process with size $N = 50K$ becomes wider as the number of rounds increases when each realization evolves under the administration of the multi drug adaptive chemo schedule, associated with the adjusted replicator system, with $e = 0$ during 8 rounds since its exact start at O. (a) round 1; (b) round 2; (c) round 3; (d) round 4; (e) round 5; (f) round 6; (g) round 7; (h) round 8

One another realization of the Moran process with a bigger population size $N = 50K$ whose trajectory moves more closely around the deterministic trajectory, $OPQO$, for the entire cycles is given in Figure 4.10a along with the associated tumor size in Figure 4.10b. For this bigger population size, the maximum of the tumor size in each cycle gradually increases as the number of rounds increases for this single simulation, and this pattern turns out to be true for the averaged trajectory of $1,000$ realizations of the Moran process and its related tumor size when $N = 50K$ (Fig.4.10c,4.10d). The trajectory under the adaptive chemotherapy schedule gradually shifts towards the S corner on average and it leads to the rise in the maximum of the tumor size attained at the end of the second $1/3$ cycle as the number of cycle increases. Finally, the tumor size that is initially equal to 1 reaches over 15 within 8 cycles though it is reduced to under 5 at the end of the 8th cycle.

Focusing on the spread of the distribution of points around O for $1,000$ realizations of the stochastic Moran process of size $N = 50K$, we indicate them as green points at the end of each cycle (Fig.4.11). They form a cloud each cycle, and it gets less thick as the number of rounds increases and some of them mostly consisted of sensitive cells. It is clear that the spread is relatively small in R_2 subpopulations but the randomness is more reflected in the proportion of S or R_1 subpopulations.

This spread is measured through the semi-major and the semi-minor axis by plotting the points in each cycle in the principal axis coordinate system (Fig.4.12). The spread overall follows the multi Gaussian distribution at the end of the first round, but it gradually starts being distorted from the following round, having the center of the cloud off the most dense part. The semi-major axis which is equal to $\sigma_1 = 0.0211$ in the first round increases roughly by 6 times in 8 cycles while the semi-minor axis being equal to $\sigma_2 = 0.0045$ in the first round increases by 3 times. The more rapid rate of increase of the semi-major axis in the number of rounds is also described in Figure 4.13a and Figure 4.13c for the population sizes $N = 10K$ and $N = 50K$, respectively, where darker dots represent the semi-major axis and lighter green dots stand for the semi-minor axis. As seen in these raw data, both metrics increase nonlinearly in the number of rounds,

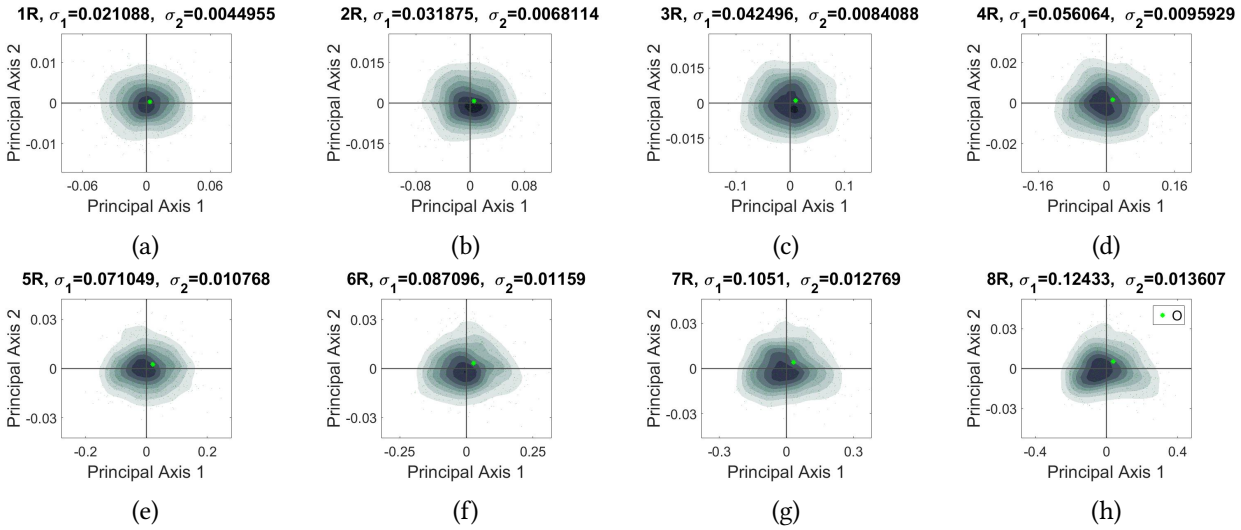

Figure 4.12: The spread of the distribution of points around O for $1,000$ realizations of the stochastic Moran process of size $N = 50K$, all starting at O and evolving under the multi drug adaptive chemo schedule with $e = 0$ during 8 rounds, shows the increase of both the semi-major axis, σ_1, and the semi-minor axis, σ_2, in the principal axis coordinate system as the number of rounds increases. (a) round 1, $\sigma_1 = 0.0211$, $\sigma_2 = 0.0045$; (b) round 2, $\sigma_1 = 0.0319$, $\sigma_2 = 0.0068$; (c) round 3, $\sigma_1 = 0.0425$, $\sigma_2 = 0.0084$; (d) round 4, $\sigma_1 = 0.0561$, $\sigma_2 = 0.0096$; (e) round 5, $\sigma_1 = 0.0710$, $\sigma_2 = 0.0108$; (f) round 6, $\sigma_1 = 0.0871$, $\sigma_2 = 0.0116$; (g) round 7, $\sigma_1 = 0.1051$, $\sigma_2 = 0.0128$; (h) round 8, $\sigma_1 = 0.1243$, $\sigma_2 = 0.0136$

definitely with the fact that both of them are bigger with a smaller population size. For each population size, we could see that the semi-major (-minor) axis has the power-law dependency on the number of rounds, and the fitted curves to the semi-major axis, σ_1, and the semi-minor axis, σ_2, with $N = 10K$ are given below in the *log-log* scale:

$$\begin{aligned} \sigma_1 &\sim 0.0412 \cdot n^{0.7782}, \\ \sigma_2 &\sim 0.0105 \cdot n^{0.4967}, \end{aligned} \tag{4.14}$$

where n is the number of rounds. Similarly, with $N = 50K$,

$$\begin{aligned} \sigma_1 &\sim 0.0186 \cdot n^{0.8602}, \\ \sigma_2 &\sim 0.0046 \cdot n^{0.5235}. \end{aligned} \tag{4.15}$$

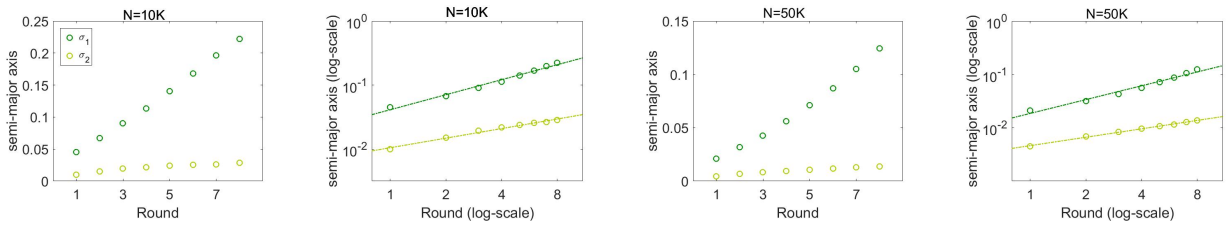

(a) (b) (c) (d)

Figure 4.13: The semi-major (and -minor) axis of the distribution of the points around O at the end of each round for $1,000$ realizations of the Moran process overall increases in the number of rounds, showing the power-law dependency, where each realization evolves under the administration of the multi drug adaptive chemo schedule associated with the adjusted replicator system with $e = 0$ during 8 rounds since its exact start at O. (a) $N = 10K$; (b) $N = 10K$, the log-log fit; (c) $N = 50K$; (d) $N = 50K$, the log-log fit

From these equations in (4.14) and (4.15), we check that the semi-major axis has a bigger increase rate than the semi-minor axis does for each N, meaning that the spread of the distribution of points near O at the end of each cycle is made more rapidly in the direction of the major principal axis than towards the both direction of the minor principal axis. It is also observed that for each i the increase rate of σ_i with $N = 50K$ is bigger in the log-log scale, however, σ_i is a dominating function with $N = 10K$ during 8 evolutionary cycles in the raw scale. In other words, despite of the fact that the distribution becomes more rapidly disseminated with a bigger population size $N = 50K$, the absolute spread with $N = 50K$ is not as larger as one with $N = 10K$ due to the stronger randomness from a smaller population size.

4.3 Adaptive control of evolutionary cycles with synergistic and antagonistic multi drug schedules

The multi drug adaptive chemotherapy schedule helps delay the saturation of cancerous cells on average for the $1,000$ realizations of the Moran process and it keeps tumor size well controlled compared to the case under no treatment when two drugs are additive for a few evolutionary cycles. In fact, the averaged trajectory circles around the closed loop, $OPQO$, that the adjusted replicator system associated with the adaptive schedule produces during one evolutionary cycle when the adaptive schedule is designed as if

each drug concentration function, $C_i(t)$, is a step function between two different levels, 0.8 and 0, across over time (Fig.4.3a). In this section, we have a similar question: how long and how well/badly the adaptive schedule overall helps postpone the direct increase of tumor volume, which would be attained if untreated, when a finite population is modeled through the Moran process with a large enough size and, more importantly, when two drugs act either synergistically or antagonistically. The drug interaction parameter, e, ranging from -1 to 1 is what it determines if the action of two drugs are antagonistic, additive or synergistic. Recall that two drugs are additive when $e = 0$, two drugs interact synergistically when $e > 0$ and they interact antagonistically when $e < 0$. For simulation, we fix the value of e as such $e = 0.3$ for synergistic and $e = -0.3$ for antagonistic drug interactions.

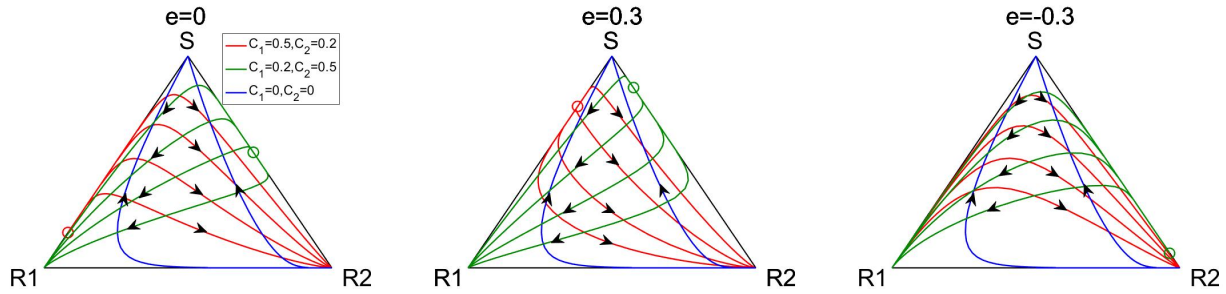

(a) (b) (c)

Figure 4.14: Deterministic trajectories describe the evolutionary stable states (ESS) of the adjusted replicator system for different constant chemotherapy values for each drug interaction. Under $C_1 = 0$ and $C_2 = 0$, the tumor saturates to the S corner regardless of the initial distribution of the three subpopulations. Under $C_1 = 0.5$ and $C_2 = 0.2$, the competitive release of the resistant subpopulations, R_2, to drug 1 drives all trajectories to the R_2 corner. Under $C_1 = 0.2$ and $C_2 = 0.5$, the competitive release of the resistant subpopulations, R_1, to drug 2 drives all trajectories to the R_1 corner. (a) $e = 0$; (b) $e = 0.3$; (c) $e = -0.3$

We also consider a new combination of two drugs of constant concentration such as $C_i(t) \equiv 0.2$ or $C_i(t) \equiv 0.5$ instead of the combination of $C_i(t) \equiv 0$ and $C_i(t) \equiv 0.8$ since this combination leads to trajectories of the adjusted replicator dynamics traversing more widely in a phase space over time when they start at the same set of initial points for each value of e that we set, and hence it allows us to more easily come up with an shared initial distribution at which the adaptive chemotherapy schedule starts its play.

We present the numerical result for additive drug interaction case as well as synergistic and antagonistic cases for comparison under this new combination of drug concentration.

The numerical simulation describes evolutionary stable states of the adjusted replicator system for different constant chemotherapy combinations of drug 1 and drug 2 in Figure 4.14. For all the values of drug interaction parameter, e, such as $e = 0, \pm 0.3$, the deterministic system is driven to the S corner regardless of the initial distribution of the three subpopulations when no treatment is carried out. The tumor saturates to the R_2 corner when a higher concentration of drug 1 is constantly administered, precisely when $C_1 = 0.5$ and $C_2 = 0.2$, and this results from the competitive release of the resistant subpopulations R_2 to drug 1. In the same manner, the competitive release of the resistant subpopulations R_1 to drug 2 drives all trajectories to the R_1 corner when a higher concentration of drug 2 is continuously delivered. With the fixed drug use, trajectories are distinguished by having a different unstable fixed point for each e though the deterministic system have the unique evolutionary stable state regardless of the value of e considered. For example, the unstable fixed point composed of only S and R_1 subpopulations, which is indicated as a red open dot in Figure 4.14, under $C_1 = 0.5$ and $C_2 = 0.2$ represents a state that consists of more S subpopulations when $e = 0.3$. This keeps consisting of more R_1 subpopulations as e decreases, and it eventually merges into the homogenous state, R_1, before it reaches $e = -0.3$. Similarly, the unstable fixed point with no R_1 population, which is marked as a green open dot, under $C_1 = 0.5$ and $C_2 = 0.2$ refers to a state having a higher proportion of S subpopulations when $e = 0.3$ while a smaller frequency of S when $e = -0.3$. Basically, the drug interaction parameter, e, plays the role of relocation of an unstable fixed point, not changing the nature of the system in terms of the evolutionary stability with this new drug combination.

It is also seen in Figure 4.14 that for each e, trajectories with three different constant chemotherapy combinations of drug 1 and drug 2 overlap at different times and generate a clear-cut closed loop. Fixing a point $O(0.812, 0.123, 0.065)$, we consider two drug adaptive chemotherapy schedules by which the

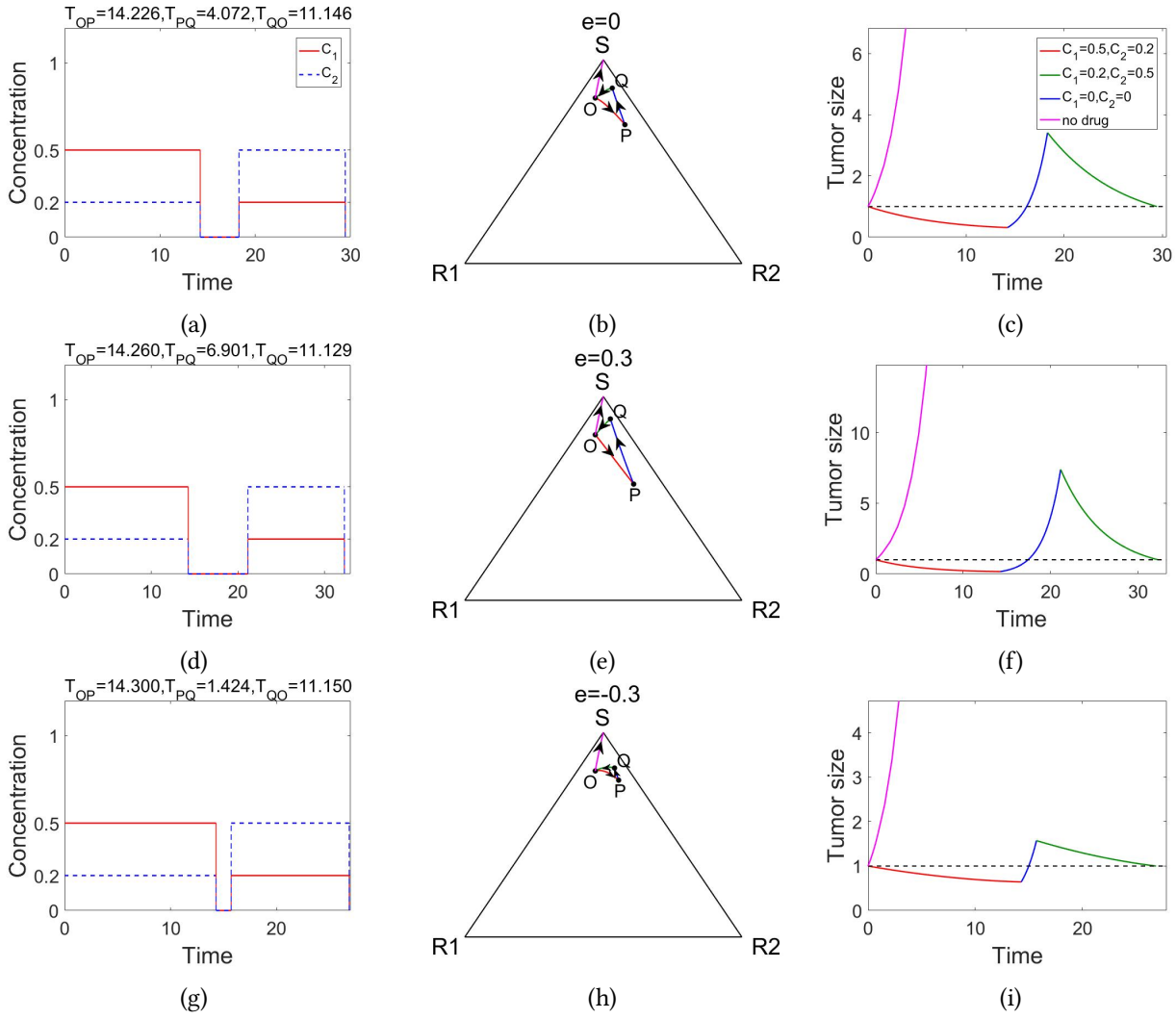

Figure 4.15: Deterministic evolution of subpopulations, S, R_1 and R_2, by the adjusted replicator system generates a closed loop, $OPQO$, when it starts at O and evolves under the multi drug adaptive chemotherapy schedule during one round, resulting in the tumor size controlled. (a) With $e = 0$, the total dose delivered to generate one evolutionary cycle is 17.7604 during 29.4440 unit time. OP: $C_1 = 0.5$, $C_2 = 0.2$ during $T_{OP} = 14.226$ unit time, PQ: $C_1 = 0$, $C_2 = 0$ during $T_{PQ} = 4.072$ unit time, QO: $C_1 = 0.2$, $C_2 = 0.5$ during $T_{QO} = 11.146$ unit time; (b) the corresponding deterministic trajectory; (c) the corresponding tumor size with the averaged background fitness, $g = 1.4527$; (d) With $e = 0.3$, the total dose delivered to generate one evolutionary cycle is 17.7723 during 32.29 unit time. OP: $C_1 = 0.5$, $C_2 = 0.2$ during $T_{OP} = 14.260$ unit time, PQ: $C_1 = 0$, $C_2 = 0$ during $T_{PQ} = 6.901$ unit time, QO: $C_1 = 0.2$, $C_2 = 0.5$ during $T_{QO} = 11.129$ unit time; (e) the corresponding deterministic trajectory; (f) the corresponding tumor size with $g = 1.4857$; (g) With $e = -0.3$, the total dose delivered to generate one evolutionary cycle is 17.8150 during 26.8740 unit time. OP: $C_1 = 0.5$, $C_2 = 0.2$ during $T_{OP} = 14.300$ unit time, PQ: $C_1 = 0$, $C_2 = 0$ during $T_{PQ} = 1.424$ unit time, QO: $C_1 = 0.2$, $C_2 = 0.5$ during $T_{QO} = 11.150$ unit time; (h) the corresponding deterministic trajectory; (i) the corresponding tumor size with $g = 1.4182$

adjusted replicator dynamic that starts at the exact O generates a closed loop, $OPQO$, in its own evolutionary cycle for each e as shown in Figures 4.15b, 4.15e, 4.15h. For all these values of e, drug delivery under $C_1 = 0.5$ and $C_2 = 0.2$ causes the deterministic system to traverse a red line and reaches P in T_{OP} unit times. When it is switched to $C_1 = 0$ and $C_2 = 0$ at P, the system reaches Q moving along a blue line in T_{PQ} unit times. Then drug starts being delivered in the concentration $C_1 = 0.2$ and $C_2 = 0.5$, and it results in the arrival of the system at O in T_{QO} unit times. Note that the initial state O is directed to the S corner for all drug interaction cases if it is chemotherapeutically untreated as seen along with a closed loop, $OPQO$.

However, the two drug adaptive chemotherapy schedule creates a closed orbit in the trajectory of the deterministic system during one evolutionary cycle avoiding the saturation of tumor though the time periods, T_{OP}, T_{PQ} or T_{QO}, under a piece of fixed constant drug combination all differ from each other for all e. These schedules with the exact time periods for each legs of OP, PQ and QO are precisely given for each case in Figures 4.15a, 4.15d, 4.15g. We agree that each e shares the same starting point O but neither P nor Q as well as neither T_{OP}, T_{PQ} nor T_{QO}. However, since no confusion arises, we use the same notations for those points at which the chemotherapy schedule changes drug concentration, and specify if needed.

e	-0.3	0	0.3
D	17.8150	17.7604	17.7723
T	26.8740	29.4440	32.2900
D/T	0.6629	0.6032	0.5504

Table 4.1: total dose (D), total time (T), and average dose (D/T) associated with adaptive chemotherapy schedules with antagonistic, additive and synergistic drug interactions during one evolutionary cycle.

Our attempt to come up with closed loops $OPQO$ that are created using, ideally, the same total dose during one evolutionary cycle for all e's numerically ended up being with closed orbits created using not a fixed but similar amount of total dose in different total times instead. All these quantities such as total

time, T (one evolutionary cycle), total dose, D, and the averaged dose, D/T, used for our simulation for one evolutionary cycle is given in Table 4.1 following the same notation in [30]. When two drugs are additive, the adaptive schedule (Fig.4.15a) uses 17.7604 dose in total from both drugs causing the system to be trapped in the closed loop $OPQO$ during one evolutionary cycle, 29.4440. When two drugs interact synergistically, the schedule (Fig.4.15d) uses 17.7723 in total and the associated trajectory creates a bigger closed loop during the longer time period, 32.2900 unit times. In contrast, using 17.8150 in total when two drugs interact antagonistically, the schedule (Fig.4.15g) generates the smallest loop during the shortest time period, 26.8740. What is understood in Table 4.1 is that using similar total dose being equal to about 17.78, the closed loop is generated distinguishably faster when two drugs interact antagonistically and this leads to the highest averaged total dose during one evolutionary cycle.

e	-0.3	0	0.3
g	1.4182	1.4527	1.4857

Table 4.2: the constant background fitness (g) associated with adaptive chemotherapy schedules for antagonistic, additive and synergistic drug interactions.

Another observation is made in terms of tumor size for all drug interactions. Tumor size that is assumed to be equal to 1 initially grows or decays according to the tumor-growth equation in (4.8), where the constant background fitness, g, is defined by the equation in (4.13). These background fitness g's associated with the adaptive chemotherapy schedules in Figure 4.15a, 4.15d, 4.15g are computed in Table 4.2 for each drug interaction, and each of these values enable tumor size to recover the initial volume at the end of one evolutionary cycle going through a series of rises and declines. What is observed in all cases in common is that tumor size initially reduces when a higher chemo dose of drug 1 is administered, rises when no chemotherapeutic treatment is done, and decreases again when a higher chemo dose of drug 2 is delivered, reaching back the initial volume in one evolutionary cycle. That is, tumor size is controlled when the two drug adaptive chemotherapy schedule is applied during one evolutionary cycle and hence as many times as

desired. This is a great advantage of the use of the adaptive schedule since tumor size dramatically soaks if no drugs are administered. In fact, tumor size under no drug surpasses its maximum in the adaptive therapy scenario even earlier than the first $1/3$ cycle ends for all drug interaction cases. Though tumor is controlled in size as a result of the adoption of the adaptive chemo schedule, it is significantly different in deviation. Compared to the additive drug interaction case, the variation in tumor size is greater when two drugs interact synergistically while it is smaller when two drugs interact antagonistically, and this is compatible with the size of the closed loop, $OPQO$. The bigger the closed loop is, the greater tumor size deviates during one cycle.

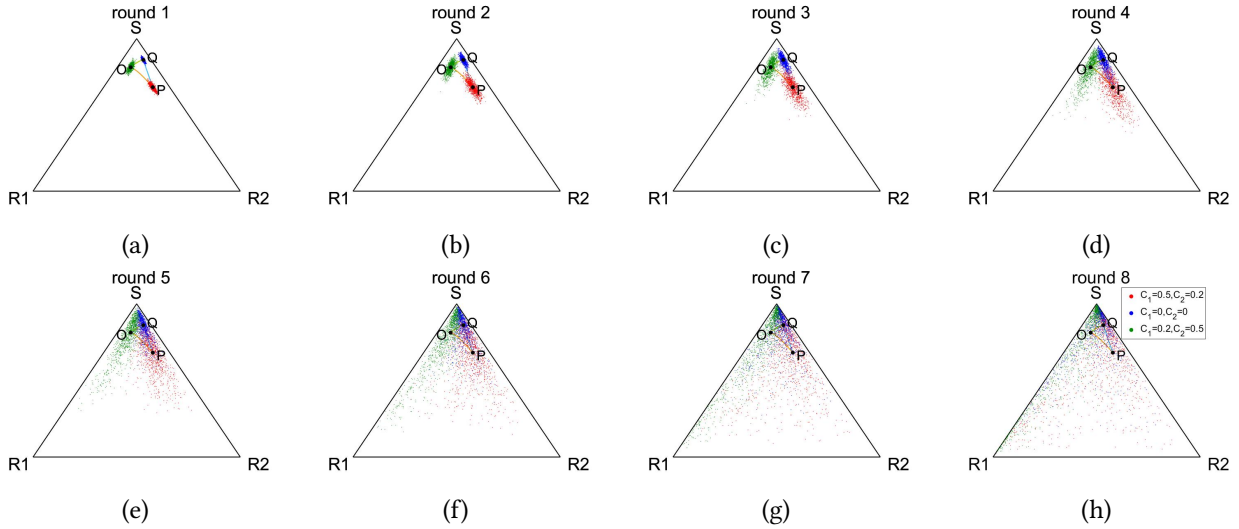

Figure 4.16: The spread of the distribution of terminal points (green dots) around O in each round for $1,000$ realizations of the stochastic Moran process with size $N = 50K$ becomes wider as the number of rounds increases when each realization evolves under the administration of the multi drug additive ($e = 0$) adaptive chemo schedule, associated with the adjusted replicator system, as in Figure 4.15a during 8 rounds since its exact start at O. (a) round 1; (b) round 2; (c) round 3; (d) round 4; (e) round 5; (f) round 6; (g) round 7; (h) round 8

Now, we apply the adaptive chemotherapy schedule associated with the deterministic adjusted replicator system to the Moran process of a large but finite population size N, $N = 50K$, starting at O, and figure out up to how many of 8 cycles this adoption is valid by comparing averaged trajectories and tumor sizes of $1,000$ realizations of the Moran process for antagonistic, additive and synergistic drug

interactions represented with parameters, $e = -0.3,\ 0,\ 0.3$, respectively. For the purpose of comparison, we will first look into the additive drug interaction case. Note that the one evolutionary cycle, $T := T_{OP} + T_{PQ} + T_{QO} = 29.4440$ unit times, associated with the adaptive chemo schedule in Figure 4.15a when $e = 0$ corresponds to the evolutionary steps, $\tau := T \cdot N = 1,472,200$, for the Moran process with $N = 50K$. In $1,472,200$ evolutionary steps, $1,000$ realizations of the Moran process that start at O form a distribution of points near O, at which each of them starts its following run during the same number of evolutionary steps.

Applying the adaptive chemo schedule during 8 cycles in this manner, we get 8 individual spreads of distribution of points around O from each round, and those points are depicted as green dots in Figure 4.16. Since the adaptive schedule that we are applying is associated with the deterministic schedule that both starts and ends at O, the gradual larger deviation in distribution in the increase of the number of runs from the continued adoption of this schedule is definitely expected not only by the stochastic structure itself but also by the fact that the initial point of each round is not the exact O but a neighborhood from the second round.

Plotting the points near O in the principal axis coordinate system and computing the semi-major axis, σ_1, and semi-minor axis, σ_2, for each run gives more comprehensive understanding (Fig.4.17). Applying the adaptive schedule one round guarantees its use for the later round since the spread of the distribution of the terminal points around O is closely centered at the initial point, O, and, in addition it follows the multi Gaussian distribution. Until the 3rd round, the application of this chemo schedule seems to suitably control the stochastic dynamic allowing the system to return back to the starting point on average although both the semi-major axis and the semi-minor axis increase as the number of rounds goes. However, the distribution starts being off the initial point, O, from the 4th round and the spreads are not anymore densely disseminated around its mean with the increasing distance from O, losing the Gaussian distribution form.

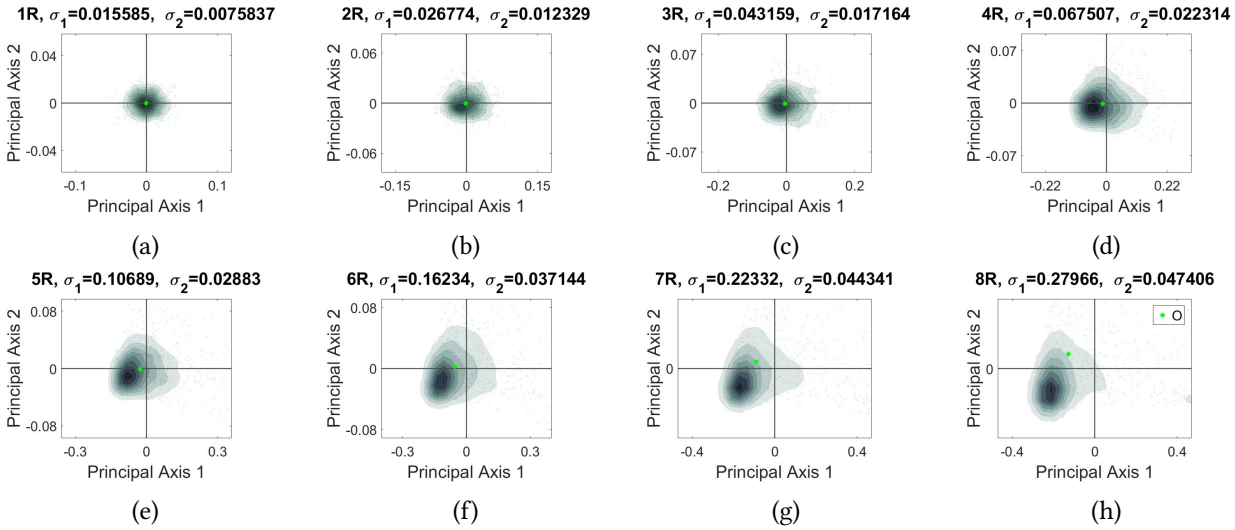

Figure 4.17: The spread of the distribution of points around O for $1,000$ realizations of the stochastic Moran process of size $N = 50K$ shows the increase of both the semi-major axis, σ_1, and the semi-minor axis, σ_2, as the number of rounds increases from 1 to 8 in the principal axis coordinate system when each realization starts at O and evolves under the multi drug additive ($e = 0$) adaptive chemo schedule as in Figure 4.15a during 8 evolutionary cycles. Though forming a multivariate Gaussian distribution nearly around O at the beginning few rounds, the spread gets further away from the initial point, O, as the adaptive schedule is repeated. (a) round 1, $\sigma_1 = 0.0156$, $\sigma_2 = 0.0076$; (b) round 2, $\sigma_1 = 0.0268$, $\sigma_2 = 0.0123$; (c) round 3, $\sigma_1 = 0.0432$, $\sigma_2 = 0.0172$; (d) round 4, $\sigma_1 = 0.0675$, $\sigma_2 = 0.0223$; (e) round 5, $\sigma_1 = 0.1069$, $\sigma_2 = 0.0288$; (f) round 6, $\sigma_1 = 0.1623$, $\sigma_2 = 0.0371$; (g) round 7, $\sigma_1 = 0.2233$, $\sigma_2 = 0.0443$; (h) round 8, $\sigma_1 = 0.2797$, $\sigma_2 = 0.0474$

One of those $1,000$ realizations of the Moran process to which the adaptive chemo schedule is applied during 8 cycles is randomly selected and its full trajectory is shown in Figure 4.18a. This realization chosen shows a similar trajectory to the associated deterministic trajectory with the adjusted replicator dynamic, depicted as a light blue line, up to the second round, but it keeps moving towards the R_1 corner as rounds go while maintaining a triangle-shaped trajectory in each cycle. We adopted the tumor-growth equation in (4.8) to describe the growth and the decay of tumor volume, and the associated tumor size with that single trajectory is given in Figure 4.18b along with the tumor size associated with the adjusted replicator dynamic in light blue. With this large population size $N = 50K$, the tumor size driven by the stochastic process almost coincides with the deterministic one during the first evolutionary cycle. However, the maximum tumor size achieved at the end of the second piece, that is no drug part, keeps increasing and it finally reaches over 30 in the 5th cycle though the tumor size reduces below 15 in the following cycle.

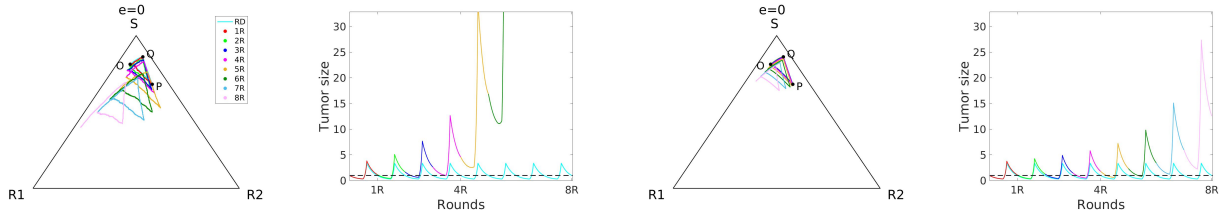

(a) (b) (c) (d)

Figure 4.18: $1,000$ realizations of the stochastic Moran process with size $N = 50K$ show that the saturation of cancer cells can be delayed when each realization evolves under the administration of the multi drug additive ($e = 0$) adaptive chemo schedule, associated with the adjusted replicator system, as in Figure 4.15a during 8 rounds since its exact start at O. (a) one realization; (b) tumor size corresponding to Figure 4.18a; (c) the averaged trajectory of $1,000$ realizations; (d) the averaged tumor size corresponding to Figure 4.18c

This pattern that the single realization has is similarly reflected in the averaged ones of $1,000$ realizations while both scale and size is reduced. Precisely, the averaged trajectory also traverse tightly near the closed loop, $OPQO$, for the first few rounds but each leg of the trajectory in each round starts being apart from the deterministic one, moving towards to the R_1 corner (Fig.4.18c). This is similar to what the single realization shows in Figure 4.18a, however, deviation is much smaller on average. The smaller deviation is also captured in the averaged tumor size that it maximally reaches only up to 10 until the 6th evolutionary cycle while it increases to over 25 in the last round. On average, tumor size increases but the rate of increase is a lot more mild compared to Figure 4.18b.

4.3.1 Synergistic multi drug schedule

Under the same constant combination of two drugs, i.e. $C_1 = 0.5, C_2 = 0.2$ during T_{OP}, $C_1 = 0, C_2 = 0$ during T_{PQ} and $C_1 = 0.2, C_2 = 0.5$ during T_{QO} unit times, we evaluate the adaptive chemotherapy applied to the Moran process of size $N = 50K$ when two drug interact synergistically. Recall from Figure 4.15d that for synergistic drug interactions ($e = 0.3$), $T_{OP} = 14.260$, $T_{PQ} = 6.901$, $T_{QO} = 11.129$, and thus the associated one evolutionary cycle, T, in this case is equal to $T = 32.29$ and the corresponding

evolutionary steps, τ, for the Moran process with $N = 50K$ is then equal to $\tau = 1,614,500$. Compared to the additive drug interaction case, this schedule has a longer cycle and hence more evolutionary steps.

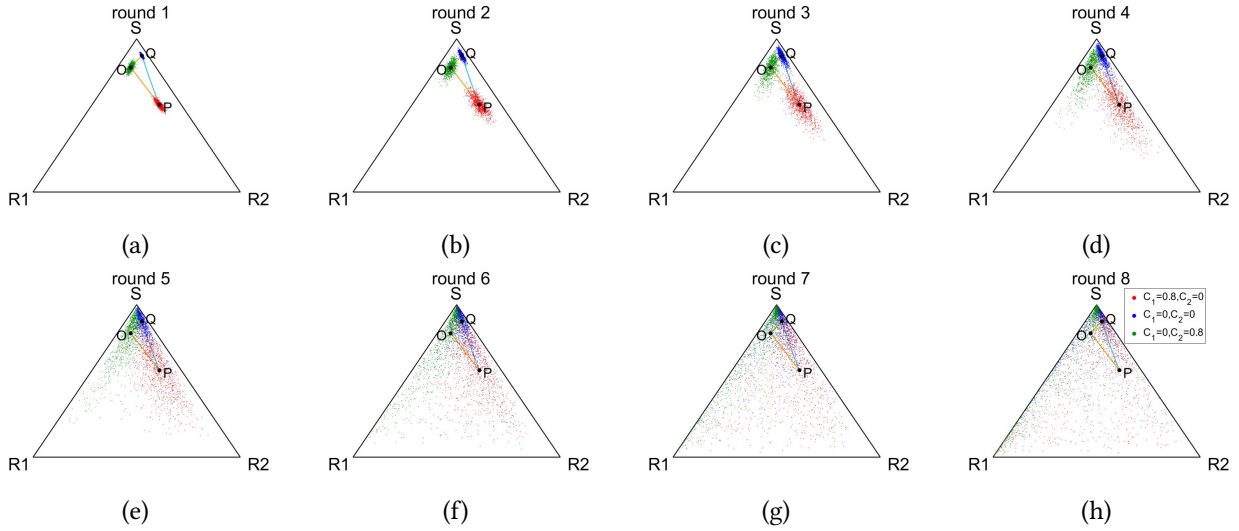

Figure 4.19: The spread of the distribution of terminal points (green dots) around O in each round for $1,000$ realizations of the stochastic Moran process with size $N = 50K$ becomes wider as the number of rounds increases when each realization evolves under the administration of the multi drug synergistic ($e = 0.3$) adaptive chemo schedule, associated with the adjusted replicator system, as in Figure 4.15d during 8 rounds since its exact start at O. (a) round 1; (b) round 2; (c) round 3; (d) round 4; (e) round 5; (f) round 6; (g) round 7; (h) round 8

Again we consider $1,000$ realizations of the Moran process that start at O. Applying the two drug adaptive chemo schedule for 8 evolutionary cycles to these individual stochastic systems provides the spread of the distribution of points around O at the end of each cycle and those points are depicted as green dots in Figure 4.19. Similar patterns that the additive drug interaction cases possess are shown for synergistic drug interactions. Expected by both the stochasticity driving the terminal point of the system to settle down on a neighborhood and the continued application of the adaptive chemotherapy associated with the closed loop, $OPQO$, at that inexact point each cycle, the points around O get more widely spread as the number of rounds increases. Moreover, for a fixed cycle, the distribution of the points vary less in the frequency of the R_2 subpopulations but more in either S or R_1 subpopulations. This is where the stochastic competitive release of R_1 as a result of the continuous delivery of a higher dose of drug 1 is reflected.

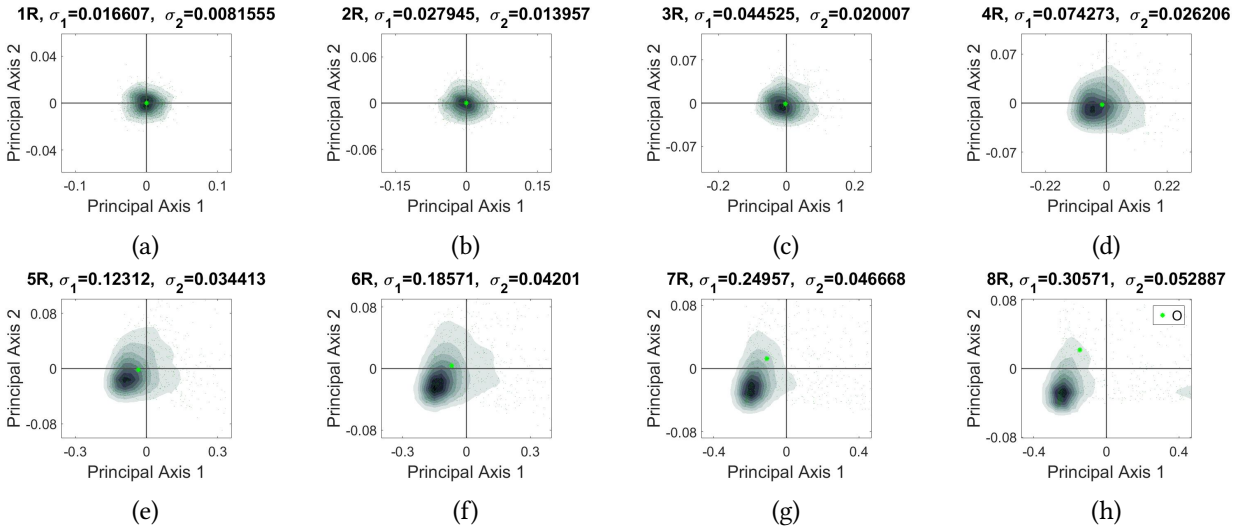

Figure 4.20: The spread of the distribution of points around O for $1,000$ realizations of the stochastic Moran process of size $N = 50K$ shows the increase of both the semi-major axis, σ_1, and the semi-minor axis, σ_2, as the number of rounds increases from 1 to 8 in the principal axis coordinate system when each realization starts at O and evolves under the multi drug synergistic ($e = 0.3$) adaptive chemo schedule as in Figure 4.15d during 8 evolutionary cycles. Though forming a multivariate Gaussian distribution nearly around O at the beginning few rounds, the spread gets further away from the initial point, O, as the adaptive schedule is repeated. (a) round 1, $\sigma_1 = 0.0166$, $\sigma_2 = 0.0082$; (b) round 2, $\sigma_1 = 0.0279$, $\sigma_2 = 0.0140$; (c) round 3, $\sigma_1 = 0.0445$, $\sigma_2 = 0.0200$; (d) round 4, $\sigma_1 = 0.0743$, $\sigma_2 = 0.0262$; (e) round 5, $\sigma_1 = 0.1231$, $\sigma_2 = 0.0344$; (f) round 6, $\sigma_1 = 0.1857$, $\sigma_2 = 0.0420$; (g) round 7, $\sigma_1 = 0.2496$, $\sigma_2 = 0.0467$; (h) round 8, $\sigma_1 = 0.3057$, $\sigma_2 = 0.0529$

Unlike the additive drug interactions, it is observed for a fixed round that the synergistic drug interactions bring in the wider distribution than the additive drug interactions entail. This deviation is quantified in terms of the semi-major and semi-minor axis by plotting the points around O in the principal axis coordinate system. As it can be seen by comparing Figure 4.17 and Figure 4.20, both the semi-major axis, σ_1, and the semi-minor axis, σ_2, are dominating in all cycles when two drugs interact synergistically. However, any significantly new feature in the form of distribution is not shown. It starts loosing the multi Gaussian structure from the 4th round and the area where points are heavily distributed gets further away from the point, O, as the additive drug interactions result.

Trajectories of one randomly chosen realization and the averaged of $1,000$ samples during 8 cycles are given in Figure 4.21. One sample in Figure 4.21a gets off much the expected trajectory quite early from the second round, and the associated tumor size explosively increases, reaching over 300 even in the 4th

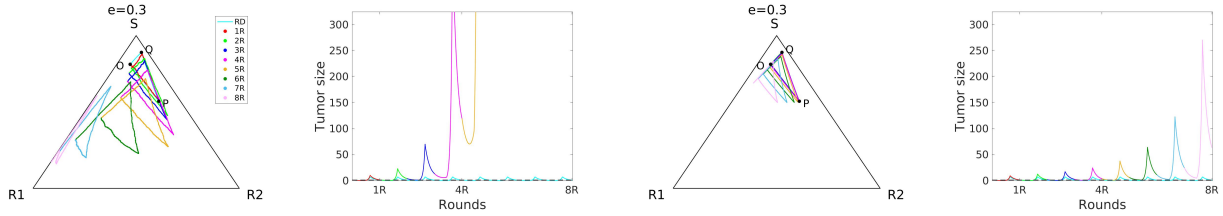

(a) (b) (c) (d)

Figure 4.21: $1,000$ realizations of the stochastic Moran process with size $N = 50K$ show that the saturation of cancer cells can be delayed when each realization evolves under the administration of the multi drug synergistic ($e = 0.3$) adaptive chemo schedule, associated with the adjusted replicator system, as in Figure 4.15d during 8 rounds since its exact start at O. (a) one realization; (b) tumor size corresponding to Figure 4.21a; (c) the averaged trajectory of $1,000$ realizations; (d) the averaged tumor size corresponding to Figure 4.21c

round (Fig.4.21b). When the observation is made on the sample average, then the mean trajectory becomes mild in the scope of movement from the closed loop, $OPQO$, maintaining its move around the loop closely until the 4th round and expanding its journey towards the R_1 corner from the next round, which is the observed feature for the additive drug interactions.

Although the additive and synergistic drug interactions do not differ much in their trajectories and the distribution of the terminal points of each round except for the deviation, things change when it comes to tumor size. Recall that tumor size is modeled by the tumor-growth equation in (4.8) where the constant background fitness, g, enters. For the numerical purpose, we set different values of g for each drug interaction as in Table 4.2 and this allows the tumor size associated with the adjusted replicator equation to be periodic with the period, T, where the one evolutionary cycle, T, also varies depending on the type of drug interactions. For both the additive and synergistic drug interactions, tumor size is well controlled with a slight increase in the maximum size for the first 3 to 4 rounds and the maximal tumor size keep increasing as the number of rounds rises. Compared to its own maximal tumor size associated with the deterministic system, the additive drug interaction causes approximately 8.2 times increase while the maximal tumor size is increased by approximately 37.23 times for the synergistic drug interaction. What it infers is that

synergistic drug interactions allow the use of two drug chemotherapy schedule for a shorter time than additive drug interactions permit.

4.3.2 Antagonistic multi drug schedule

Evaluation of the two drug adaptive chemotherapy schedule composed of the same constant combination of two drugs, i.e. $C_1 = 0.5, C_2 = 0.2$ during T_{OP}, $C_1 = 0, C_2 = 0$ during T_{PQ} and $C_1 = 0.2, C_2 = 0.5$ during T_{QO} unit times, is to be made with $1,000$ realizations of the Moran process of size $N = 50K$ for antagonistic drug interactions. With the choice of the drug interaction parameter, $e = -0.3$, and those constant combination of drugs, the time period for each leg is given in Figure 4.15g as $T_{OP} = 14.300$, $T_{PQ} = 1.424$ and $T_{QO} = 11.150$, which in turn results in the total time period, T, being equal to $T = 26.8740$. With the selected size $N = 50K$ of the Moran process, it gives rise to the evolutionary steps, τ, being equal to $\tau = 1,343,700$, and it is the shortest number of steps among all drug interactions considered.

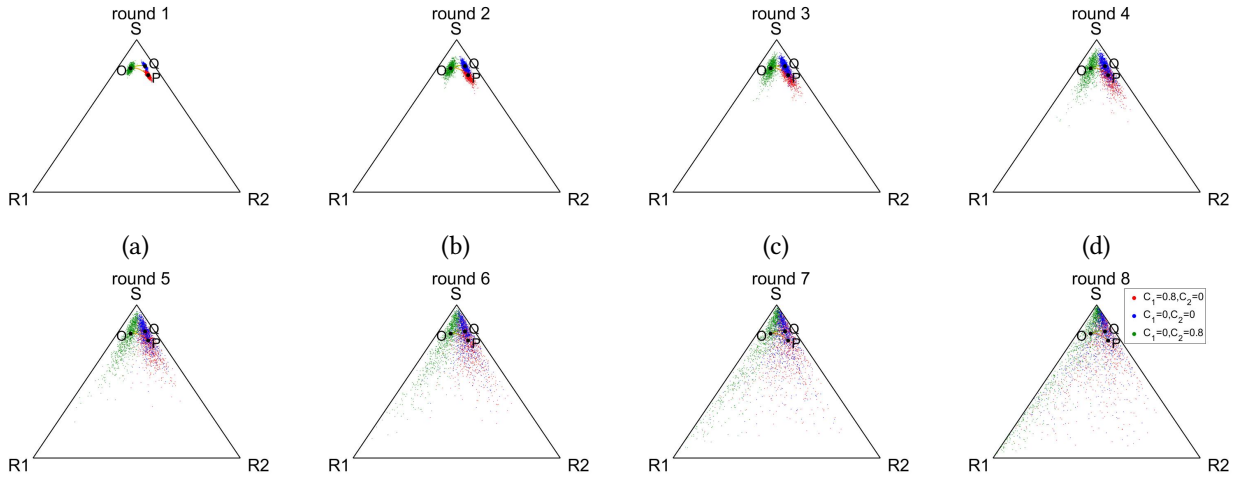

Figure 4.22: The spread of the distribution of terminal points (green dots) around O in each round for $1,000$ realizations of the stochastic Moran process with size $N = 50K$ becomes wider as the number of rounds increases when each realization evolves under the administration of the multi drug antagonistic ($e = -0.3$) adaptive chemo schedule, associated with the adjusted replicator system, as in Figure 4.15g during 8 rounds since its exact start at O. (a) round 1; (b) round 2; (c) round 3; (d) round 4; (e) round 5; (f) round 6; (g) round 7; (h) round 8

Indicating the last points of each run for $1,000$ individual simulations of the Moran process as green dots visualizes the spread of the distribution of points around O in Figure 4.22. The distribution obviously gets more widely disseminated in the rise of the number of rounds as similarly shown for other drug interaction cases. It is also apparently seen that the antagonistic drug interaction preserves thick mass around O for a longer cycle in comparison with the additive drug interaction.

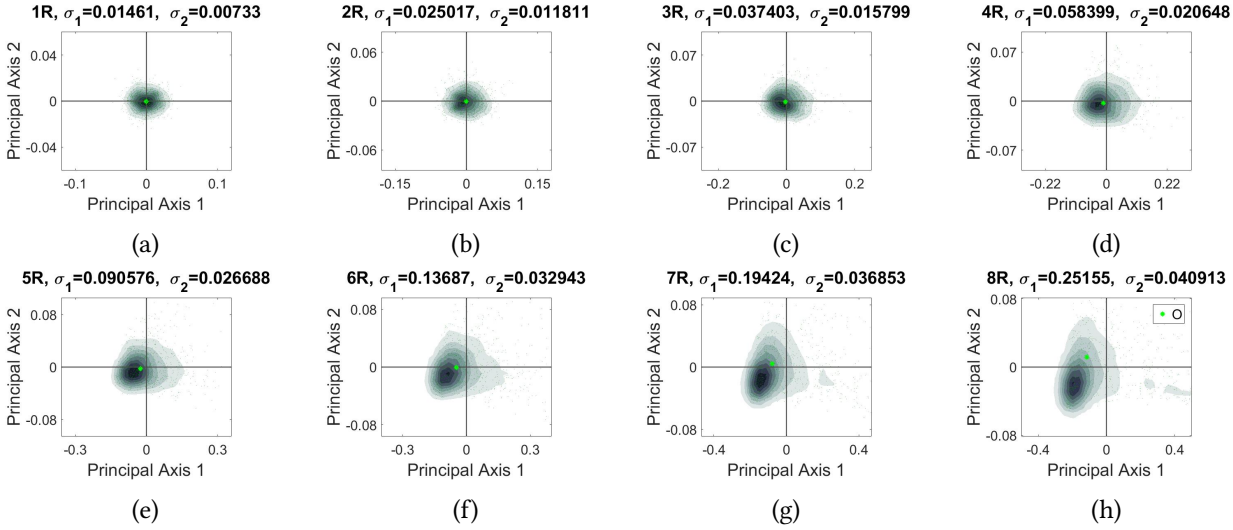

Figure 4.23: The spread of the distribution of points around O for $1,000$ realizations of the stochastic Moran process of size $N = 50K$ shows the increase of both the semi-major axis, σ_1, and the semi-minor axis, σ_2, as the number of rounds increases from 1 to 8 in the principal axis coordinate system when each realization starts at O and evolves under the multi drug antagonistic ($e = -0.3$) adaptive chemo schedule as in Figure 4.15g during 8 evolutionary cycles. Though forming a multivariate Gaussian distribution nearly around O at the beginning few rounds, the spread gets further away from the initial point, O, as the adaptive schedule is repeated. (a) round 1, $\sigma_1 = 0.0146$, $\sigma_2 = 0.0073$; (b) round 2, $\sigma_1 = 0.0250$, $\sigma_2 = 0.0118$; (c) round 3, $\sigma_1 = 0.0374$, $\sigma_2 = 0.0158$; (d) round 4, $\sigma_1 = 0.0584$, $\sigma_2 = 0.0206$; (e) round 5, $\sigma_1 = 0.0906$, $\sigma_2 = 0.0267$; (f) round 6, $\sigma_1 = 0.1369$, $\sigma_2 = 0.0329$; (g) round 7, $\sigma_1 = 0.1942$, $\sigma_2 = 0.0369$; (h) round 8, $\sigma_1 = 0.2516$, $\sigma_2 = 0.0409$

When the points are plotted in the principal axis coordinate system in Figure 4.23, we observe that the distribution in the form of multi Gaussian structure is maintained up to the third cycle similarly to two other drug interaction cases, but the distance between the area where points are heavily crowded and the exact point, O, slowly increases in this case. In fact, the point, O, in the principal axis coordinate system is located at the border line in the last round for both the additive and synergistic cases when the plots are smoothened using the kernel density estimation method while Figure 4.23h shows the heavy mass is

still close to the point, O, even in the 8th evolutionary cycle. In addition, the deviation of the distribution around O for the antagonistic drug interaction turns out to be smallest in all cycles. It must be due to that administering a similar amount of the total dose, the adaptive chemotherapy schedule results in the smallest closed loop for the expected system, the adjusted replicator dynamic, in its one evolutionary cycle when drugs interact antagonistically as shown in Figure 4.15. Thus the stochastic Moran process has less chance to reflect its randomness on its path as it evolves. The exact values of the semi-major axis, σ_1, and the semi-minor axis, σ_2, are given on top of each plot in Figure 4.23.

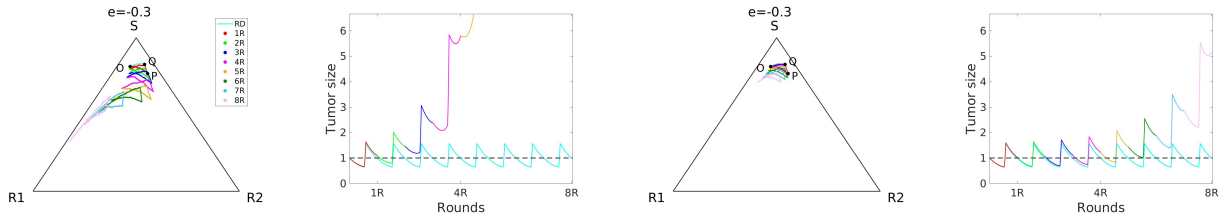

(a) (b) (c) (d)

Figure 4.24: $1,000$ realizations of the stochastic Moran process with size $N = 50K$ show that the saturation of cancer cells can be delayed when each realization evolves under the administration of the multi drug antagonistic ($e = -0.3$) adaptive chemo schedule, associated with the adjusted replicator system, as in Figure 4.15g during 8 rounds since its exact start at O. (a) one realization; (b) tumor size corresponding to Figure 4.24a; (c) the averaged trajectory of $1,000$ realizations; (d) the averaged tumor size corresponding to Figure 4.24c

The trajectories of one realization chosen at random and the mean for the $1,000$ realizations of the Moran process are provided in Figure 4.24. One realization of the stochastic system in Figure 4.24a evolves as much as there are more R_1 subpopulations at the end of 8 cycles, showing the early development of the group of the R_1 subpopulations as a result of the competitive release caused by the higher dose of drug 2. However, the stochastic Moran process can only be understood in terms of a realistic estimate, and we take it to be the sample mean since it is of a finite but large population size. The trajectory in Figure 4.24c corresponding to the sample mean moves tightly to the deterministic path until the 5th round and gradually starts being off towards to the R_1 corner, but not as much as the one realization shows. Except that the averaged trajectory under the antagonistic drug interaction generates a smaller open-triangle-like

shape in each cycle than under two other drug interaction cases, it shares the same pattern with other two cases.

However, the considerable advantage of the antagonistic drug interactions is proven when we focus on tumor size. With the choice of the constant background fitness, g, as in Table 4.2, tumor size is not only controlled relatively longer with little increase in its maximum until the 4th round but also the increase that starts from the 5th round is much slower compared to either the additive or synergistic drug interactions. Precisely, the maximal tumor size obtained at the end of the second $1/3$ cycle in each round is increased by approximately 3.56 times in 8 evolutionary cycles, and this is a considerably smaller rate if we note that the rates were 8.2 and 37.23 for the additive and synergistic drug interactions, respectively. The fact that the maximum tumor size even in the last round is less than only 6 is also notable. Set the threshold of tumor size to be equal to, say, 10, then the two drug adaptive chemotherapy schedule can be applied during 5 cycles for the additive drug interaction as seen in Figure 4.18d but it can be only applied during one cycle for the synergistic drug interaction as verified in Figure 4.21d. Figure 4.24d finally justifies that the most powerful drug interaction in controlling tumor size when applying the adaptive chemo schedule is the antagonistic one since tumor size most slowly grows and it grows much less than it is allowed.

As mentioned before, one of reasons that the antagonistic drug interaction when applying the adaptive chemotherapy schedule is that the spread of the distribution of points around O keeps centered near O with the smallest deviation as the number of rounds increases, making the adoption of the adaptive chemo schedule for the next round more feasible. The measures, the semi-major and semi-minor axis, to explain the deviation in the distribution in each round are depicted in Figure 4.25 to summarize that the largest deviation is obtained with the synergistic interaction while the smallest one with the antagonistic drug interaction. We also present the fitted curves of both σ_1 and σ_2 in log-log scale in Figure 4.25d, 4.25e, 4.25f

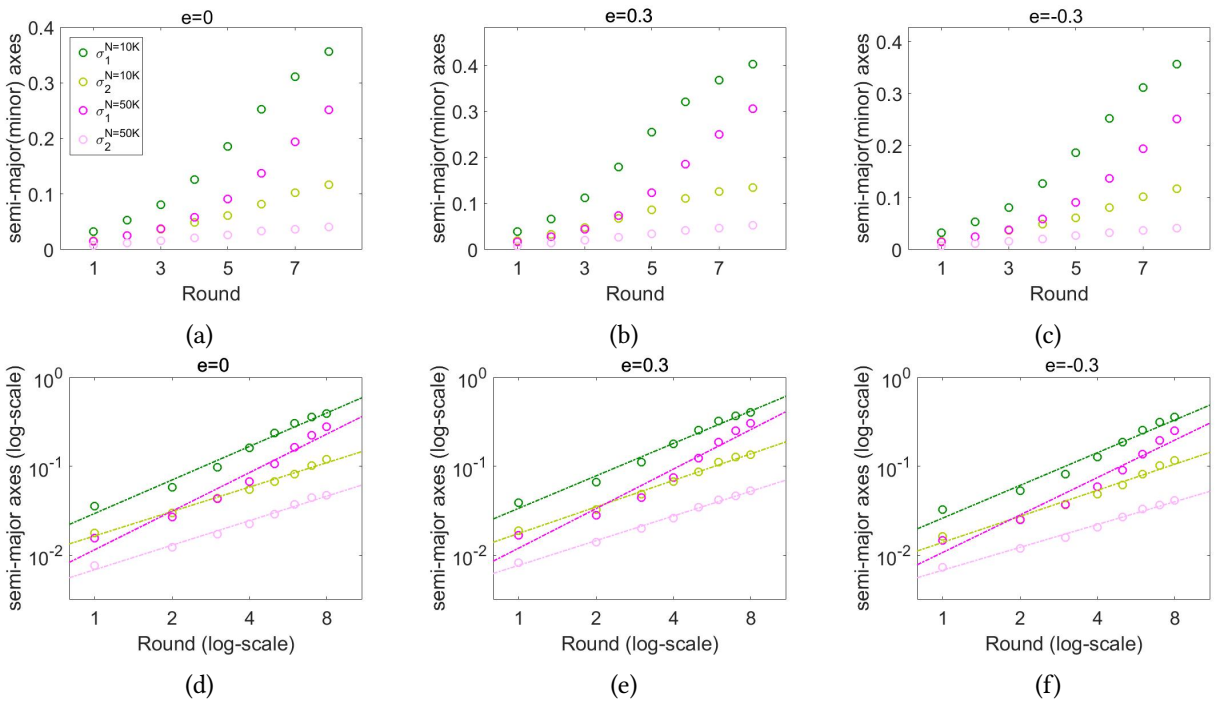

Figure 4.25: The semi-major (and -minor) axis of the distribution of the points around P at the end of each evolutionary cycle for $1,000$ realizations of the Moran process with $N = 10K$ or $N = 50K$ overall increases in the number of rounds, showing the power-law dependency, where each realization evolves under the administration of the adaptive schedule associated with the adjusted replicator system during 8 evolutionary cycles since its exact start at O. (a) $e = 0$; (b) $e = 0.3$; (c) $e = -0.3$; (d) $e = 0$, the log-log fit; (e) $e = 0.3$, the log-log fit; (f) $e = -0.3$, the log-log fit

for the additive, synergistic and antagonistic interaction, respectively, and all of them show the power-law dependency in the number, n, of rounds as follows with $N = 10K$:

$$\begin{aligned}
\sigma_1^{e=0} &\sim 0.0295 \cdot n^{1.2504}, \\
\sigma_2^{e=0} &\sim 0.0165 \cdot n^{0.9114}, \\
\sigma_1^{e=0.3} &\sim 0.0337 \cdot n^{1.2108}, \\
\sigma_2^{e=0.3} &\sim 0.0175 \cdot n^{0.9904}, \\
\sigma_1^{e=-0.3} &\sim 0.0261 \cdot n^{1.2214}, \\
\sigma_2^{e=-0.3} &\sim 0.0139 \cdot n^{0.9734}.
\end{aligned} \tag{4.16}$$

Similarly, with $N = 50K$:

$$\begin{aligned}
\sigma_1^{e=0} &\sim 0.0115 \cdot n^{1.4387}, \\
\sigma_2^{e=0} &\sim 0.0069 \cdot n^{0.9152}, \\
\sigma_1^{e=0.3} &\sim 0.0120 \cdot n^{1.4752}, \\
\sigma_2^{e=0.3} &\sim 0.0077 \cdot n^{0.9216}, \\
\sigma_1^{e=-0.3} &\sim 0.0107 \cdot n^{1.3981}, \\
\sigma_2^{e=-0.3} &\sim 0.0068 \cdot n^{0.8525}.
\end{aligned} \tag{4.17}$$

4.4 Comparison of adaptive multi drug chemotherapy schedule with standard clinical approaches

The evaluation of the adaptive two drug chemotherapy schedule for a few cycles with the fixed amount of the total dose was made in the previous section across the different types of drug interactions when it is applied to the Moran process that starts at a fixed point. It was concluded that the therapy associated with the closed loop, $OPQO$, turns out to be the most efficient when two drugs interact antagonistically in the sense that it gives rise to the smallest trajectory and the lowest increase in tumor size during the whole cycles. On the other hand, when two drug interact synergistically, it involves the largest trajectory with the greatest deviation in the spread of the distribution of point around the initial point, O. On top of that, it provides the significantly rapid increase in tumor size compared to two other drug interactions.

In this section, fixing a drug interaction, we evaluate the adaptive two drug chemotherapy schedule by comparing it to the most frequently used standard clinical schedules: the maximum tolerated dose schedule (MTD) and the low-dose metronomic schedule (LDM). We already considered these two clinical schedules in Section 3.4 with a single drug chemotherapy model, where we had only one controller of the system which is the concentration function of the single drug with a constraint $0 \leq C(t) \leq 1$ for all t. In

two drug chemotherapy model, we have two controllers, $C_1(t)$ and $C_2(t)$, that are concentration functions of drug 1 and drug 2, and these functions have come with one more constraint

$$C_1(t) + C_2(t) \leq 1 \tag{4.18}$$

for all t as well as $0 \leq C_i(t) \leq 1$.

The comparison of two drug chemotherapy schedules is made by fixing both a type of drug interaction, more precisely a value of the drug interaction parameter, e, and the same total dose delivered over a finite time, where the total dose, $D(T)$, of two drugs delivered during T unit time is similarly defined to the equation in (3.13) by:

$$D(T) := \int_0^T C_1(t) + C_2(t)dt. \tag{4.19}$$

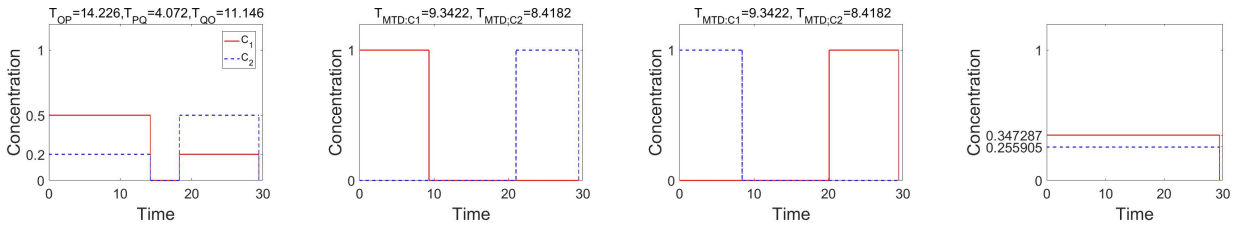

(a) (b) (c) (d)

Figure 4.26: The multiple additive ($e = 0$) standard clinical approaches are designed to have the same total dose, being equal to 17.7604, as the amount that is delivered during one round (29.4440 unit time) according to the adaptive chemo schedule in Figure 4.15a. (a) adaptive; (b) MTD_1: the drug 1 is maximally administered during the beginning $T_{MTD:C_1} = 9.3422$ unit time while the drug 2 is delivered during the last $T_{MTD:C_2} = 8.4182$ unit time. (c) MTD_2: the drug 2 is maximally administered during the beginning $T_{MTD:C_2} = 8.4182$ unit time while the drug 1 is delivered at largest during the last $T_{MTD:C_1} = 9.3422$ unit time. (d) LDM: both the drug 1 and drug 2 are constantly administered during the whole rounds at the level of $C_1 = 0.347287$ and $C_2 = 0.255905$, respectively.

Our two drug adaptive chemotherapy schedule in Figure 4.15a associated with the closed loop, $OPQO$, in Figure 4.5b for the additive drug interaction ($e = 0$) has the total dose $D = 17.7604$ for one evolutionary cycle which we set T to be. Having in mind that MTD delivers the highest dose of a drug by which any significantly unacceptable side effects are not caused, we may naturally come up with two MTD schedules

with the same total dose, D, during $T = 29.4440$ unit time forcing them to satisfy the equation (4.18). One MTD, which we denote by MTD_1, is to deliver the highest dose of drug 1 first until the total dose of drug 1 under MTD_1 meets half the total dose of drug 1 under the adaptive schedule, that is $D/2$. For the rest $D/2$, the highest dose of drug 2 is delivered at the end of one cycle during the time over which the total dose of drug 2 under MTD_1 is equal to $D/2$. Let $T_{MTD:C1}$ and $T_{MTD:C2}$ be the time period over which drug 1 and drug 2, respectively, is maximally delivered so that the total dose of both drugs during one evolutionary cycle is equal to D. Then $T_{MTD:C1} = 9.3422$, $T_{MTD:C2} = 8.4182$ for the additive drug interaction, and MTD_1 is well described in Figure 4.26b.

Another MTD schedule is exactly the same as MTD_1, except that the delivery order of drugs is switched so that drug 2 is delivered first during $T_{MTD:C2}$ unit times and drug 1 is administered at the end of the cycle during $T_{MTD:C1}$ unit times, having a pause between. We denote this schedule by MTD_2 and it is depicted in Figure 4.26c. For both MTD schedules, we simply put the delivery times of two drugs apart, at the beginning and at the end, so that the area of the maximal concentration is not overlapped during one cycle in order to make sure the constraint in (4.18). However, it is true that we may design infinitely many MTD schedules by adjusting time window as long as two maximal windows are not overlapped.

LDM is one other typical clinical approach where the low dose is continuously delivered during a finite time period. It is straight forward to design LDM by simply averaging the total dose of each drug under the adaptive schedule for the entire time period. From the adaptive schedule in Figure 4.15a for the additive drug interaction, the constant low dose of drug 1 turns out to be 0.347287 and the one of drug 2 is lower and equal to 0.255905. This LDM schedule for the additive interaction is given in Figure 4.26d. Thus we so far have 4 two drug chemotherapy schedules that have the same total dose for a fixed one evolutionary

cycle in hand to compare when two drugs are additive. Denoting the type of schedule as superscript for the concentration functions, $C_i(t)$, of drug i, all the schedules in Figure 4.26 satisfies

$$\begin{aligned} D &= \int_0^T C_1^{\text{Adaptive}}(t) + C_2^{\text{Adaptive}}(t)dt \\ &= \int_0^T C_1^{MTD_1}(t) + C_2^{MTD_1}(t)dt \\ &= \int_0^T C_1^{MTD_2}(t) + C_2^{MTD_2}(t)dt \\ &= \int_0^T C_1^{LDM}(t) + C_2^{LDM}(t)dt \end{aligned} \tag{4.20}$$

, where $T = T_{OP} + T_{PQ} + T_{QO} = 29.4440$ and $D = 17.7604$. Note that we omit indicating here the type of drug interaction since the comparison to be made is within a fixed type and the construction of MTD's and LDM is designed in the same manner to satisfy the equation in (4.20) with simply different values of D and T for each drug interaction as determined in Table 4.2.

Recall from Figure 4.18c,4.18d that applying the adaptive chemotherapy schedule to the $1,000$ realizations of the Moran process of the population size, $N = 50K$, successfully controls both trajectory and tumor size for the first few rounds on average when two drugs are additive as the well designed schedule eventually plays the role of delaying the competitive release of R_1 or R_2. Although the stochasticity drives the system gradually to be off the expected route in the direction towards the R_1 corner resulting in the growth of tumor in size, its increase is below 30 during 8 evolutionary cycles. These trajectory and tumor size for the adaptive schedule are depicted in pink in Figure 4.27.

On the other hand, when MTD schedules are applied, the first maximal dose of a drug helps the system shortly build up the resistant subpopulations even though the duration of the maximal dose is relatively shorter than the first $1/3$ piece of the adaptive schedule. For MTD_1 which administer the drug 1 first, the resistant R_2 subpopulations to drug 1 starts quickly proliferating in a population and it nearly overtakes the entire population at the end of the delivery of the maximal dose even in the first round. However, a

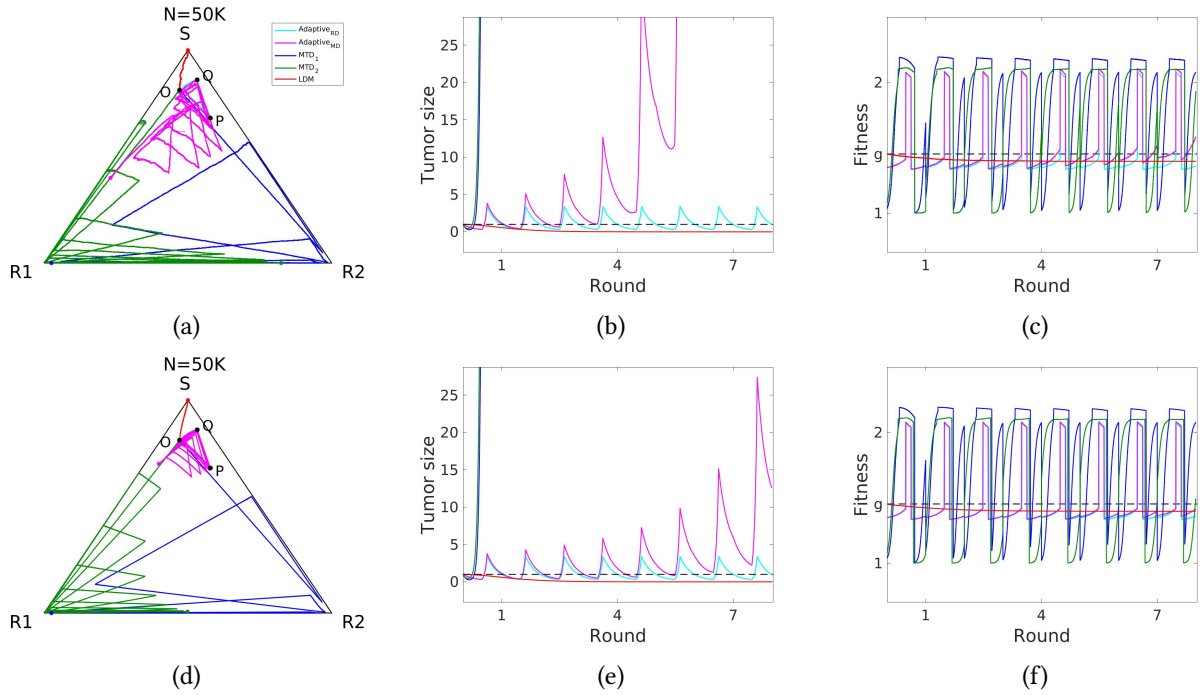

Figure 4.27: $1,000$ realizations of the stochastic Moran process with size $N = 50K$ show that the saturation of cancer cells can be delayed longer on average compared to being under either LDM and MTD's when each realization evolves under the administration of the multi drug additive ($e = 0$) adaptive chemo schedule, associated with the adjusted replicator system, during 8 rounds since its exact start at O. (a) one single realization; (b) tumor size corresponding to Figure 4.27a; (c) the averaged fitness of S, R_1 and R_2 cells corresponding to Figure 4.27a; (d) the averaged trajectory of all realizations; (e) the averaged tumor size corresponding to Figure 4.27d; (f) the averaged fitness of S, R_1 and R_2 cells corresponding to Figure 4.27d

pause, that is no drug, between two maximal dose administration of different drugs allows the system to step back towards the S corner for a while. When the administration of the maximal dose of drug 2 begins, the resistant R_1 subpopulations to drug 2 starts growing and the population finally has a higher frequency of R_1 than others at the end of the first round. This pattern continues as the number of rounds increases, but the absent mutation kills the whole sensitive subpopulations early and the population becomes full of resistant populations. In fact, the maximal dose administration of a drug let the selection functions of sensitive cells to the drug used vanish while it lets resistant cells to the drug used have the strongest selection regardless of the value of e according to the equation (4.1) and the payoff matrix, A, in (4.6). Then the expected fitness of those sensitive cells become less fitter, being equal to 1. This is reflected to

our stochastic simulation under MTD. MTD_1 administers drug 2 in the last and it leads to the proliferation of the resistant subpopulations R_1 to that drug 2 as can be seen from the terminal point of the last cycle marked as a blue dot in Figure 4.27a, 4.27d. The whole trajectory corresponding to MTD_1 is described in a blue line in Figure 4.27.

MTD_2 acts exactly in an opposite way since it interchanges the order of administration of two drugs. The maximal dose of drug 2 at the beginning leads the dynamic of the stochastic system to nearly the R_1 corner since the highest dose of drug 2 rapidly help the resistant subpopulations R_1 to drug 2 develop. We noticed that this nearly fixation to R_2 is reached even in a shorter time $T_{MTD:C2} = 8.4182$ than MTD_1 results in the almost full growth of R_2 subpopulations for $T_{MTD:C1} = 9.3422$ unit times. It is hard to tell that one drug is stronger or less effective than another, but it is related to the distance from the starting point, O, in fact the initial distribution, O, is closer to the R_1 corner in a phase space. Then MTD_2 takes a pause for a while and it causes the sensitive subpopulations to recover some, and when the highest dose of drug 1 begin its delivery, the development of the resistant subpopulations of R_2 to drug 1 is achieved though it is smaller in extent as there are more sensitive subpopulations. Again, this pattern continues for the following rounds, leading the stochastic system to eventually have more and more R_1 subpopulations on its way. The trajectories or tumor size, of both one single simulation and the averaged one, corresponding to MTD_2 are shown in green in Figure 4.27. The dynamics determined by both MTD schedules are different in directions especially in the growth and decay of resistant subpopulations, however, they are almost the same in their induced tumor size as can be seen in Figure 4.27e. The rapid development of the resistant subpopulations and the dramatic decrease in the number of sensitive cells brings out the explosive increase in tumor size even before the first pause ends though tumor size is initially decreased sensitively reacting to the drug that is first delivered due to the high dose.

The low-dose metronomic schedule (LDM) shows somewhat different dynamic from both the adaptive and the maximum tolerated dose schedules. This constant schedule guides the stochastic system to the

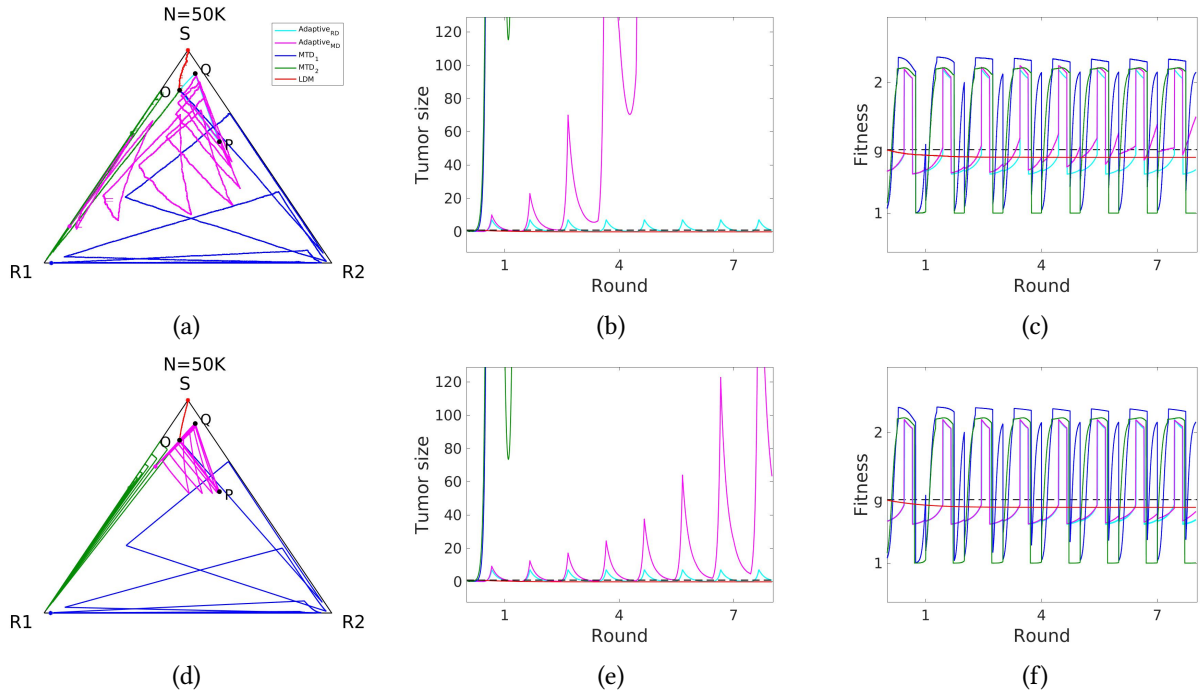

Figure 4.28: $1,000$ realizations of the stochastic Moran process with size $N = 50K$ show that the saturation of cancer cells can be delayed longer on average compared to being under either LDM and MTD's when each realization evolves under the administration of the multi drug synergistic ($e = 0.3$) adaptive chemo schedule, associated with the adjusted replicator system, during 8 rounds since its exact start at O. (a) one single realization; (b) tumor size corresponding to Figure 4.28a; (c) the averaged fitness of S, R_1 and R_2 cells corresponding to Figure 4.28a; (d) the averaged trajectory of all realizations; (e) the averaged tumor size corresponding to Figure 4.28d; (f) the averaged fitness of S, R_1 and R_2 cells corresponding to Figure 4.28d

fixation to S on average and the associated trajectory is given in Figure4.27d as a red line. For one realization chosen at random also shows the direct approach to the S corner. In fact, S is an asymptotically stable fixed point and trajectories converge to the S corner regardless of initial distributions as long as both drugs are delivered at a low dose. The exact description of the ESS is explained in [30] for additive drug interactions. In detail, $C_1 = 7/18$ is a bifurcation value where the fixed point R_2 changes its stability from unstable to stable, and S changes its stability from stable to unstable at $C_1 = 1/2$. For drug 2, $C_2 = 1/3$ is a bifurcation value and R_1 changes from an unstable to a stable fixed point. At $C_2 = 1/2$, S changes its stability from stable to unstable. In LDM schedule, $C_1 = 0.347261$ and $C_2 = 0.255905$, and the initial point, O, is laid in the basin of attraction for S for this combination. As a result, the averaged

trajectory of $1,000$ realizations of the Moran process of a large population size shows the convergence to the evolutionarily stable strategy S under LDM.

Though the populations is fixated to one of cancerous state, S, the associated tumor size surprisingly reduces during 8 cycles as shown in red in Figure 4.27e. It seems to conflict with the exponentially increasing tumor size associated with the adjusted replicator system when no drug is used shown in Figure 4.15c. However, recall that tumor size is modeled using the tumor-growth equation in (4.8) by which it grows whenever the averaged fitness, $< f >$, of S, R_1 and R_2 in the entire population is greater than the constant background fitness, g, that is set to be equal to $g = 1.4527$, and that $< f >$ is a function of selections w^S, w^{R_1} and w^{R_2} as in (4.1) where C_i's enters a population through. Thus, a different set of C_i's gives rise to a different value of $< f >$ even at a fixed state and this possibly brings out a totally opposite destiny in tumor size. We computed the averaged fitness, $< f >$, for the averaged Moran process during 8 evolutionary cycles and it shows that $< f >$ is less fitter than the constant background fitness, g, during the entire time period as seen in Figure 4.27f and this allows the tumor size under LDM to decrease.

We have investigated how successfully 4 different two drug chemotherapy schedules work when they are applied to the Moran process that starts a fixed point, O, for the additive drug interaction. We conclude that both MTD's work the worst showing the immediate nearly full development of resistant subpopulations and the extraordinarily rapid growth rate of tumor size too early in the whole 8 cycles. The adaptive schedule associated with the deterministic adjusted replicator system is successful in controlling both the trajectory and tumor size by preventing the competitive release of a resistant subpopulation for the first few cycles. Depending on how much big threshold of tumor size we set, this schedule can be applied longer or shorter. However, it does not work as effectively as LDM does which completely kills out tumor. What LDM does is that the continuous low dose administration helps lower the averaged fitness of cancerous cells, S, R_1 and R_2, making the fitness other factors such as healthy cells or any environment that contribute to tumor development fitter.

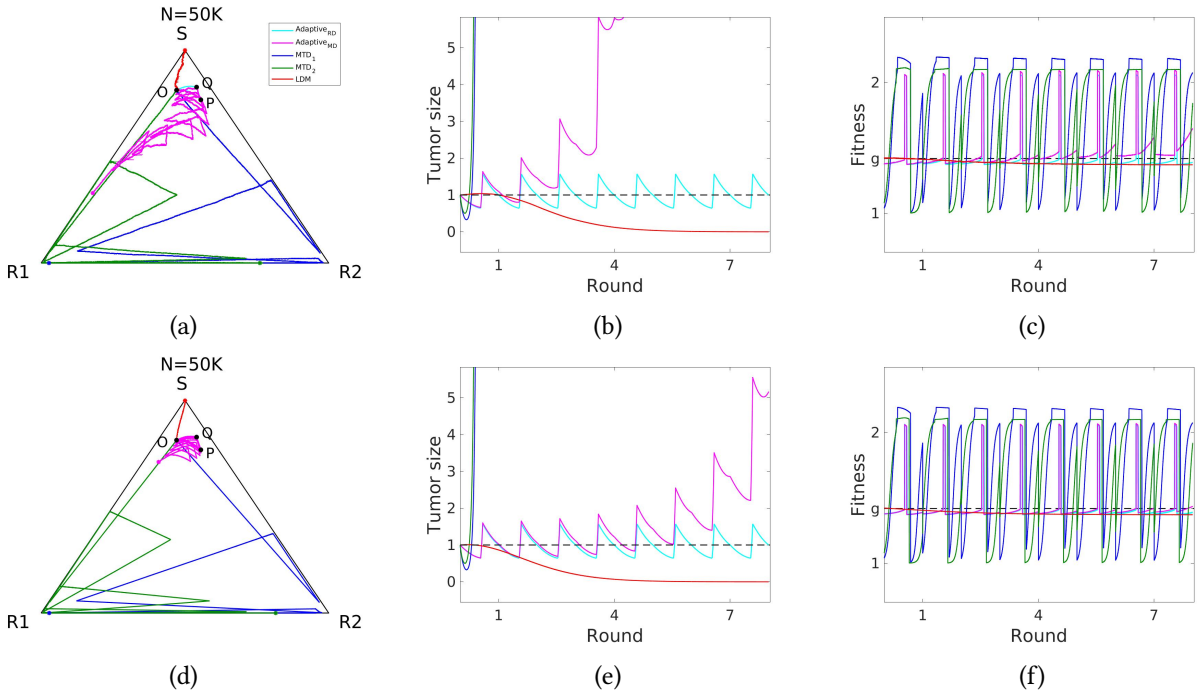

Figure 4.29: $1,000$ realizations of the stochastic Moran process with size $N = 50K$ show that the saturation of cancer cells can be delayed longer on average compared to being under either LDM and MTD's when each realization evolves under the administration of the multi drug antagonistic ($e = -0.3$) adaptive chemo schedule, associated with the adjusted replicator system, during 8 rounds since its exact start at O. (a) one single realization; (b) tumor size corresponding to Figure 4.29a; (c) the averaged fitness of S, R_1 and R_2 cells corresponding to Figure 4.29a; (d) the averaged trajectory of all realizations; (e) the averaged tumor size corresponding to Figure 4.29d; (f) the averaged fitness of S, R_1 and R_2 cells corresponding to Figure 4.29d

Two MTD's and LDM schedules can be easily constructed for synergistic and antagonistic drug interactions referring to its own adaptive schedule associated with each $OPQO$ and total dose, D, during one evolutionary cycle, T. Then applying those 4 schedules to the same number of realizations of the Moran process with size, $N = 50K$ is processed in the same manner for each $e = 0.3, -0.3$. We present a set of trajectory, tumor size, and the averaged fitness, $< f >$, for both one randomly chosen realization and the averaged of $1,000$ individuals in Figure 4.28 for the synergistic interaction and in Figure 4.29 for the antagonistic drug interaction. Regardless of the drug interaction parameter, e, the maximum tolerated dose schedules turn out to be the worst in efficacy of controlling tumor size and the adaptive chemo schedule is successful for a few cycles while it may be applied longer if two drug interact antagonistically but shorter

if synergistically. LDM wins all other three chemo schedules delivering the same total dose for 8 cycles since the low dose of both drugs at that starting point, O, helps either noncancerous cells or environment fitter and hence it gradually reduces tumor size.

However, remember that one point in a phase space corresponds to a unique status of a patient. Thus the change in the initial status of a patient leads to a different starting point instead of O, then to a different closed loop, a new associated adaptive chemo schedule, and a different MTD or LDM. The result in this thesis proves LDM as the most powerful chemotherapeutic method at one point, and the conclusion may vary depending on the given initial stage.

Chapter 5

Future directions

Originating from this thesis, generalization of our model can be made in many different ways. First, for both single and two drug chemotherapy models, we assumed for simplicity that no further mutation is allowed as the system evolves since the population initially attains the minimally required ingredients (e.g. resistant cells) by preexisting mutation. However, mutation is one of key factors in the Darwinian evolutionary theory along with heredity and natural selection, and there are a lot of literatures that describe an evolving population allowing mutation during the whole evolution process. Allowing mutation during evolution process also gives rise to qualitatively different but desired results in asymptotic behavior such as the emergence of cooperation as it was shown for both a finite and infinite population by in [7, 24, 26].

Thus, it can be our one possible generalization of our model to introduce a mutation rate to each group of cells and let them evolve according to either the replicator-mutator equations for an infinite populations or the Moran process with mutation for a finite population, and examine if the introduction of mutation helps us have more promising results in terms of the maximum number of cycles during which the application of the adaptive schedule to the Moran process is successful in regulating tumor volume.

Second, for two drug chemotherapy model, tumor volume is designed using the tumor-growth equation in (4.8) where the background fitness, that captures the information of healthy cells or surrounding environment, is set to be constant. However, when drug concentration enters the total population that

contributes tumor development, not only it changes the fitness of cancer cells but also whatever ingredients that influence on forming the background fitness also adapt, making the background fitness fluctuate rather than stay constant. Representing the background fitness as a function of $C_1(t)$ and $C_2(t)$ is more realistic and generalizes our model. This should be designed along with clinical and laboratory observations about reproduction rate of healthy cells and surrounding environment.

The last but not the least important interest for the next study stems from the evaluation of the adaptive two drug chemotherapy model where the low-dose metronomic schedules turns out to be the best chemotherapeutic strategy for the Moran process that starts at one exact point, O, regardless of drug interactions in the sense that it was the most efficient in reducing the tumor volume. However, in reality, the different patients' initial status are assigned to all different points from O and from each other in a phase space, and the conclusion of the evaluation of 4 discussed chemotherapy schedules might vary depending on initial states. For that reason, we would like to visualize the area of initial points in a phase space, at which each of those schedules work the best.

Bibliography

[1] P. M. Altrock and A. Traulsen. “Deterministic evolutionary game dynamics in finite populations”. In: *Physical Review E* 80.1 (2009), p. 011909.

[2] P. M. Altrock and A. Traulsen. “Fixation times in evolutionary games under weak selection”. In: *New Journal of Physics* 11 (2009), p. 013012.

[3] R. Axelrod. *The evolution of cooperation*. New York, USA: Basic Books, 1984.

[4] S. Bernstein. “Démonstration du théorème de Weierstrass fondée sur le calcul des probabilités (Proof of the theorem of Weierstrass based on the calculus of probabilities)”. In: *Communications of the Kharkov Mathematical Society* 13.1 (1912), pp. 1–2.

[5] C. I. Bliss. “The toxicity of poisons applied jointly”. In: *Annals of Applied Biology* 26.3 (1939), pp. 585–615.

[6] I. M. Bomze. “Lotka-Volterra equation and replicator dynamics: A two-dimensional classification”. In: *Biological Cybernetics* 48 (1983), pp. 201–211.

[7] I. M. Bomze and R. Burger. “Stability by mutation in evolutionary games”. In: *Games and Economic Behavior* 11.2 (1995), pp. 146–172.

[8] “Changes associated with the development of resistance to imatinib (STI571) in two leukemia cell lines expressing p210 Bcr/Abl protein”. In: *Cancer* 100.7 (2004), pp. 1459–1471.

[9] T. C. Chou and D. C. Rideout. *Synergism and antagonism in chemotherapy*. San Diego, CA, USA: Academic Press, 1991.

[10] J. C. Claussen and A. Traulsen. “Non-Gaussian fluctuations arising from finite populations: Exact results for the evolutionary Moran process”. In: *Physical Review E* 71.2 (2005), p. 025101.

[11] J. H. Connell. “The influence of interspecific competition and other factors on the distribution of the barnacle Chthamalus stellatus”. In: *Ecology* 42.4 (1961), pp. 710–723.

[12] C. R. Darwin. *On the origin of species*. London, UK: John Murray, 1859.

[13] J. D. Davidson and et al. “An increase in the expression of ribonucleotide reductase large subunit 1 is associated with gemcitabine resistance in non-small cell lung cancer cell lines”. In: *Cancer Research* 64.11 (2004), pp. 3761–3766.

[14] R. Dawkins. *The selfish gene*. Oxford, UK: Oxford University Press, 1976.

[15] E. M. Ferreira and A. G. M. Neves. “Fixation probabilities for the Moran process with three or more strategies: general and coupling results”. In: *Journal of Mathematical Biology* 81 (2020), pp. 277–314.

[16] R. A. Fisher. *The genetical theory of natural selection*. Oxford, UK: Clarendon Press; Oxford University Press, 1930.

[17] D. Foster and P. Young. “Stochastic evolutionary game dynamics”. In: *Theoretical Population Biology* 38.2 (1990), pp. 219–232.

[18] R. A. Gatenby. “A change of strategy in the war on cancer”. In: *Nature* 459 (2009), pp. 508–509.

[19] R. A. Gatenby, A. S. Silva, R. J. Gillies, and B. R. Frieden. “Adaptive therapy”. In: *Cancer Research* 69.11 (2009), pp. 4894–4903.

[20] A. Gautam and G. Bepler. “Suppression of lung tumor formation by the regulatory subunit of ribonucleotide reductase”. In: *Cancer Research* 66.13 (2006), pp. 6497–6502.

[21] C. Hauert, S. D. Monte, J. Hofbauer, and K. Sigmund. “Replicator dynamics for optional public good games”. In: *Journal of Theoretical Biology* 218.2 (2002), pp. 187–194.

[22] J. Hofbauer and K. Sigmund. “Evolutionary game dynamics”. In: *Bulletin of the American Mathematical Society* 40 (2003), pp. 479–519.

[23] J. Hofbauer and K. Sigmund. *Evolutionary games and population dynamics*. Cambridge, UK: Cambridge University Press, 1998.

[24] L. A. Imhof, D. Fudenberg, and M. A. Nowak. “Evolutionary cycles of cooperation and defection”. In: *Proceedings of the National Academy of Sciences of the United States of America* 102.31 (2005), pp. 10797–10800.

[25] L. A. Imhof and M. A. Nowak. “Evolutionary game dynamics in a Wright-Fisher process”. In: *Journal of mathematical biology* 52 (2006), pp. 667–681.

[26] L. A. Imhof and M. A. Nowak. “Stochastic evolutionary dynamics of direct reciprocity”. In: *Proceedings of the Royal Society B: Biological Sciences* 277.1680 (2010), pp. 463–468.

[27] W. S. Kendal. “Gompertzian Growth as a consequence of tumor heterogeneity”. In: *Mathematical Biosciences* 73.1 (1985), pp. 103–107.

[28] S. Lessard and V. Ladret. “The probability of fixation of a single mutant in an exchangeable selection model”. In: *Journal of Mathematical Biology* 54 (2007), pp. 721–744.

[29] E. Lieberman, C. Hauert, and M. A. Nowak. “Evolutionary dynamics on graphs”. In: *Nature* 35 (2005), pp. 312–316.

[30] Y. Ma and P. K. Newton. “Role of synergy and antagonism in designing multidrug adaptive chemotherapy schedules”. In: *Physical Review E* 103.3 (2021), p. 032408.

[31] P. A. P. Moran. “Random process in genetics”. In: *Mathematical Proceedings of the Cambridge Philosophical Society* 54.1 (1958), pp. 60–71.

[32] P. A. P. Moran. *The Statistical Processes of Evolutionary Theory*. Oxford, UK: Clarendon Press; Oxford University Press, 1962.

[33] O. Morgenstern and J. V. Neumann. *Theory of games and economic behavior*. Princeton, NJ, USA: Princeton University Press, 1953.

[34] J. F. Nash. “Equilibrium points in n-person games”. In: *Proceedings of the National Academy of Sciences of the United States of America* 36.1 (1950), pp. 48–49.

[35] J. V. Neumann. “Zur Theorie der Gesellschaftsspiele [On the Theory of Games of Strategy]”. In: *Mathematische Annalen [Mathematical Annals] (in German)* 100 (1928), pp. 295–320.

[36] P. K. Newton and Y. Ma. “Nonlinear adaptive control of competitive release and chemotherapeutic resistance”. In: *Physical Review E* 99.2 (2019), p. 022404.

[37] M. A. Nowak. *Evolutionary dynamics: Exploring the equations of life*. Cambridge, MA, USA: Harvard University Press, 2006.

[38] M. A. Nowak and R. M. May. “Evolutionary games and spatial chaos”. In: *Nature* 359 (1992), pp. 826–829.

[39] M. A. Nowak and R. M. May. “The spatial dilemmas of evolution”. In: *International Journal of Bifurcation and Chaos* 3.1 (1993), pp. 35–78.

[40] M. A. Nowak, A. Sasaki, C. Taylor, and D. Fudenberg. “Emergence of cooperation and evolutionary stability in finite populations”. In: *Nature* 428 (2004), pp. 646–650.

[41] M. A. Nowak and K. Sigmund. “Evolutionary dynamics of biological games”. In: *Science* 303.5659 (2004), pp. 793–799.

[42] M. A. Nowak and K. Sigmund. “The evolution of stochastic strategies in the Prisoner’s dilemma”. In: *Acta Applicandae Mathematicae (in Netherlands)* 20 (1990), pp. 247–265.

[43] K. M. Page and M. A. Nowak. “Unifying evolutionary dynamics”. In: *Journal of Theoretical Biology* 219.1 (2002), pp. 93–98.

[44] F. C. Santos, M. D. Santos, and J. M. Pacheco. “Social diversity promotes the emergence of cooperation in public goods games”. In: *Nature* 454 (2008), pp. 213–216.

[45] P. Schuster and K. Sigmund. “Replicator dynamics”. In: *Journal of Theoretical Biology* 100.3 (1983), pp. 533–538.

[46] J. M. Smith. *Evolution and the theory of games*. Cambridge, UK: Cambridge University Press, 1982.

[47] J. M. Smith. *On evolution*. Edinburgh, Scotland: Edinburgh University Press, 1972.

[48] J. M. Smith. “The theory of games and the evolution of animal conflicts”. In: *Journal of Theoretical Biology* 47.1 (1974), pp. 209–221.

[49] J. M. Smith and G. R. Price. “The logic of animal conflicts”. In: *Nature* 246 (1973), pp. 15–18.

[50] G. Szabo and C. Toke. “Evolutionary prisoner’s dilemma game on a square lattice”. In: *Physical Review E* 58.1 (1998), p. 69.

[51] C. Taylor, D. Fudenberg, A. Sasaki, and M. A. Nowak. “Evolutionary game dynamics in finite populations”. In: *Bulletin of Mathematical Biology* 66 (2004), pp. 1621–1644.

[52] P. D. Taylor and L. B. Jonker. “Evolutionary stable strategies and game dynamics”. In: *Mathematical Biosciences* 40.1–2 (1978), pp. 145–156.

[53] A. Traulsen, J. C. Claussen, and C. Hauert. “Coevolutionary dynamics in large, but finite populations”. In: *Physical Review E* 74.1 (2006), p. 011901.

[54] A. Traulsen, J. C. Claussen, and C. Hauert. “Coevolutionary dynamics: from finite to infinite populations”. In: *Physical Review Letters* 95.23 (2005), p. 238701.

[55] A. Traulsen and M. A. Nowak. “Evolution of cooperation by multilevel selection”. In: *Proceedings of the National Academy of Sciences of the United States of America* 103.29 (2006), pp. 10952–10955.

[56] A. Traulsen, M. A. Nowak, and J. M. Pacheco. “Stochastic dynamics of invasion and fixation”. In: *Physical Review E* 74.1 (2006), p. 011909.

[57] A. Traulsen, J. M. Pacheco, and L. A. Imhof. “Stochasticity and evolutionary stability”. In: *Physical Review E* 74.2 (2006), p. 021905.

[58] A. Traulsen, J. M. Pacheco, and M. A. Nowak. “Pairwise comparison and selection temperature in evolutionary game dynamics”. In: *Journal of Theoretical Biology* 246.3 (2007), pp. 522–529.

[59] J. West, Y. Ma, and P. K. Newton. “Capitalizing on competition: An evolutionary model of competitive release in metastatic castration resistant prostate cancer treatment”. In: *Journal of Theoretical Biology* 455 (2018), pp. 249–260.

[60] S. Wright. “Evolution in Mendelian populations”. In: *Genetics* 16.2 (1931), pp. 97–159.

[61] B. Wu, P. M. Altrock, L. Wang, and A. Traulsen. “Universality of weak selection”. In: *Physical Review E* 82.4 (2010), p. 046106.